Rochester Institute of Technology

RIT Digital Institutional Repository

Theses

6-1-2011

Fabrication and life cycle assessment of organic photovoltaics

Annick Anctil

Follow this and additional works at: https://repository.rit.edu/theses

Recommended Citation

Anctil, Annick, "Fabrication and life cycle assessment of organic photovoltaics" (2011). Thesis. Rochester Institute of Technology. Accessed from

This Dissertation is brought to you for free and open access by the RIT Libraries. For more information, please contact repository@rit.edu.

FABRICATION AND LIFE CYCLE ASSESSMENT OF ORGANIC PHOTOVOLTAICS

by

ANNICK ANCTIL

A DISSERTATION

Submitted in partial fulfillment of the requirements
For the degree of Doctor of Philosophy
in
Sustainability
at the
Rochester Institute of Technology

June 2011

Author: _____
Sustainability Program

Certified by: _____
Dr. Ryne P. Raffaelle
Professor of Physics and Microsystems Engineering

_____
Dr. Brian J. Landi
Professor of Chemical Engineering

Approved by: _____
Dr. Thomas W. Smith
Interim Academic Director of Sustainability Program

Certified by: _____
Dr. Nabil Nasr
Assistant Provost and Director, Golisano Institute of Sustainability

NOTICE OF COPYRIGHT

© 2011

Annick Anctil

REPRODUCTION PERMISSION STATEMENT

Permission Granted

TITLE:

"Fabrication and Life Cycle Assessment of Organic Photovoltaics"

I, *Annick Anctil*, hereby grant permission to the Wallace Library of the Rochester Institute of Technology to reproduce my dissertation in whole or in part. Any reproduction will not be for commercial use or profit.

Signature of Author: _____ Date: _____

Fabrication and Life Cycle Assessment of Organic Photovoltaics

by

Annick Anctil

Submitted by Annick Anctil in partial fulfillment of the requirements for the degree of Doctor of Philosophy in Sustainability and accepted on behalf of the Rochester Institute of Technology by the dissertation committee.

We, the undersigned members of the Faculty of the Rochester Institute of Technology, certify that we have advised and/or supervised the candidate on the work described in this dissertation. We further certify that we have reviewed the dissertation manuscript and approve it in partial fulfillment of the requirements of the degree of Doctor of Philosophy in Sustainability.

Approved by:

Dr. Ryne P. Raffafelle _____
(Committee Chair and Dissertation Co-Advisor) Date

Dr. Brian J. Landi _____
Dissertation Co-Advisor

Dr. Callie Babbitt _____

Dr. Gabrielle Gaustad _____

SUSTAINABILITY PROGRAM
ROCHESTER INSTITUTE OF TECHNOLOGY
June 2011

ABSTRACT

Golisano Institute for Sustainability
Rochester Institute of Technology

Degree Doctor of Philosophy **Program** Sustainability

Name of Candidate Annick Anctil

Title : Fabrication and Life Cycle Assessment of Organic Photovoltaics

Increasing demand for renewable energy has resulted in a new interest for alternative technologies such as organic photovoltaics. With efficiencies exceeding 8% for both polymer and small molecule photovoltaics, organic photovoltaics are now being commercialized due to their flexibility and low weight which allow for their adoption in new applications such as portable electronics, smart fabrics, and building-integrated photovoltaics. To date, most research efforts have been focused on increasing power efficiency with little assessment of potential negative impacts associated with their large scale production. It is generally assumed that organic photovoltaics have low environmental impacts and are by nature inexpensive to produce since they are often solution processed. In the present work, a comprehensive analysis of the life cycle embodied energy for C_{60} and C_{70} fullerenes which are the most common acceptor molecules in organic photovoltaics, has been performed from cradle-to-gate, including the relative contributions from synthesis, separation, purification, and functionalization processes. The embodied energy of all fullerenes was calculated to be an order of magnitude higher than most bulk chemicals. These results have enabled the life cycle impact associated with the production of various types of organic photovoltaics to be calculated, including polymer, small molecule and multi-junction devices. An outcome of the life cycle assessment for organic photovoltaics shows that small molecule devices require significant fabrication energy from high vacuum processing and their efficiency is limited by poor absorption in the near-infrared (NIR). Therefore, a solution processing approach with novel NIR absorbing molecules in multi-junction devices has been developed in order to minimize the total cumulative energy. The combined efforts have led to the first demonstration of a spray-coated small molecule photovoltaic NIR device, using a combination of ZnPc and AlPc which is projected to have an embodied energy similar to single junction polymer devices.

ACKNOWLEDGMENTS

I would like to thank both of my advisors, Dr. Ryne Raffaelle for giving me the opportunity to work at the NanoPower Research Lab and Dr. Brian Landi for his continuous support and availability. I would also like to show my gratitude to members of my committee, my family, friends and colleagues for their help and moral support.

TABLE OF CONTENTS

LIST OF FIGURES

LIST OF TABLES

LIST OF SYMBOLS

BCP	bathocuproine
BHJ	Bulk heterojunction
BPhen	bathophenanthroline
CED	Cumulative Energy Demand
C_{60}PCBM	Phenyl-C_{61}-butyric acid methyl ester
EBL	Electron blocking layer
EPBT	Energy payback time
EQE	External Quantum Efficiency
FF	Fill factor
HBL	Hole blocking layer
HOMO	Highest occupied molecular orbital
ISO	International Organization for Standardization
ITO	Indium tin oxide
I-V	Current-voltage measurement
LCA	Life cycle assessment
LCI	Life cycle inventory
LUMO	Lowest occupied molecular orbital
MEH-PPV	Poly (2-methoxy, 5-(2-ethylhexoxy)-1,4-phenylene vinylene)
MPc	Metal phthalocyanine
η	Power conversion efficiency
NIR	Near infrared
OPV	Organic photovoltaics
P3CT	Poly-(4-(2,3-dihydroxypropoxy)-2-methylbutan-2-yl5,5'-dimethyl-[2,2'-bithiophene]-4-carboxylate
P3HT	Poly (3-hexylthiophene)
PBDTTT	poly[4,8-bis-substituted-benzo [1,2-b:4,5-b0]dithiophene-2,6-diyl-alt-4-substituted-thieno[3,4-b]thio- phene-2,6-diyl]
PC	Phthalocyanine
PCDTBT	poly[N-9'-hepta-decanyl-2,7-carbazole-alt-5,5-(4',7'-di-2-thienyl-2',1',3'-benzothiadiazole)
PEDOT:PSS	Poly(3,4-ethylenedioxythiophene) poly(styrenesulfonate)
PET	Polyethylene
PTB7	Poly[4,8-bis[(2-ethylhexyl)oxy]benzo[1,2-b:4,5-b']dithiophene-2,6-diyl][3-fluoro-2-[(2-ethylhexyl)carbonyl]thieno[3,4-b]thiophenediyl]
RF	Radio-frequency
SQ	2,4-bis[4- (N,N-diisobutylamino)-2,6-dihydroxyphenyl]squaraine
SM	Small molecules
SubNc	Chloroboron subnaphthalocyanine
SubPc	Chloroboron subphthalocyanine
TRACI	Tool for the reduction and assessment of chemical and other environmental impacts
Wp	Watt-peak generation

I. INTRODUCTION

After many years of debate, there is now a general agreement within the scientific community that humans have played a role toward climate change [1]. While looking at the major source of emissions in Figure 1a, electricity production stands out as not only the largest contributor of greenhouse gases, but also the one that has steadily increased over the last 35 years. In order to limit the impacts related to climate change, stabilization at the current level will not suffice. The next fifty years are expected to be critical since carbon dioxide emissions should be reduced even with an increasing world population without constraining economic growth. Historically, energy consumption has increased by 2% per year which has translated into 1.5% increase in CO_2 over the last 30 years [2]. While developed countries are often held responsible for the current situation, Figure 1b shows that over the last 30 years, Europe and North America have only slightly increased there energy consumption while most of the increase is a result of other regions of the world, trying to reach the same level of development.

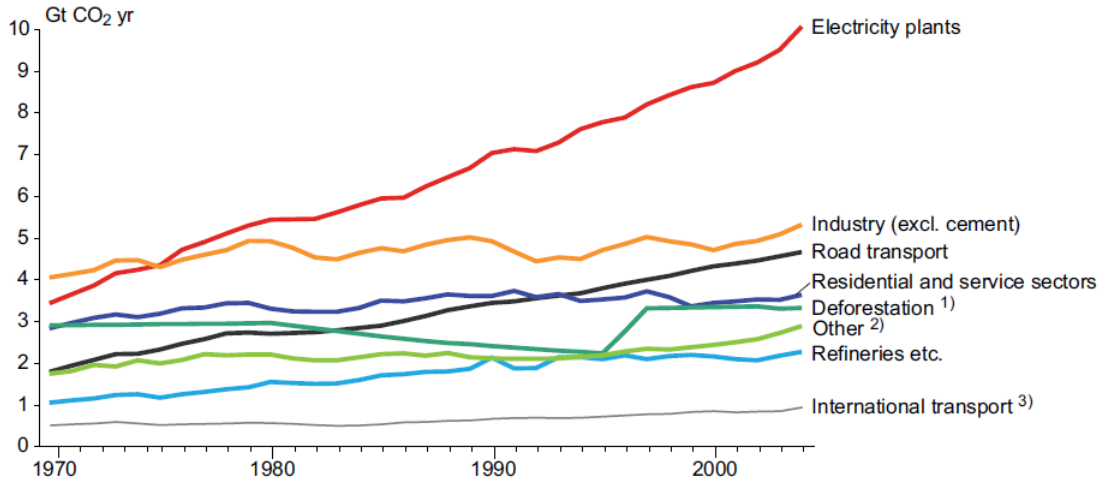

(a)

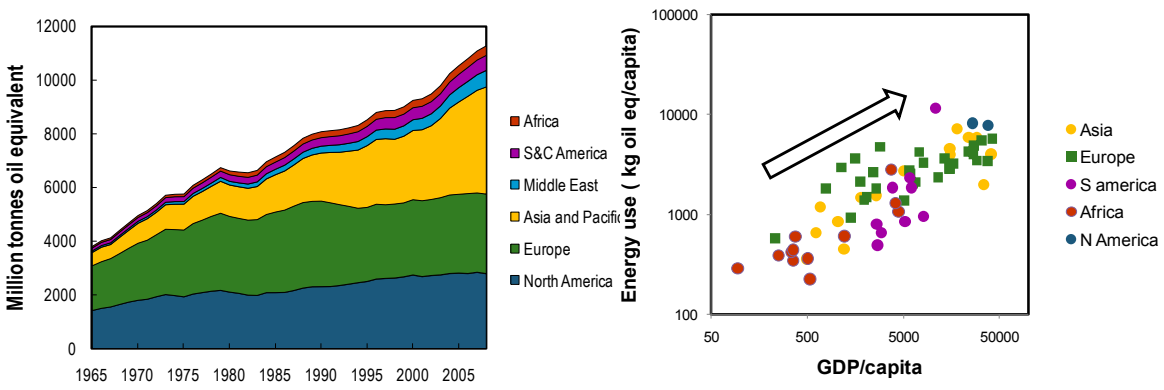

(b) (c)

Figure 1: (a) Source of global CO_2 emissions 1970-2004 by sectors [3], (b) energy consumption over time [4] and (c) energy use as a function of GDP/capita [4, 5].

Energy poverty is used to describe the lack of access to modern, cost-effective and sustainable energy services, which is recognized as a major impediment to human development in many areas of the world. While energy is not part of the millennium development goals as defined by the United Nations, it is recognized that energy poverty has negative impacts on education, health, gender and prosperity. As illustrated in Figure 1c, the energy poor countries are mainly situated in sub-Saharan Africa and South Asia where the greatest population growth is happening. Limiting energy consumption would limit development, which would not be a desirable outcome. The same is true for developed countries such as the United Sates, where the energy consumptions is expected to grow by 14% over the 2008-2035 period, which would cause an increase of 8.7% in CO_2 eq emissions [6]. Therefore, there is a need for cleaner energy sources to prevent further increase in greenhouse gases emissions for both developed and developing countries.

In addition to the need for cleaner energy sources, renewable energy could provide increased energy security. There is a large uncertainty regarding the amount of reserves left from traditional fossil fuels, but recent estimates suggest that the current oil reserves will

be exhausted in about 40 years and natural gas in about 60 years [7]. On the other hand there should be enough coal left for 250 years and uranium for 80 years. Therefore, the need for energy independence is not sufficient to justify the development of renewable and sustainable energy. The main driving force for those technologies is the desire for energy sources with lower environmental impact. The operation of renewable energy devices like solar and wind do not contribute to air pollution through emissions of NO_x and SO_2, thereby also reducing air pollution.

With over 101,000 terawatts of available power, solar energy is the most promising source of renewable energy as shown in Figure 2a, as it would be more than enough to fulfill the 15 terawatts average of power consumed annually world-wide. Solar energy is free and available, but due to the high cost of the technology, it is not expected to represent a large portion of the energy portfolio over the next 20 years as shown in Figure 2b.

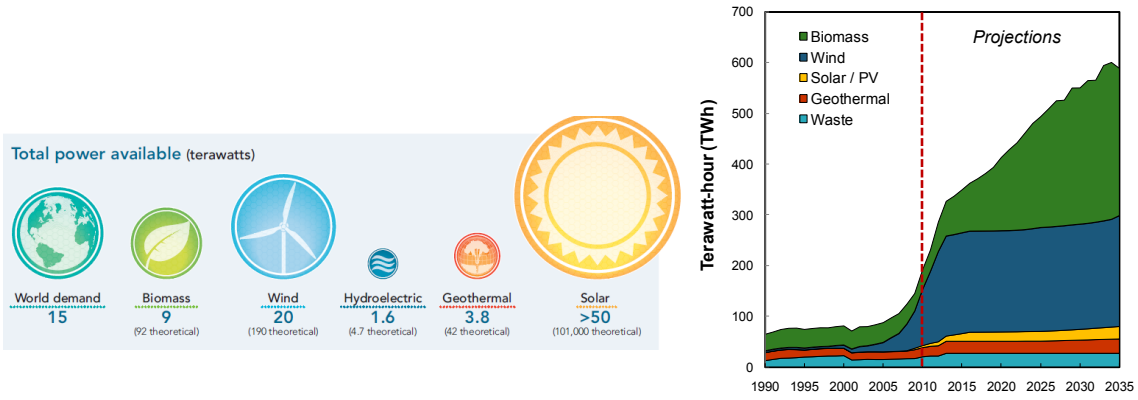

(a) (b)

Figure 2: (a) power available from renewable resources [7] and (b) projection for worldwide energy supply [8].

To understand the current limitation of the technology and its low market penetration, it is useful to distinguish various types of technologies. First generation photovoltaics, which are made of silicon, have been around for more than fifty years. With

this type of technology, it is difficult to decrease the cost below the desirable US$1/Wp as illustrated in Figure 3, because the maximum conversion efficiency is limited by the bandgap of the silicon and the cost is associated with the energy intensive process required to produce monocrystalline silicon ingots. Alternatively, second generation technologies, which corresponds to thin film technologies such as CdTe, CIGS, and amorphous silicon are flexible and cheaper to produce than the first generation solar cells. However, they currently have lower efficiencies but in the case of CdTe, technology price has reached a cost of $0.77/Wp for 11.2% modules [9] providing a rapid growth of the thin film sector. Finally, third generation multi-junction solar cells have been developed for high efficiency applications such as space exploration. However they are now being adapted for terrestrial applications. These devices have more complex geometry and use vapor phase deposition on single crystal substrates, and therefore, are much more expensive than previous generation solar cells. However, because of their high efficiency and use of concentrated sunlight, the energy cost is expected to be lower than other generations' solar cells.

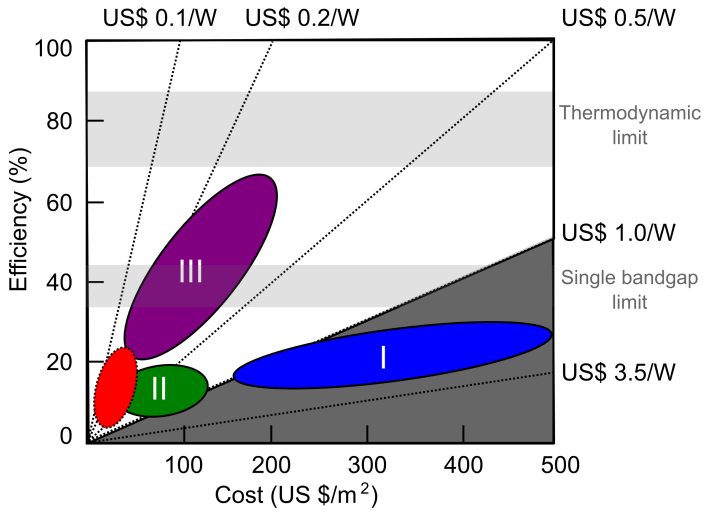

Figure 3: Efficiency vs. cost for various solar cells generations [10].

The category of interest for this dissertation is organic photovoltaics (OPV) which position in Figure 3 is not clear as some refer to them as third generation, based on the time

of their discovery, while other believe they should belong to the second generation since they share the flexibility and low cost of this type of solar cell. However, compared to inorganic materials, the maximum efficiency of organic materials is not fixed. This is because the material can be modified to obtain the desired properties, and therefore, there is no simple theory that can predict their maximum efficiency. For this reason, organic photovoltaics could be considered to be in the red area of Figure 3 since they should be cheaper than second generation but likely to have lower efficiency than third.

While it took 20 years to increase device power efficiencies from 0.1% to 3.5% in 2005 [11], device efficiencies have now reached 8.3% for both small molecule and polymer photovoltaics [12]. Because of their low cost, organic photovoltaics have been recently commercialized by Konarka [13] and production is expected to begin this year for both Solarmer [14] and Heliatek [15]. Organic photovoltaics have reached commercialization earlier than expected, mainly because they can be used in new applications, which counterbalance their low efficiency. One advantage of incorporating low efficiency organic solar cells into electronics products is to increase the lifetime of the battery by charging the devices while not in use. Smart fabrics (also referred to as wearable technology) add new functionality to traditional applications, for example in clothing, tents, military uniform, etc. Applications are numerous for off-grid remote locations, in particular to provide lighting at night or play a double role of shading an area while providing electricity for another usage in the case of shade structures [13].

For building-integrated photovoltaics (BIPV), the low absorption of organic films allows light reduction without completely blocking the light. It could help provide power for buildings during the day when demand is at its peak. It also allows considerable design

improvements compared to traditional semiconductors since organic molecules can be tuned to the desirable colors by slightly changing their chemical properties; therefore, adding an aesthetic aspect allowing OPV to be part of the design. There are also potential applications in windows, skylights, roof and walls where the lower efficiency is balanced by the ancillary attributes.

Motivation

Based on the availability of solar resources, photovoltaic technologies have the potential to provide a significant amount of the energy required to fulfill current and future energy demand while reducing greenhouse gases emissions. So far, the high cost of photovoltaics compared to other energy sources has limited their use. However, emerging technologies such as organic photovoltaics, which take advantage of man-made materials and solution processing hold the promise for future inexpensive devices.

Various challenges have limited OPV use; in particular the large bandgap of most organic polymers is responsible for low power conversion efficiency since a large portion of the solar spectrum remains unabsorbed. Photon absorption is the first step towards high efficiency photovoltaics and lowering the bandgap of the donor material is necessary in that direction. However, to allow efficiencies higher than 13% [16], it also requires a multi-juction approach. While multi-junction devices increase efficiency, they also increase device complexity and require additional processing steps and materials. Those aspects have yet to be considered when estimating the future cost of the technology and ensure that OPV remains a low cost option. For large-scale production, the fabrication methods also need to be considered as current devices use a mixture of solution and vacuum methods which are difficult to scale-up.

While cost and efficiency are often discussed as major challenges of photovoltaics, there are other aspects that need to be considered to make OPV a sustainable technology. According to the Brundtland Commission, sustainable development is " Development that meets the needs of the present without compromising the ability of future generations to meet their own needs" [17]. In that perspective, energy solutions developed today should also be desirable in the future, and most importantly, not at the expense of creating new issues. Sustainability considers the economic, social and environmental aspects altogether. Therefore, goals such as lowering the cost below 1$/Wp or reducing greenhouse gases emissions alone are not sufficient as each of those goal solely address economic or environmental aspects. To be a sustainable technology, other aspects need to be considered, such as the scarcity of material, risk, safety, toxicity, social acceptance and end of life.

So far, there has been a lot of attention towards device efficiency and cost of the technology, but little attention has been given to the environmental impact of OPV production. Therefore, the first goal of this dissertation is to look at current OPV technologies to establish the environmental impact associated with their production. The method used for this purpose is Life Cycle Assessment (LCA) [18] where all the stages from raw material extraction to the module assembly are considered. Since the quality of a LCA study is strongly dependent on the quality of the inventory data, the first step is to characterize the impact of fullerene production. Chapter IV provides a comprehensive analysis of the life cycle embodied energy for C_{60} and C_{70} fullerenes, which are the most common acceptor molecules in organic photovoltaics. The analysis is performed from

cradle-to-gate, including the relative contributions from synthesis, separation, purification, and functionalization processes.

These results are later used in Chapter V to perform the most comprehensive life cycle impact analysis associated with the production of various types of organic photovoltaics, including for the first time: low bandgap polymers, small molecule and multi-junction devices. Using the results from the life cycle inventory, an analysis of proposed greener options is presented as well an alternative method to calculate the cost of organic technologies. An outcome of the life cycle assessment for organic photovoltaics shows that small molecule devices require significant fabrication energy from high vacuum processing and their efficiency is limited by poor absorption in the near-infrared (NIR). Therefore in Chapter VI, a solution processing approach with novel NIR absorbing molecules in multi-junction devices is presented which is expected to have lower embodied energy to produce than current multi-junction photovoltaic devices.

II. BACKGROUND

2.1. Principles of Photovoltaics

The most common device structure for OPV uses a mixture of donor and acceptor materials reffered to as a bulk heterojunction (BHJ) which resides between two electrodes. A typical BHJ made of Poly (3-hexylthiophene) (P3HT) and Phenyl-C_{61}-butyric acid methyl ester (C_{60}PCBM) is illustrated in Figure 4. The photogeneration proceeds according to the following steps. The illumination of an organic semiconductor donor (1) generates excitons (2) with a binding energy of about 0.4 eV instead of free charges [19]. To be separated into free charges, the exciton needs to diffuse until it reaches a donor/acceptor interface (3) with a difference in electron affinities and ionization potential large enough to overcome the binding energy (as illustrated in Figure 4b. The free charges can then travel through either the donor or acceptor material (5) to the electrodes (6). The overall device efficiency is therefore determined by the optical absorption and the efficiency of each of those steps.

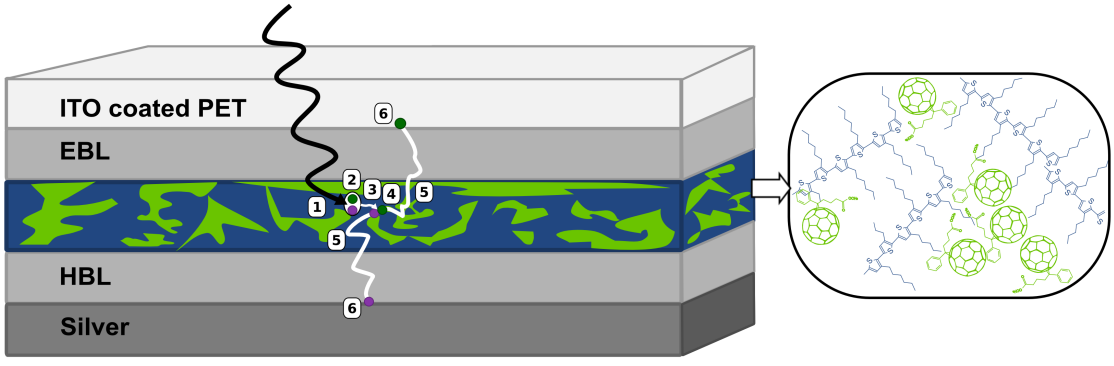

(a)

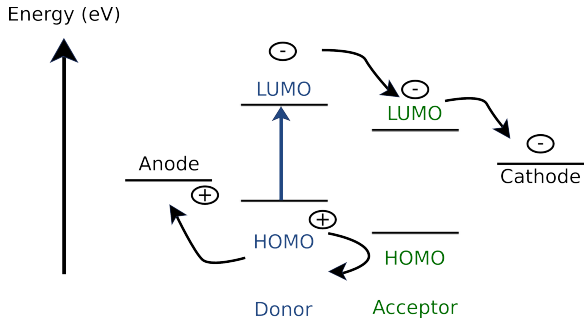

(b)

Figure 4: (a) Photovoltaic effect in a bulk heterojunction organic solar and detail about the chemical structure of P3HT:C_{60}PCBM material used in the active layer and (b) conditions for charge transfer in a donor/acceptor photovoltaic device

The multi-junction approach allows the absorption of a larger portion of the solar spectrum, but for OPV it is also advantageous to overcome the poor charge carrier mobility and lifetime of carriers which prevents the fabrication of a thick absorbing layer [20]. In comparison with inorganic material, organic semi-conductors absorb only a narrow portion of the spectrum as illustrated in Figure 5 and therefore a combination of multiple materials is necessary to absorb a larger portion of the spectrum.

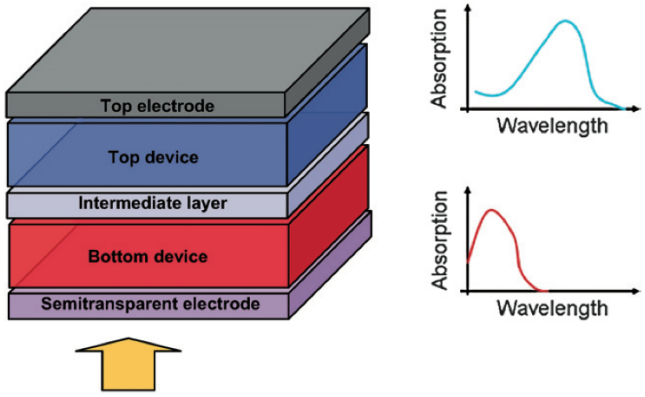

Figure 5: Organic photovoltaic with two sub-cells having different complementary absorption spectra [20].

Multi-junction devices can either be connected in series or in parallel depending on the nature of the intermediate layer. The most common type of connection is in series where the voltage across the whole device is equal to the sum of the voltage of each sub-cell and the current is limited by the lowest sub-cell current.

2.2. Organic Semiconductors

Organic semiconductors require alternating single and double carbon bonds where each carbon binds only to three adjacent atoms, resulting in one electron left in the P_z orbital. The overlap of these P_z orbitals causes the formation of π bonds along the backbone, and delocalizaton of the π electrons. Molecules with a delocalized π electron system can absorb sunlight, create photogenerated charge carriers, and transport these charge carriers. The organization of the semi-conducting material is critical as the π-π bonds need to be close enough to allow charge transport. Organic semiconductors are divided in two categories: polymer, which can be solution processed and small molecules that are generally evaporated under high vacuum. Both types of semi-conductor materials have been used in this dissertation and therefore will be further discussed.

2.2.1 Polymer semiconductors

Current interest in OPV can be attributed to regioregular poly(3-hexylthiophene) (P3HT) which allowed device efficiencies to reach 5% for the first time. Morphology has been found to be critical, requiring a precise control over the donor:acceptor ratio, solvent choice, and post-treatment annealing to induce reorganization and crystallization of the polymer. While efficiencies have constantly improved over the last few years, there is still work required to reach the 10% benchmark, generally considered necessary for large scale commercialization. One major limitation of organic solar cells is related to the poor

absorption of the semi-conductor material compared to the solar spectrum as illustrated in Figure 6a. The maximum efficiency is therefore limited by the bandgap of the polymer and is estimated to be lower than 10% for both P3HT and Poly(2-methoxy, 5-(2-ethylhexoxy)-1,4-phenylene vinylene) (MEH-PPV) as illustrated in Figure 6b. In theory, to have an optimal solar cell, the acceptor bandgap should be around 1.4 eV, for which the maximum efficiency would be 31% under 1 sun AM1.5 [21]. The majority of initially developed semiconducting polymers have bandgaps higher than 2 eV (620 nm), which limits their maximum efficiency.

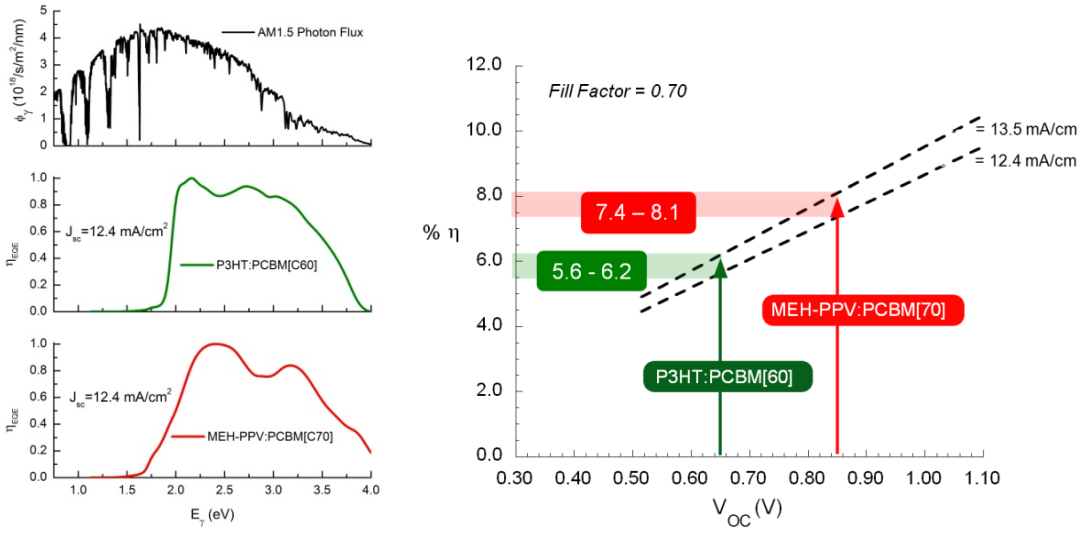

(a) (b)

Figure 6: (a) Comparison of the spectral response for P3HT and MEH-PPV:C_{60}PCBM devices and the calculated limiting J_{sc} = 12.4 mA/cm^2 from the normalized EQE; (b) plot of the maximum theoretical efficiency as a function of V_{oc} for the normalized EQE data from (a). The arrows and shading for each polymer system reflect experimentally observed V_{oc} values [22].

To increase device efficiency, there are mainly two alternatives: lower bandgap and multi-junction. One which has received considerable interest in the last few years and resulted in the actual record efficiency, consists of lower bandgap polymers, closer to the optimal bandgap, used with the same acceptor material (fullerenes) as previous generation

organic solar cells. By lowering the bandgap from 2eV to 1.5 eV, the maximum theoretical efficiency increases from 8% to 13% [16]. The second approach uses 2 different cells to form a multi-junction device, which can capture broader range of the solar spectrum.

2.2.2 Small molecule semiconductors

While polymers have received the greatest attention in the last few years, small molecule devices were actually responsible back in 1985 for the first 1% efficient solar cell which is often considered the beginning of organic photovoltaics [23]. Metal phthalocyanines (MPc) have been used for over 20 years with only modest success, but there is still considerable interest for this class of materials since they can be easily synthesized and modified by changing the central metal atom (M = Zn, Mg, Cd, Cu, Co, etc.) as illustrated in Figure 7a. While MPc are traditionally synthesized by reacting phthalonitrile with the desired metal chloride, phthalic anhydride is used to obtain a metal phthalocyanine chloride (MPcCl), such as aluminum phthalocyanine chloride (AlPcCl) and indium phthalocyanine chloride (InPcCl) which are considered in this work [24, 25] The last class of phthalocyanine molecules considered include chloroboron subnaphthalocyanine (SubNc) and chloroboron subphthalocyanine (SubPc) which are also synthesized using phthalic anhydride according to the reaction shown in Figure 7c.

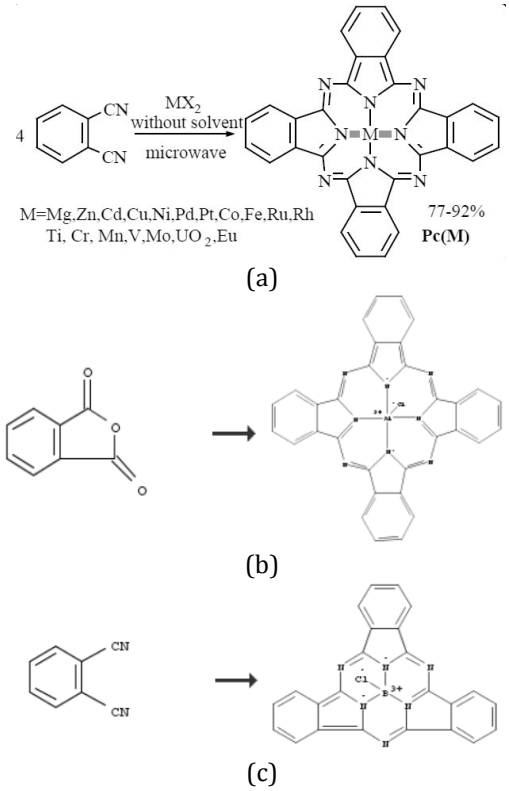

Figure 7: (a) General reaction for the synthesis of metal phthalocyanies using microwave conditions [24], (b) synthesis of AlPcCl using phthalic anhydride and (c) synthesis of SubPc.

One main disadvantage of small molecules such as phthalocyanines is the need for high vacuum equipment to evaporate the material. Therefore, there is a growing interest in developing solution processable small molecules such as squaraine derivatives which have recently been synthesized [26].

III. METHODS

The work in this dissertation initially evaluates the impact of current technologies using LCA and then uses the results to propose alternative multi-junction photovoltaics using a NIR approach. Therefore, a general overview of LCA as well as device fabrication and testing is provided in this section.

3.1. Life cycle assessment (LCA)

As illustrated in Figure 8a, a complete life cycle assessment (LCA) is a "cradle-to-grave" method approach, which begins with raw material extraction (cradle) and ends when the material returns to the earth (grave). The cumulative environmental impacts from all stages in a product life cycle are included, by providing a comprehensive view of the environmental impacts, which allow the evaluation of trade-offs in product and process selection. By performing a comprehensive analysis, including all product life cycle stages and multiple metrics, LCA helps to avoid shifting environmental problems.

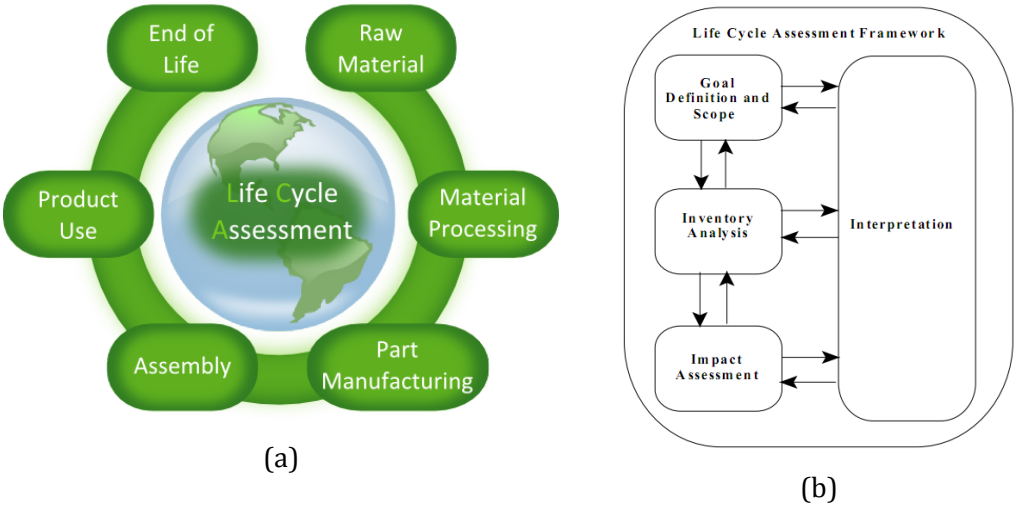

Figure 8: (a) Cradle-to grave Life Cycle Assessment and (b) phases of LCA [27].

LCA is a ISO standardized method which requires specific methodology. It consists of four stages as illustrated in Figure 8b [18, 27] which are:

1- **Goal definition and scoping:** Define and describe the product, process or activity and define the system boundaries and metrics being used. This stage must include the type of information needed and how the results of the LCA should be interpreted and used. During this stage, the distinction between foreground and background data has to be established. The foreground system is the system of primary concern while the background system uses aggregated datasets which are similar for all the various scenarios being considered.

2- **Inventory Analysis:** All relevant data is collected and organized. The level of accuracy and detail will influence the quality of the analysis. Assumptions and limits of data collection such as cut-off rules have to be clearly defined. The goal and scope stage has defined general system boundaries which need to be further detailed and analyzed using the following 4 stages:

   a. Develop a flow diagram of the processes being evaluated
   b. Develop a data collection plan
   c. Collect data
   d. Evaluate and report results

   Part of the system description is the identification of co-products which are process outputs that have value, and therefore, are not treated as wastes. The ISO standards suggest to avoid allocation if possible and to prefer physical relationships methods rather than economics if allocation is necessary. In this work, allocation is always performed on a gravimetric basis.

3- **Impact Assessment:** Using appropriate metrics and using the inventory analysis, assess the potential human and ecological impacts.

4- **Interpretation:** Evaluate the results of the inventory analysis and impact assessment to select the preferred product, process or service.

The use of LCA software facilitates the compilation and analysis, and SimaPro® was choosen for this purpose. Inventory data from an existing database (ecoInvent) and previously published primary literature are used for common materials. Process inventory data for chemicals not publicly available are estimated using default values and stoichiometric reactions according to previously published guidelines [28, 29].

3.2. Fabrication and testing of photovoltaics

Organic solar cells are generally fabricated using either spin-coating for polymer photovoltaics or vacuum-deposition for small molecules. ITO coated glass is cleaned with acetone and isopropanol, dried for half an hour prior to the spin-coating of Poly(3,4-ethylenedioxythiophene) poly(styrenesulfonate) (PEDOT:PSS) which acts as the electron blocking layer (EBL). Evaporation of the small molecules as well as the aluminum contact is done using a multi-source Lesker PVD75 evaporator.

Current-Voltage (J-V)

The principal method for photovoltaics characterization is current-voltage (J-V) measurement where the device is exposed to a simulated solar spectrum. The standard illumination condition for terrestrial applications is an AM1.5 spectrum which represents a light intensity of 1000 W/m^2, with a spectral intensity distribution matching that of the sun on the earth's surface at an incident angle of 48.2° [30]. Figure 9 illustrates a typical

current-voltage curve. The fill factor (FF), which corresponds to the darker square area, represents the ratio of delivered power over the maximum potential power. The power conversion efficiency (η) is the ratio of the power delivered over the incident power (1000 W/m^2).

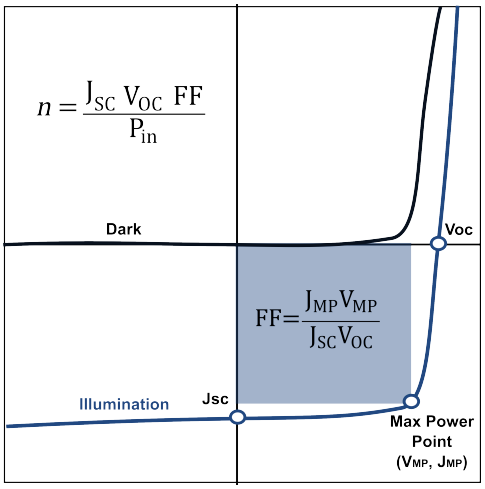

Figure 9: Current-Voltage (J-V) curve

External Quantum Efficiency (EQE)

The current-voltage characterization provides information about the total amount of incident power converted into electrical power. For device optimization, in particular for multi-junctions, it is useful to know what wavelengths of the solar spectrum are being converted. The external quantum efficiency (EQE) measures the number of electrons collected under short circuit conditions divided by the number of incident photons.

$$\boldsymbol{E.Q.E} = \frac{\boldsymbol{1240\ Isc}}{\boldsymbol{\lambda P_{in}}} \qquad (1)$$

IV. MATERIAL AND ENERGY INTENSITY OF FULLERENE PRODUCTION

Previous to the work presented in this dissertation, the life cycle assessment of OPV had only been performed for one type of device, corresponding to the best device developed five years ago, and therefore not relevant to currently commercialized devices. Since the quality of a LCA study is strongly correlated to the quality of the inventory data, the first step is to ensure quality data for the new organic materials. For OPV, the most common acceptor molecules are fullerenes for which there exists no detailed inventory information. Therefore, this chapter analyses the impact of fullerene production, in particular considering the types of fullerenes derivatives and purity requirement necessary for application in organic photovoltaics. This work has been published as A. Anctil, C. W. Babbitt, R. P. Raffaelle, and B. J. Landi, "Material and Energy Intensity of Fullerene Production," *Environmental Science and Technology,* vol. 45, pp. 2353-2359, 2011. Additional information regarding data sources for life-cycle assessment, production, separation and functionalization of fullerenes process diagrams, inventory for the production of C_{60} and various fullerenes derivatives and price of fullerenes is available in section A.1.

INTRODUCTION

Carbon can be arranged under various configurations ranging from amorphous carbon to the highly organized diamond structure to nanomaterials like carbon nanotubes and fullerenes, depending on conditions that prevail during synthesis [31]. Fullerenes have been one of the most prevalent carbon allotropes in chemical research since their discovery in 1985 by Sir Harold Kroto and coworkers [32]. Fullerenes in their pure form are carbon atoms organized in an empty closed cage structure which comprises twelve 5-member rings

and various numbers of 6-member rings depending on the size of the fullerene (i.e. C_{60}, C_{70} C_{84}, C_{96}). The representative structure for C_{60} is depicted in Figure 10a and has been the building block for derivative synthesis using covalent, supramolecular, and/or endohedral chemistry, which can lead to numerous derivatives [33-35] So far, fullerenes have found applications in medicine (e.g. fate and transport of drugs through dense tissues like cancerous cells, for DNA photocleavage, and gene delivery [34], environmental remediation (e.g. pathogen decontamination [31], and energy systems (e.g. organic solar cells).

The most common modification to fullerenes consists of adding either one or two methyl ester functional groups to form [6,6]-phenyl-C_{61}-butyric acid methyl ester (PCBM) (Figure 10b) or bis [6,6]-phenyl-C_{61}-butyric acid methyl ester (bis-PCBM) (Figure 10). Using the same process, methyl ester groups can be added to larger fullerenes such as C_{70} as illustrated in Figure 10d. The fullerene derivatives illustrated (Figure 10 b-d) are commonly used as an acceptor molecule when mixed with a conducting polymer to create a bulk heterojunction of donor/acceptor material (Figure 10e) in organic solar cells. Under illumination, the polymer (e.g. polyhexylthiophene (P3HT)) generates bound electron-hole pairs that are dissociated into free charges at the junction with the fullerene materials. The free electrons can then travel to the anode using the fullerene pathway and the holes through the polymer resulting in a photocurrent. This type of organic solar cell can potentially provide inexpensive, large area solar energy conversion.

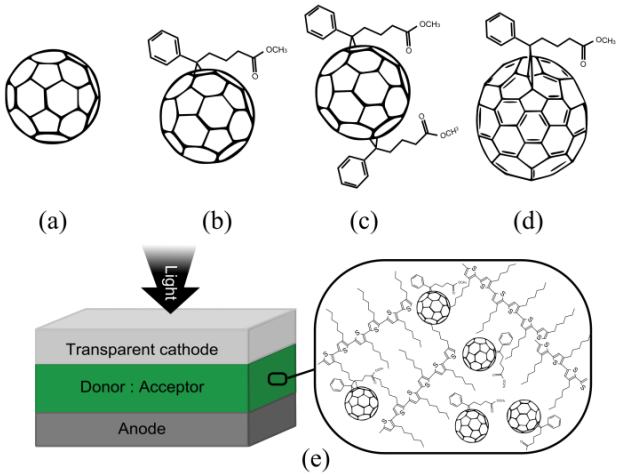

Figure 10: Pure fullerene (a) C_{60} and fullerene derivatives (b) C_{60}-PCBM , (c) C_{60}-bisPCBM and (d) C_{70}-PCBM and (e) schematic of (C_{60}-PCBM) fullerenes derivatives used in a bulk heterojunction organic solar cells.

The prospect for nanomaterials like fullerenes to be adopted in organic solar cells and other emerging products motivates the need to understand what the impact of these nanomaterials will be in the overall product [36-38]. Organic solar cells containing fullerenes have already been commercialized since 2008 by Konarka [39] and with other companies in the development phase, there is a real need to proactively evaluate the impact of fullerenes.

The contribution from nanomaterials in developing products has generally not been studied in detail and only a small fraction of studies use current data for nanomaterial production methods[40]. An unfounded assumption that is present in some studies is the notion that a small amount of nanomaterials in a product will result in minimal environmental impact [36, 40]. This can lead to application of cut-off rules based on weight to simplify life-cycle assessment of products containing nanomaterials. However, there are legitimate concerns with such an approach since existing impact data are often based on limited analysis of upstream material inputs and system boundaries [36]. Therefore, it is

considered a priority to publish detailed and updated inventory data [40-41] for nanomaterials like fullerenes, which are likely to have a high potential for future industrial applications [38].

In this work, life cycle assessment (LCA) is used to assess energy intensity of producing C_{60} and C_{70} fullerenes and corresponding derivatives that are being considered in present day medical and energy applications. Whereas previous studies have limited the LCA scope to direct energy input (e.g. electricity usage) during fullerene synthesis [42-43], this study quantifies total material intensity and embodied energy with a scope that includes all direct and upstream feedstock and fuel energy inputs for modern production methods. The variation in synthesis method and purification processes is included to more accurately quantify the impact from factors as synthesis reaction, purity of reactants and solvents, low reaction yields, repeated purification steps, and toxic chemicals or solvents. The primary goal of this study is to use the calculated energy intensity of modified fullerene production to determine opportunities for future process innovations to minimize environmental impact. As secondary objectives, this study serves both to fully document a life cycle inventory of fullerene production and to investigate the relative importance of nanomaterials in the products in which they are used, as demonstrated through examples of C_{60} used in an aluminum composite and PCBM derivative used in organic solar cell applications.

METHODOLOGY

The goal of this study is to assess the cradle-to-gate embodied energy associated with producing fullerenes and modified derivatives using a process-based life cycle assessment (LCA) methodology. Analysis of the various fullerenes products is intended to

provide a baseline to evaluate future product developments and guide product design and research [44]. The scope includes two types of fullerene production methods (pyrolysis and plasma with different precursors for both techniques) and two types of fullerenes (C_{60} and C_{70}) as well as one type of derivative [6,6]-phenyl-C61-butyric acid methyl ester (PCBM). The LCA scope is illustrated in Figure 11 and corresponds to the four stages of fullerene production: synthesis, separation, purification, and functionalization.

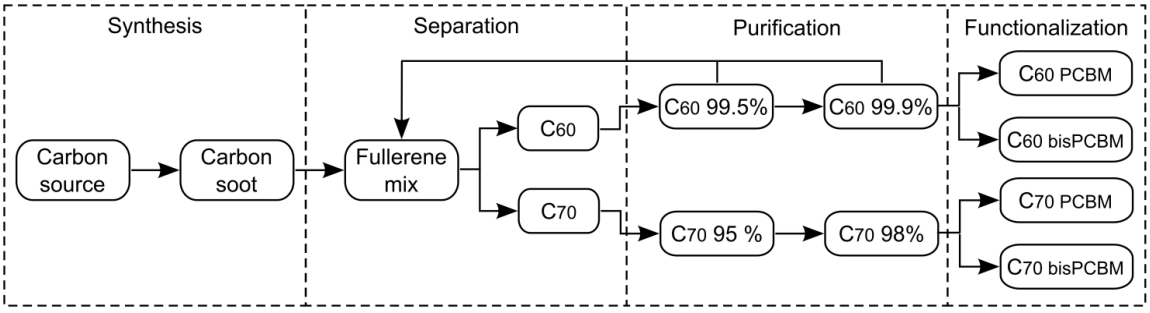

Figure 11: Overview of the process flow for the production of modified fullerene compounds for use as functional materials in organic solar cells.

The cradle-to-gate inventory is based on the functional unit of 1 kg of product (either C_{60} or C_{70}), such that results can be used to compare fullerenes to other raw materials and assess downstream uses of these materials in a variety of applications. Energy inputs are allocated to C_{60} and C_{70} by their mass ratio on an as-produced basis. The life cycle assessment results are obtained from analysis using SimaPro® (PRe Consultants, The Netherlands) using inventory data from an existing database (ecoInvent, ecoinvent Centre, Switzerland) and previously published primary literature. Inventory data for chemicals not publicly available were estimated using default values and stoichiometric reactions according to previously published guidelines [28,29]. Solvent regeneration is assumed for all purification steps using the procedure developed specifically for the production of fine chemicals [29]. Detailed information about processes involved in the

four stages of fullerene production, data sources, and life cycle inventory calculations is available in A1.

RESULTS AND DISCUSSION

1. Synthesis and separation

Plasma techniques are often viewed as a greener option than pyrolysis methods as they don't produce direct gaseous emissions during synthesis [45]. However, this analysis demonstrates that comparative environmental impact is dependent on how the carbon precursor is transformed into the desired fullerenes by each of four synthesis methods of interest: pyrolysis with either tetralin (1,2,3,4-tetrahydronaphthalene) or toluene as feedstock and radio frequency (RF) or arc plasma with graphite as a feedstock. The carbon material flow for each, per 1 kg of C_{60} produced, is shown in Figure 12.

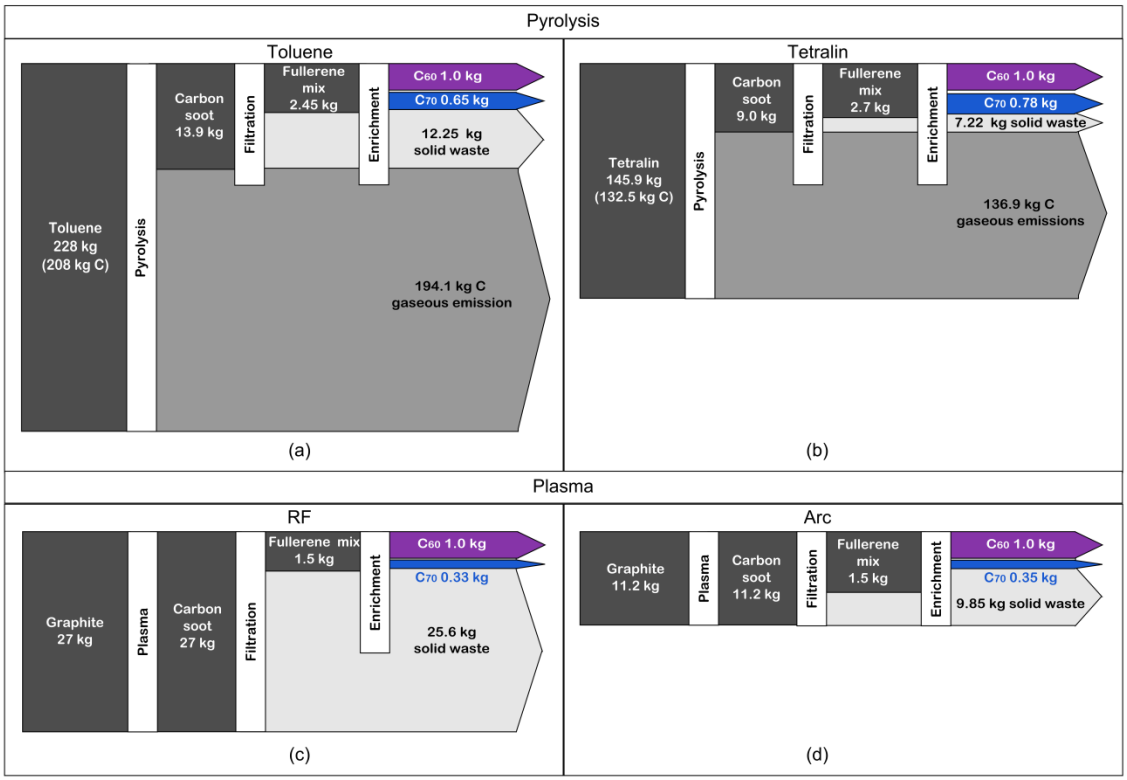

Figure 12: Material flow for the four synthesis methods (a) pyro-toluene, (b) pyro-tetralin, (c) RF plasma and (d) arc plasma.

As shown in Figure 12, pyro-toluene requires 228 kg of toluene to produce 1 kg of C_{60} with over 93% (194.1 kg) of the carbon being released as gaseous emissions. Since the fullerenes result from an incomplete combustion process, carbon emissions depend on the specific process conditions. In particular, conditions such as the temperature profile in the reactor, the ratio of oxygen, and precursor used, will influence the amount and nature of gaseous emissions. This is similar to what was recently measured for production of carbon nanotubes [46], and therefore cannot be simply estimated.

Using tetralin instead of toluene reduces the amount of solvent required to produce the same 1 kg of C_{60}. It is important to note that the amount of C_{70} in the fullerene mix depends on the hydrocarbon used as a carbon source. The amount of C_{70} that can be co-produced while synthesizing 1 kg C_{60} can be increased 20% when using tetralin instead of toluene. In comparison, plasma methods generate mainly C_{60}, and therefore, are not well suited for synthesis of C_{70}. In particular, RF plasma produces almost 60% less C_{70} than pyro-tetralin for the same 1 kg C_{60} product.

While the carbon flow is informative on the efficiency of the process in terms of products, wastes, and co-product yields, to adequately compare the various methods it is necessary to consider the full life cycle, including raw material production and energy requirement. Due to the unknown nature of carbon emissions that result from pyrolysis, it is not yet possible to fairly compare the four production methods using midpoint impact assessment categories (e.g., carbon footprint or human toxicity). Instead, this study calculates the embodied energy (the total of all direct and indirect energy inputs), to characterize the life cycle impact of fullerene production.

Previous work on estimating the life cycle energy of fullerenes has only considered direct process energy for plasma [42] or embodied energy of the carbon feedstock [42-43] for pyrolysis synthesis techniques, using in most cases outdated production methods. (A1). By comparison, this work quantifies embodied energy inclusive of all upstream inputs and is based on production methods published in the last five years. Figure 13a shows the embodied energy disaggregated by process step for all four synthesis methods. (Inventory data is available in A1). It is evident that pyrolysis methods have a much lower energy impact than plasma methods by nearly an order of magnitude.

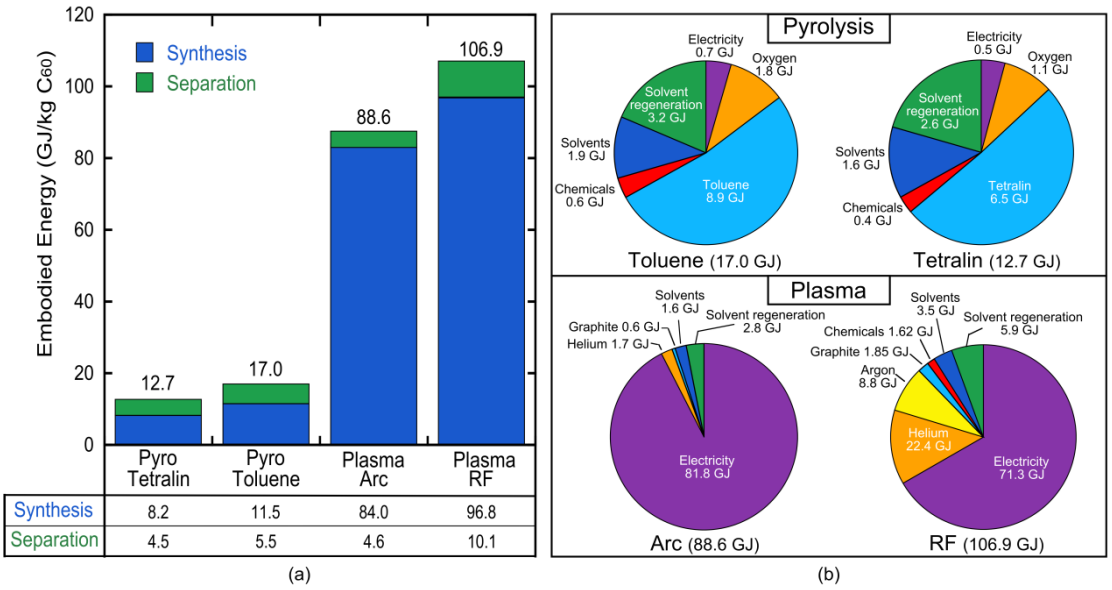

Figure 13: (a) Embodied energy of 1 kg of C_{60} after synthesis and separation, as produced by pyrolysis (tetralin and toluene) and plasma methods and (b) contribution of various components for the total embodied energy for each type of synthesis methods after fullerenes separation.

Previous estimates of the embodied energy for C_{60} produced using the same pyro-toluene process were 48% lower (8.8 GJ/kg) [43] than our current estimate (Figure 13). This discrepancy is due in large part to the more comprehensive system boundary used here (including direct and upstream energy inputs) for both the synthesis with pyro-tetralin

and separation steps required to obtain the separated C_{60} and C_{70} fullerenes. By including this level of detail, it becomes obvious that the separation step for pyrolysis methods cannot be neglected. As previously illustrated in Figure 12, the amount of fullerenes that can be extracted from the carbon soot is less than 30%. Due to the low solubility of fullerenes in *o*-xylene, a large amount of organic solvent is required. While most of the solvent can be regenerated, the energy associated with solvent production, solvent regeneration, and separation electricity increases the total embodied energy for pyro-toluene from 11.5 (after synthesis) to 17.0 GJ/kg C_{60} (after separation). Similarly, the separation step is significant for the pyro-tetralin process, as the embodied energy increases from 8.2 to 12.7 GJ/kg C_{60} with its inclusion.

When disaggregating the various contributors to the total embodied energy (Figure 13b), the carbon feedstock for pyrolysis is the largest component, but accounts for around 50% of the total embodied energy. The other part of the combustion reaction is the high purity oxygen required to improve the fullerene yield [47], which accounts for 10% of the embodied energy. These results suggest that studies that only include feedstock energy may underestimate the total energy intensity of fullerene production. Furthermore, the results are consistent with our findings from Figure 13a on the importance of including the separation stage. Figure 13b also shows that solvent production and solvent regeneration account for 30% of the embodied energy of fullerenes produced when using pyrolysis.

In the case of plasma synthesis, an updated set of techniques with improved yields for C_{60} were used as the reference (see A1). The overall embodied energy for arc is 88.6 GJ/kg C_{60} while it is 106.9 GJ /kg C_{60} for RF, which is similar to previously calculated values [42]. The direct electricity consumption is still the most important component and accounts

for up to 92% of the embodied energy of C_{60} produced using arc plasma. In the case of RF plasma, however, the electricity is 67% and the required argon and helium gases represent 29% of the total embodied energy. While the overall embodied energy might seem similar with previous "outdated" results (see A1), including details about all input materials allows identification of critical inputs where greatest resource reduction could be achieved and fair comparison between processes. The inclusion of plasma gases in the life cycle assessment makes RF plasma the most energy intensive technology, rather than the arc plasma method.

2. Purification

Synthesis and separation are only the first steps of functional fullerene production, as higher purity material is required for commercial applications. Therefore, the true embodied energy in a product is related to the solvents, chemicals, and electricity required to isolate the purified product. Based on the best-case synthesis scenario (pyro-tetralin), the impact of purification on the embodied energy of fullerenes is further illustrated in Figure 14, which shows how the embodied energy of C_{60} and C_{70} varies at different product stages.

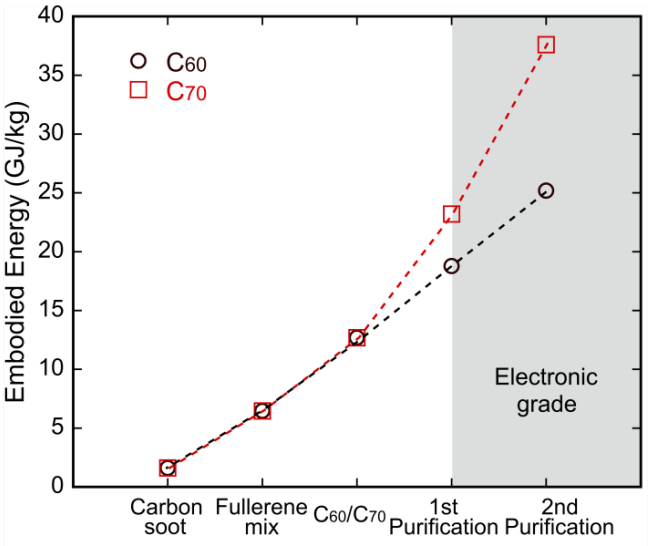

Figure 14: Embodied energy for C_{60} and C_{70} products as a function of product stage.

The grey region illustrates the typical purity onset required for electronic grade applications like organic solar cells. C_{70} is produced along with C_{60} in the carbon soot for each of the synthesis methods, albeit in ratios varying relative to the synthesis technique. As shown in Figure 12, the pyro-tetralin technique produces the largest ratio of C_{70}/C_{60}. Since C_{70} is more difficult to separate from the other higher order fullerenes than C_{60}, 2.6 kg of C_{70} after separation is required to produce 1 kg of high purity C_{70} (after 2nd purification) while only 1.7 kg of C_{60} is required for an equivalent amount of high purity material. The super-linear increase in embodied energy with purification is to be expected for fine chemicals [29], like modified fullerenes, intended for use in next-generation applications. The embodied energy is an indicator of the cost of a product and a similar trend in price can be observed for C_{60}, with typical price increases from \$31 to \$59/g from 1st to 2nd purification (See A1). For C_{70}, prices are significantly higher and increase from \$258 to \$338/g for the same purification steps, therefore indicating the increased difficulty in producing larger fullerenes. The purification steps double the embodied energy for C_{60} and triple it for C_{70}, making clear that both fullerene size and purity of the materials are essential specifications to estimate embodied energy of these nanomaterials.

3. Functionalization

While a high degree of purity is required for most electronic applications, in certain cases there is an additional need to modify the fullerene structure to increase utility. This is the case for fullerenes used in organic solar cells (Figure 10e), which need to have high purity to avoid impurity trap states, but also need to be modified to PCBM to increase solubility for solution processing and device viability. The additional embodied energy associated with each of the various chemicals, solvents, and solvent regeneration steps further increases the embodied energy up to 64.7 GJ/kg for C_{60}-PCBM; more than five-fold

greater than embodied energy calculated for C_{60} synthesized by pyro-tetralin. Although considerable research has utilized C_{60}-PCBM for organic solar cells, recent results show that C_{70}-PCBM can promote higher device efficiencies [48], thereby increasing interest in the larger fullerenes. Figure 15 illustrates the contribution from each component along the complete process required to produce either 1 kg of C_{60}-PCBM or C_{70}-PCBM. Due to the increased energy intensity associated with purification and the functionalization reactions, the embodied energy of C_{70}-PCBM is 90.2 GJ/kg as compared to 64.7 GJ/kg for C_{60}-PCBM. Therefore, each modified fullerene has a significantly different embodied energy, which in turn influences the embodied energy of the product in which they are ultimately incorporated. (Inventory results for various fullerenes are available in A1).

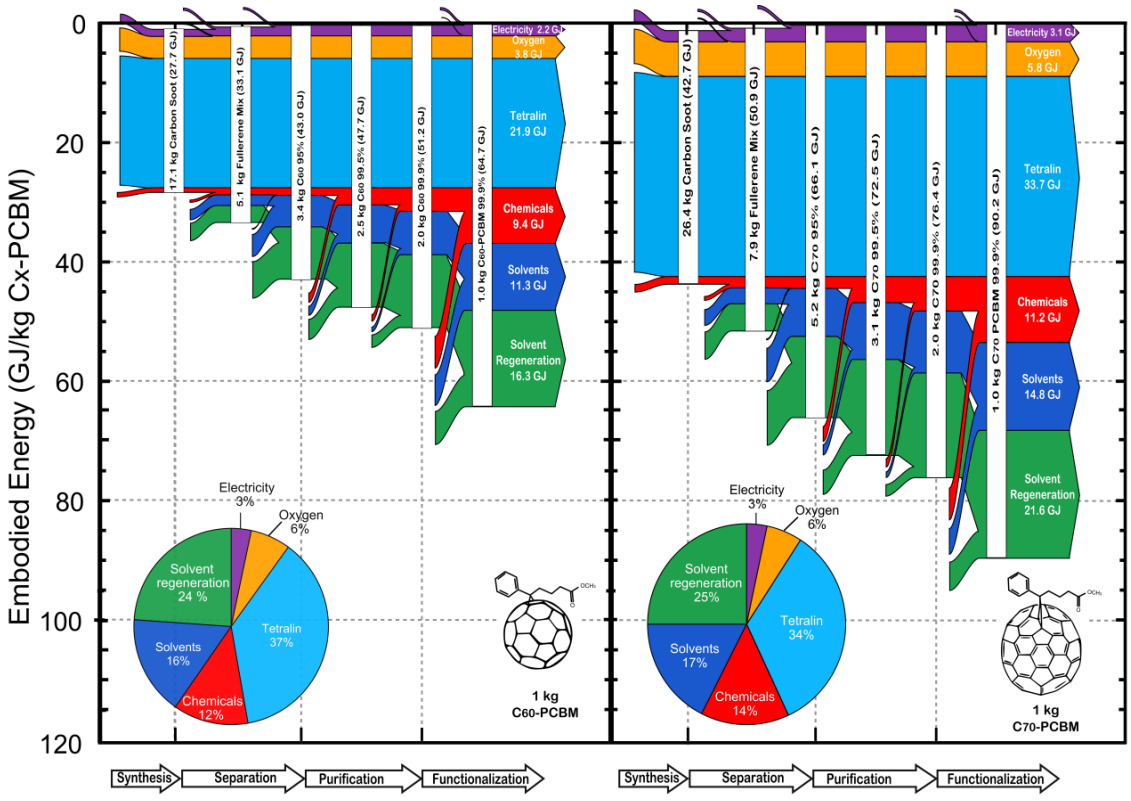

Figure 15: Energy flow diagram for production using the pyro-tetralin synthesis method of (a) 1 kg of C_{60}PCBM compared to (b) 1kg of C_{70}PCBM.

BROADER IMPLICATIONS

The cradle-to-gate assessment of fullerene embodied energy reported herein not only serves to characterize the environmental impact of these materials, but at a broader level also illustrates the methodological considerations essential for LCA studies conducted on nanomaterials. Regarding the first point, it has been shown here that pyrolysis techniques are a preferable alternative to plasma techniques on the basis of producing fullerenes with the lowest embodied energy. Although the scope of this study was limited to embodied energy, future work on the combustion products from pyrolysis can expand this analysis to include environmental or health impacts such as global warming potential and carcinogenicity, all of which may change as a function of synthesis conditions.

This work also illustrates the impact of purification and modification of fullerenes on the embodied energy of a specific product for electronic applications. Each process step increases the amount of direct energy inputs, but also leads to material losses that require additional raw materials. For example, using the embodied energy of C_{70} after separation rather than after modification as C_{70}-PCBM for organic solar cells would result in underestimating the impact of C_{70}-PCBM production by 85%. Such a knowledge gap has been addressed here by broadening the range of inputs in the synthesis reaction as well as considering the impact of purification and functionalization, which allowed differentiation in the embodied energy of various fullerenes products. This points to an opportunity for process innovation to increase yield and decrease solvent usage in each additional material processing stage.

The embodied energy of all fullerenes are an order of magnitude higher than most common chemicals, and therefore, are likely to influence the embodied energy of the

product they will be used in, even though they might only represent a small fraction of its total mass. For example, an aluminum/C_{60} composite has been developed for higher strength applications [49] where 5% weight of C_{60} is added to an aluminum matrix. Considering the range of embodied energy for C_{60} after separation to be between 12.7 and 106.9 GJ/kg C_{60} (Figure 13a), the embodied energy of the aluminum will increase from 137 MJ/kg [50] to a minimum of 765 MJ/kg, and could reach 5475 MJ/ kg for the composite, if fullerenes were synthesized using RF plasma. In the case of organic solar cells, while fullerenes are undeniably essential for charge transport, they are only required in small quantity compared to other materials.

For a typical organic solar cell (P3HT:PCBM), the fullerene would only account for 0.3% of the total weight according to previous work [51] and would be excluded based upon recent reports using mass based cut-off rule [52-53]. However, in the case of the active layer for an organic solar cell, the addition of C_{60}-PCBM 99.9% (pyro-tetralin) to the polyhexylthiophene will increase the polymer embodied energy from 160 MJ/kg [42] to 32, 400 MJ/kg. Scaling this increase up to the level of the full device, fullerenes would then represent up to 19% of the total embodied energy of the solar cell [51]. It is clear that the high embodied energy of nanomaterials will have a significant impact on the final product embodied energy, and therefore, cut-off rules based on mass should not be applied routinely to simplify life-cycle assessment of products containing nanomaterials.

V. LIFE CYCLE ASSESSMENT OF ORGANIC PHOTOVOLTAICS

Using the results from Chapter IV, the life cycle assessment (LCA) of various polymers, small molecules, single and multi-junction photovoltaics, representing the best devices efficiencies over the last five years is performed. The number of solar cells devices analyzed in the present work using LCA increases from 1 to 26. While LCA is useful to compare current technologies, it can also be used to compare alternative solutions. As an example, the environmental impact of water-soluble organic photovoltaics is compared to current technologies in section 5.2. The detailed information collected to generate the life cycle inventory can also be useful to estimate the cost of the technology as shown in section 5.3. Additional information regarding input-output for chemicals used in the life cycle assessment as well as supporting system information are available in A2 and A3, respectively.

5.1. Cumulative Energy Demand for Small Molecule and Polymer Photovoltaics

INTRODUCTION

Since the maximum theoretical efficiency of a single junction organic photovoltaics with a 1.5 eV bandgap is 13% [16], there is an increasing interest to pursue a multi-junction approach where two or more devices are built on top of each other to absorb a larger portion of the solar spectrum. While this approach can significantly improve device power efficiency, it also increases the amount of processing and amount of material in a single photovoltaic cell. A second approach is the development of low bandgap polymer, which allows the absorption of a larger portion of the solar spectrum compared to polythiophenes derivatives. The most successful method so far has been through the use of block copolymers, which combines one electron-rich monomer (fluorene, carbazole, dibenzosiloe,

benzodithiophene, etc.) and one electron-deficient monomer (benzodiathiazole, diketopyrrolopyrrole,etc.) [54] which has produced an efficiency of 7.7% [55]. Although significant progress in device efficiency is underway, there has been minimal effort to assess potential negative impacts associated with their large scale production. It is generally cited that organic photovoltaics have low environmental impact, or have the potential to be inexpensive to produce [56-57] since they take advantage of solution processing. For example, fullerenes are the most common acceptor molecule in organic photovoltaics, and it has been suggested that they are an environmentally-friendly material because of being made only of carbon [58]. However, as shown in Chapter IV, fullerene production is energy intensive [59], and will directly influence the cumulative energy and environmental impact of organic photovoltaics. To evaluate the impact of OPV, life-cycle assessment (LCA) can be used to evaluate the total environmental impact of a product from raw material extraction to end-of-life. The first step requires the compilation of all materials and energy input to create the life-cycle inventory (LCI). This inventory is then used to characterize various impacts such as human health, ecosystems, climate change and resource uses. While there have been life cycle studies on basic bulk heterojunctions made of polyhexylthiophene and [6,6]-phenyl-C61 butyric acid methyl ester (P3HT: C_{60}PCBM) as they were first developed [42, 60, 61] these reports underestimated the fullerene contribution.

The present work applies LCA to OPV to compare products, materials and processes during the development process which leads to solutions with lower environmental impact as well as faster reduction in manufacturing cost. This work is unique from previous studies in that it compares small molecules and polymer photovoltaics and examines various methods used to increase power conversion efficiency such as the use of thermal

treatment, interface layers, low bandgap polymer and the multi-junction approach. The most recent device architectures are considered and updated embodied energy calculation for newer and organic photovoltaic materials is calculated. In addition, the present LCA is performed to determine if the additional processing steps and material used to create a multi-junction photovoltaic are a sustainable tradeoff with the gain in device efficiency. Another outcome of the present study is to quantify the energy associated with the synthesis of low bandgap polymers which will likely be significantly higher than the original P3HT. Overall, the results of this work provide a framework to identify critical steps in the organic photovoltaic life cycle where the greatest reduction in resource and emissions could be achieved.

METHODOLOGY

The LCA results are obtained from analysis using SimaPro® based upon existing inventory data obtained from available databases and previously published primary literature. Inventory data for chemicals not available in databases are estimated using default values and stoichiometric reactions according to previously published guidelines [28-29]. The life cycle impact of OPV is performed using the specific data from the life cycle of fullerene production, semiconductor polymer, small molecule, and interfacial material processing. Different donor/acceptor combinations are examined in conjunction with the reported efficiencies and specific processing conditions. The life cycle assessment characterization is done using the cumulative energy demand (CED) method using the Ecoinvent electricity profile form the United States. CED has been shown to be correlated with most environmental indicators [62-63] and since comprehensive data related to environmental impact, in particular emissions in term of toxicology and releases, are rather

scarce in the current inventories, it often provides a better estimate of the environmental impact and informs indirectly on the expected costs.

1. Goal definition and scoping

The primary goal of this LCA is to compute the CED of various organic photovoltaic technologies, including single junction small molecule and polymer photovoltaics as well as the multi-junction counterparts which are responsible for the rapid increase in device efficiency. A secondary goal is to examine the effect of specific processing conditions such as the use of thermal treatments, interface layers, low bandgap polymers and the type of heterojunction approach. The functional unit of this study is the CED to produce a power of 1 watt-peak (CED/Wp). As illustrated in Figure 16, the substrate (ITO coated PET), the silver contact and encapsulation constitute the background system. The focus of this work is the material used in the active and interface layers as well as the process energy associated with the deposition and annealing of those layers. Devices illustrated in Figure 16, represent the most complex case, where interfacial layers are used between each active layer. Two types of interfacial layers are used: the electron blocking layer (EBL) and the hole blocking layer (HBL). As illustrated in Figure 16, there is one active layer for polymer photovoltaics but in the case of small molecules, the active layer is actually made of multiple layers to create either planar or planar-mixed heterojunctions.

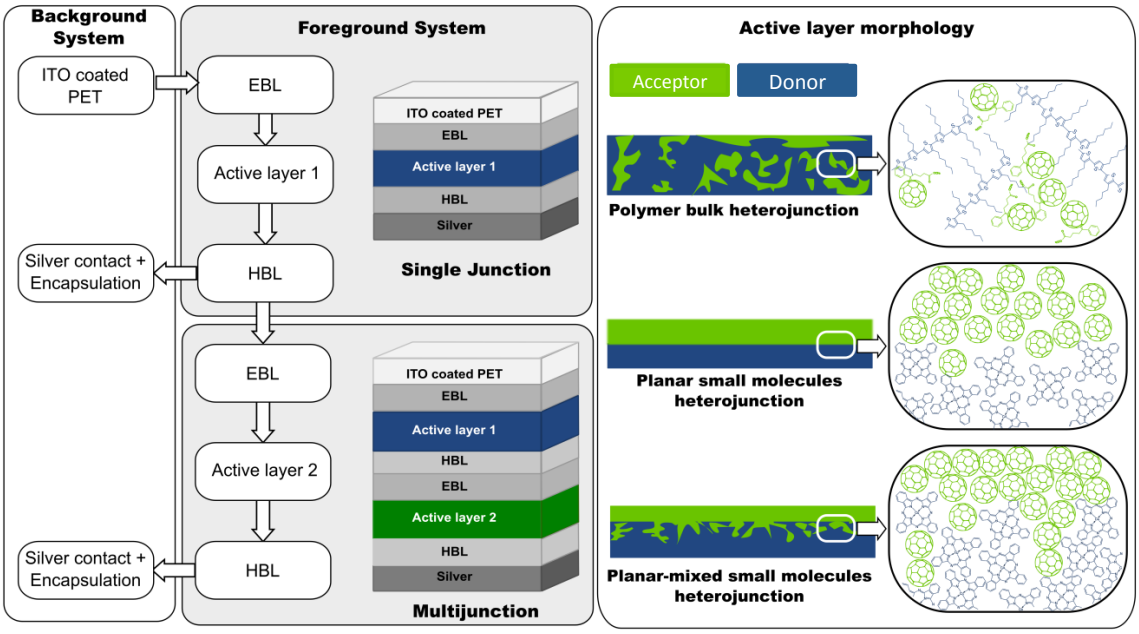

Figure 16: Overview of the process flow for the production of organic photovoltaics and active layer morphologies for polymer and small molecule photovoltaics.

2. Embodied energy of OPV materials

Organic photovoltaics (OPV) are made of high purity materials which comprise newly synthesized materials (e.g. nanomaterials, novel absorbing dye conjugates, and block co-polymers) with no existing life cycle inventory (LCI) data. Therefore, the first step is to calculate the embodied energy of the materials on a gravimetric basis using life cycle assessment from cradle to gate. In general, OPV materials fall into 3 categories: electron accepter (e.g. modified fullerenes), donor (polymer and small molecule), and interfacial materials (HBL and EBL). Fullerenes are the most common acceptor material and are used directly with small molecules or after functionalization for improved solubility in polymer photovoltaics. The embodied energy of fullerene production was previously calculated [59] and will be included in the present work. In addition to methanofullerene derivatives (PCBM and *bis*-PCBM), the impact of an alternative indene derivative recently synthesized,

ICBA [64], is calculated for the first time since it has produced a higher efficiency (6.5% vs. 5.1%) as a replacement for C_{60}PCBM with P3HT [65].

Another factor in the recent increase in device efficiency can be attributed to the development of suitable polymers with bandgaps that extend from the visible into the near-infrared. The embodied energy of polyhexylthiophene (P3HT) [66] is compared to two types of low bandgap block copolymers: a polybenzodiathiazole (PTCDTBT) [67] and a poly(benzo[1,2-b:4,5-b']dithiophene)s (PTB7) [68]. These two block copolymers are selected based upon the demonstrated device efficiencies of 6.1 % and 7.4% for PTCDTBT and PTB7, respectively.

Two classes of small molecules are compared, namely phtahlocyanines and squaraines. Phthalocyanines (Pc) can be synthesized by reacting the desired metal chloride with either phthalonitrile (to produce ZnPc, InClPc, CuPc, PdPc, SubPc) or phthalic anhydride (to produce AlPcCl) [24, 25]. The original Pc synthesis methods required extensive high temperature reactions (i.e. > 180 °C for 4 hours), and considerable amounts of solvent and catalyst. The newer methods developed largely for electronic applications, employ high energy microwave reactors which allow for solvent-free reactions, while producing a higher yield of Pc in a shorter amount of time and lowering the amount of required purification steps [24]. Although Pc has shown tremendous potential, it is typically processed using high vacuum equipment; therefore, a second type of small molecule relevant for OPV is one that can be solution-processed for device fabrication. The most successful to date based upon device efficiency is the squaraine derivative 2,4-bis[4-(N,N-diisobutylamino)-2,6-dihydroxyphenyl]squaraine (SQ) produced through condensation of an aniline intermediate with squaric acid [26].

Various interfacial materials are used to improve the electrode contacts in order to enhance charge collection of electrons and holes in organic photovoltaics. For organic photovoltaics, the material inventory for solution processed TiO_x used as a HBL [69] is calculated in the present study, while previous published values are used for PEDOT:PSS, a common EBL [42] and ZnO an alternative EBL [61]. In the case of small molecules, the CED of bathophenanthroline (BPhen) [70], bathocuproine (BCP) [70] both HBL and MoO_3, an EBL [71] are each calculated.

3. Photovoltaics

Using the material cradle-to-gate life cycle inventory, the cumulative energy required to fabricate photovoltaics with 1 watt-peak generation (CED/Wp) is calculated. The focus of this work is the active layer and interface layers, therefore, the other components are assumed constant for a given photovoltaic area. Table 1 provides information about the reference values for the background system. The energy required for evaporation is calculated for each type of photovoltaic structure considering the specific conditions (i.e. material, thickness and complete structure) and is available in the SI. The energy required for annealing is adjusted according to the specific temperature and duration, based on previous study of large area photovoltaics produced through a roll-to-roll process [61]. Since reported device areas are generally smaller than 0.2 cm^2 for both polymer and small molecule photovoltaics, the efficiency of the solar panel is assumed 20% lower than the best published efficiency. The area is adjusted to 85% to account for the non-active area of a solar panel.

Table 1. References and values for materials and energy commodities of the background system used in the inventory analysis (adjusted for 85% active area)

Stage	Details	Embodied Energy (MJ/m^2)	Reference
ITO coated PET	Polyethylene terephthalate film (130 um thick)	16.9	[72]
	Sputtering 180 nm ITO (including production ITO)	68.3	[73]
Contacts Printing	Silver	4.9	[61]
	Screen-printing	9.9	[61]
Encapsulation	PET Covers + epoxy	11.7	[61]
	Lamination energy	0.1	[61]

3.1 Sensitivity Analysis of OPV Fabrication

Sensitivity analysis is performed by varying single parameter values over realistic ranges for the embodied energy of fullerenes, the amount of material used in the active layer and the process energy for device processing. Details about the base case assumptions and the range of values considered in the best and worst-case scenarios are given in Table 2. There are several prevalent methods to synthesize fullerenes, including plasma techniques (arc and RF), as well as pyrolysis of carbon precursors [(toluene and 1,2,3,4-tetrahydronaphthalene (tetralin)]. The main production method for fullerenes is pyrolysis, [74] so accordingly the base case scenario assumes 90% of the fullerene mix from pyrolysis with an equal weighting between carbon precursors (see Table 2). The best case scenario assumes that all fullerenes are produced from pyro-tetralin, which was previously reported to be the production method with the lowest embodied energy [59]. In comparison, the worst case scenario increases the proportion of fullerenes produced from the two plasma methods from 10 in the base scenario to 20% of the total mix.

The amount of polymer in the base case scenario is 0.3 g/m^2 to produce a 100 nm polymer layer. It is adjusted based on the optimal layer thickness for various photovoltaics

assuming 85% active area and 10% loss according to optimized conditions [61]. For the polymer as well as all the other variables in the sensitivity analysis, the best and worst case scenarios correspond to ±25% of the base case scenario.

The best small molecule material utilization efficiency reported is 50% and corresponds to an optimized organic vapor phase deposition method [75]. Previous LCA studies only considered aluminum evaporation and assumed material utilization from 16.7% [61] to 100% [42]. In this case, 40% is used as the base case scenario and the best and worst are adjusted by 10%, accordingly. The base case scenario for slot-die coating is based on previous values for large area production of organic photovoltaics [61] while the energy consumption for evaporation is based on actual measured values, and is adjusted using an energy consumption factor of +/- 25%.

Table 2: Scenarios for sensitivity analysis.

	Best	Base	Worst
Fullerene mix % (pyro-tetralin / pyro-toluene/ Arc Plasma / RF Plasma)	100/ 0/ 0 / 0	**45 / 45 / 5 / 5**	40 / 40 / 10 / 10
Polymer usage per layer (g/m²)	0.225	**0.3**	0.375
Small molecules material utilization efficiency (%)	50	**40**	30
Slot-die coating (MJ/m²)	0.975	**1.3**	1.625
Evaporator energy consumption factor	0.75	**1**	1.25

3.2 Polymer photovoltaics

Polymer photovoltaics, are made by mixing the donor and acceptor materials to form a bulk heterojunction in between electrical contact materials. Due to the low mobility of the semiconducting material, the maximum thickness of the device is generally between 50-200 nm, therefore limiting the total amount of material being used. The initial improvement from 3.5% to 5% using the same P3HT: C_{60}PCBM combination was a result of better processing conditions such as thermal annealing and solvent optimization as well as

addition of interface layers to improve charge collection [76]. Specific solvents, annealing conditions, and interface materials can significantly influence the analysis results. Figure 17a shows the structure of a typical single junction photovoltaic where the donor: acceptor bulk heterojunction is changed using the various conditions described in Figure 17b. All photovoltaics use PEDOT:PSS as an EBL which is commonly annealed at 150°C for 10 minutes [76]. For slot-die coating, the amount of solvent is calculated using a polymer concentration of 1% weight in the coating solution. The impact of using TiOx as a HBL is also compared for P3HT and PCDTBT-based devices.

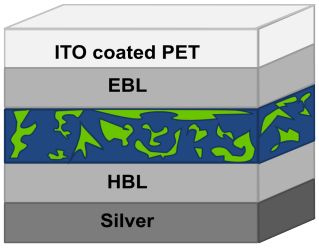

(a)

Donor	Acceptor	D/A ratio	η (%)	Solvent	HBL (nm)	Annealing	Ref
P3HT	C_{60} PCBM	1 / 0.8	5.1	CB		150 °C (30 min)	[77]
	C_{60} PCBM	1 / 0.8	5.0	CB	TiOx (30)	150 °C (10 min)	[78]
	C_{60} bisPCBM	1 / 1.2	4.5	o-DCB		110 °C (5 min)	[79]
	C_{60} ICBA	1 / 1	6.5	o-DCB		150 °C (10 min)	[65]
	C_{70} ICBA	1 / 1	5.6	o-DCB		150 °C (10 min)	[80]
PSiF-DBT	C_{60} PCBM	1 / 2	5.4	CB		-	[81]
PTB1	C_{60} PCBM	1 / 1	4.8	o-DCB		-	[82]
	C_{70} PCBM	1 / 1.2	5.3	o-DCB		-	[82]
PCDTBT	C_{70} PCBM	1 / 2	5.5	o-DCB		-	[83]
	C_{70} PCBM	1 / 4	6.1	o-DCB	TiOx (10)	70 °C (60 min) + 80 °C (10 min)	[84]
PIDTBT	C_{70} PCBM	1 / 3	6.3	o-DCB		-	[85]
PTB7	C_{70} PCBM	1/ 1.5	7.4	o-DCB		-	[86]
PBDTTT	C_{70} PCBM	1 / 1.5	7.7	CB		-	[55]

(b)

Figure 17: (a) Schematic of a single OPV bulk heterojunction between electrical contact layers and (b) best devices efficiencies reported for various donor/acceptor combinations with and without hole blocking layer (HBL). The solvent is in reference to CB is chlorobenzene and o-DCB: is *ortho*-dichlorobenzene.

The impact of a solution processed multi-junction photovoltaic is compared for two polymer bulk heterojunction multi-junction devices described in Figure 18b.

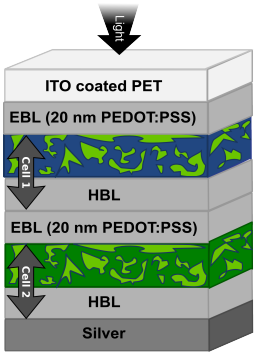

(a)

	PCDTBT: P3HT		PFTBT : pBBTDPP2	
η (%)	6.5		4.9	
Ref.	[87]		[88]	
	Cell 1	Cell 2	Cell 1	Cell 2
D/A	PCDTBT: C_{60}PCBM	P3HT: C_{70}PCBM	PFTBT:C_{60}PCBM	pBBTDPP2: C_{60} PCBM
D/A ratio	1 / 3.6	1 / 0.7	1 / 4	1/2
Solvent	CB	C	CB	C /oDCB (1 :1)
Active layer thickness (nm)	130	170	180	125
HBL (nm)	TiOx (20)	TiOx (20)	ZnO (30)	
Annealing	HBL (10 min 80 °C) EBL (10 min 140 °C)	HBL (10 min 80 °C) Device (5 min 160 °C)	HBL (10 min 80 °C) EBL (10 min 140 °C)	

(b)

Figure 18: (a) Schematic of a multi-junction OPV bulk heterojunction between electrical contact layers and (b) device structures considered based on best reported efficiencies and processing conditions.

3.3 Small molecule photovoltaics

Small molecule photovoltaics use various combinations of thin heterojunction and diffuse heterojunction structures prepared by deposition of multiple materials. The most common type of small molecule employed is phthalocyanines which are deposited with C_{60} using thermal evaporation under vacuum, and typically without an EBL. The evaporation process allows the molecules to self-organize, therefore, increasing the carrier mobility [26] compared to polymers such as P3HT which requires annealing to increase long range order.

Recently, the solution-processable squaraine derivative 2,4-bis[4- (N,N-diisobutylamino)-2,6-dihydroxyphenyl]squaraine (SQ) [26] has been synthesized and used as an alternative to vacuum processed phthalocyanines devices. SQ photovoltaics have a slightly different device structure since they require the evaporation of a 8 nm MoO_3 EBL prior to the deposition of the SQ using solution processing. The C_{60} and HBL layers are evaporated prior to thermal annealing at 110 °C for 20 minutes [26].

Details about all single junction small molecule photovoltaics being analyzed are available in Figure 19 a-b for planar and planar-mixed heterojunctions. Multi-junction structures as illustrated in Figure 19c are made by successive evaporation of each layer. For small molecule multi-junction, device efficiency has been shown to increase from 3.6 % for a single junction chloroboron subnaphthalocyanine (SubPc) to 5.2% by adding a chloroboron subphthalocyanine (SubNc) device [89].

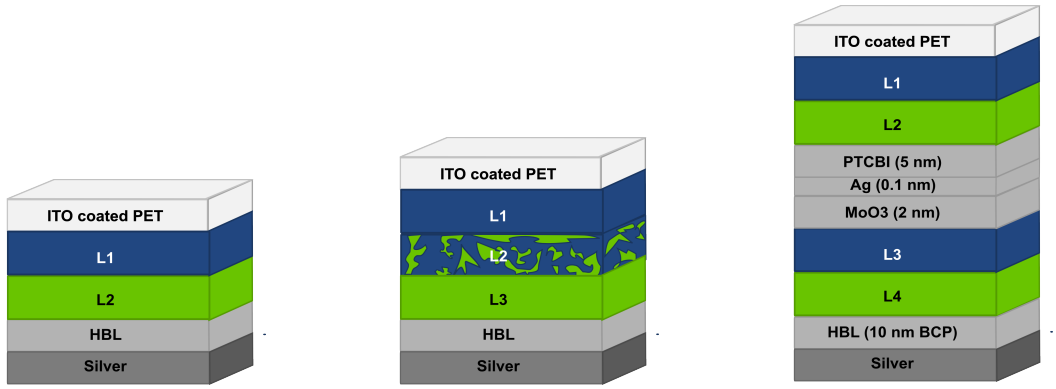

(a) (b) (c)

Donor	L1 (nm)	L2 (nm)	L3 (nm)	L4 (nm)	HBL (nm)	η (%)	Ref.
Single junctions							
AlPcCl	AlPcCl (24)	C_{60} (40)			BCP (10)	3.0	[89]
ClInPc	ClInPc (20)	C_{60} (40)			BCP (10)	3.3	[90]
SubNc	SubNc (7.5)	C_{60} (40)			BCP (10)	3.5	[89]
SubPc	SubPc (22)	C_{60} (35)			BCP (10)	3.6	[89]
ZnPc	ZnPc:C_{60} (1:1) (35)	C_{60} (25)			Bphen (7)	3.9	[91]
ZnPc	PdPc (15)	ZnPc:C_{60} (1:1) (20)	C_{60} (30 nm)		BCP (15)	3.7	[92]
CuPc	CuPc (20)	C_{60} (40)			BCP (10)	3.7	[93]
CuPc	CuPc (15)	CuPc:C_{60} (1:1) (10)	C_{60} (35 nm)		BCP (10)	5.0	[93]
SQ	SQ (6.2)	C_{60} (40)			BCP (10)	4.6	[26]
Multi-junctions							
SubNc + AlPcCl	AlPcCl (16)	C_{60} (20)	SubPc (16)	C_{60} (20)	BCP (10)	4.1	[89]
SubNc + SubPc	SubNc (7.5)	C_{60} (16)	SubPc (16)	C_{60} (20)	BCP (10)	5.2	[89]

Figure 19: Schematic of (a) planar (b) planar-mixed and (c) planar multi-junction small molecules devices and (d) structure considered for single and multi-junction small molecules photovoltaics highlighted in grey represent the planar-mixed devices.

RESULTS AND DISCUSSION

1. Embodied energy of OPV materials

1.1 Fullerenes

The most common acceptor molecules for organic photovoltaics are fullerenes, either in their native form for small molecule photovoltaics or structurally modified (e.g. PCBM, ICBA, etc.) for polymer photovoltaics. In the recent analysis, the fullerene embodied energy from four production methods was detailed [59], and has been summarized in Figure 20 for the three different sensitivity scenarios described in Table 2. As illustrated, C_{70} structures (both native and functionalized) have consistently higher embodied energy than C_{60} ones. There are also significant differences between the modified and native fullerenes, where the "Best" case PCBM scenario for each structure is higher than the worst case native one (e.g. C_{60}PCBM is s more than double the embodied energy for pure C_{60}). New analysis calculation in the present work evaluates the C_{60} and C_{70} indene bisadduct (ICBA)[64]. The comparison between PCBM and ICBA derivatives shows that the ICBA derivatives have a dramatically lower embodied energy, on the order of 40% less for both C_{60} and C_{70} structures. Such a reduction is attributed to a simpler reaction scheme for ICBA derivatives based upon fewer chemicals required during synthesis and processing which results in less embodied energy to produce.

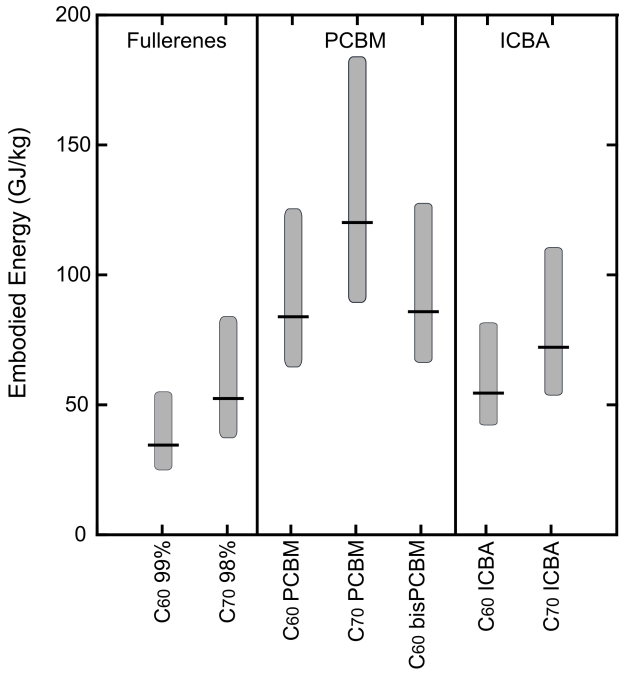

Figure 20: Embodied energy of fullerenes and fullerene derivatives used in organic photovoltaics where the grey bar spans the best and worst case scenarios and the line, represents the base case.

1.2 Polymer

The semiconducting polymers used in OPV require multiple steps to build the specific monomer prior to the final polymerization stage. This is illustrated Figure 21 for three types of semiconducting polymers commonly used to achieve the highest efficiencies to date. Increasing the number of steps from 4 for P3HT to 11 for PTB7 increases the embodied energy by 2.5. The details of the synthesis and calculations are provided in the Supporting Information. In comparison, many common polymers in the chemical industry have 1-2 steps, resulting in an embodied energy typically less than 20 MJ/mol.

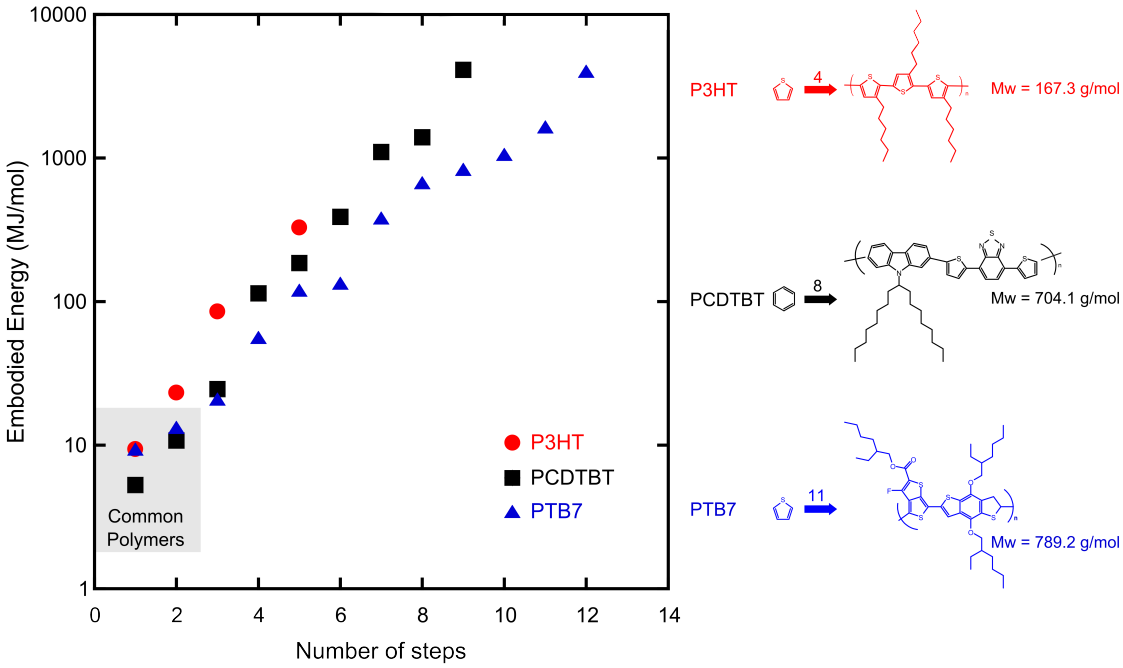

Figure 21: Embodied energy of 3 types of semi-conducting polymer used in organic photovoltaics as a function of synthesis stage.

However, it is important to recognize that even with the additional energy required for multiple synthesis steps, the total embodied energy of each of the commonly used semiconducting polymers for OPV is 1-2 order of magnitude lower than for fullerenes, ranging from 1.9 GJ/kg for P3HT to 5.8 GJ/kg for PCDTBT. It is evident at this stage of the analysis, that since similar amounts of polymer and fullerene are used in an organic photovoltaic, the fullerene embodied energy will dominate the active layer impact.

1.3 Small molecules

Each of the phthalocyanine small molecules has 2 synthesis steps and there is a small contribution in each case to the type of coordinated metal atom present. The details of the synthesis and calculations are available in the Supporting Information. The embodied energy is nearly the same between the small molecules examined, except for PdPc due to the scarcity of palladium (see **Figure 22**). The comparison between SQ and Pc small

molecules shows very similar embodied energy values, thus indicating that any difference in cumulative energy demand from the photovoltaic device will largely be from the type and extent of processing methods employed.

1.4 Interface materials

There are several prevalent interfacial materials being used to improve charge collection in organic photovoltaics either in a single junction device or as a junction between the two devices in a tandem photovoltaic. Figure 22 summarizes the embodied energy of each interface material used in this work. In the case of solution processed interface materials for polymer photovoltaics like TiO_x, ZnO, and Pedot:PSS, the major component is the solvent since dilute solutions (15-30 mg/mL) are necessary to achieve a layer less than 20 nm during deposition. TiO_x has a higher embodied energy than the other two materials since it uses a sol-gel solution during synthesis which needs to be refluxed with a ligand [84]. Comparison of BCP and BPhen shows similar embodied energy since they have similar structure and require the same number of synthesis steps. Overall, the interfacial layers have the lowest impact of typical active materials in the device, and since they are used in small quantities, they are unlikely to have a dominant contribution.

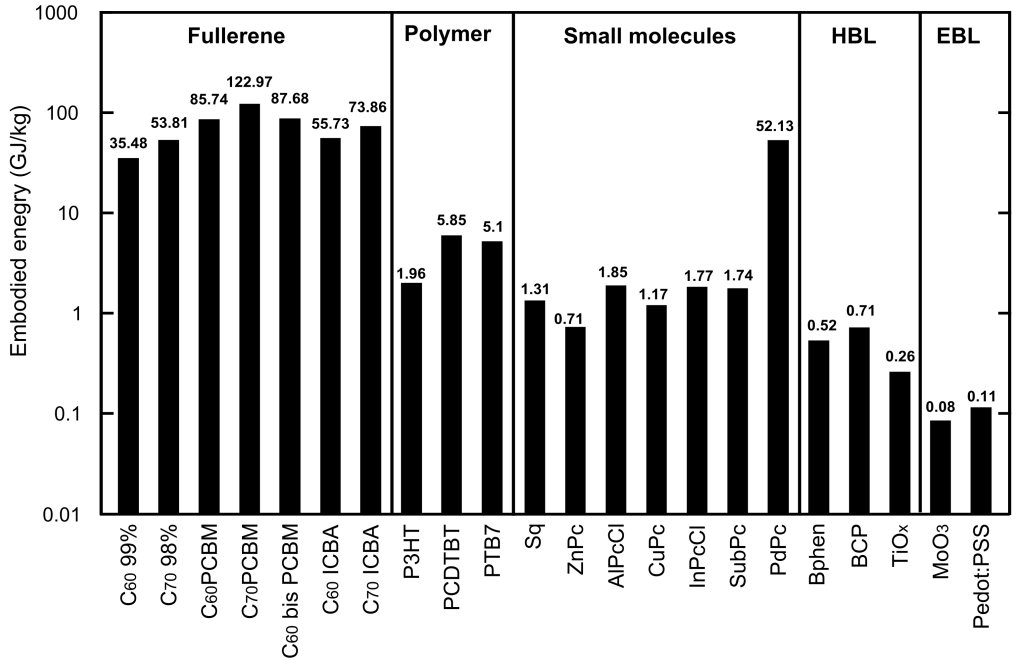

Figure 22: Embodied energy for all types of material considered in this work.

2. Single junction organic photovoltaics

The CED for single junction photovoltaics is calculated using the embodied energy of the individual materials according to the processing conditions described in Figure17b for polymer and Figure19b for small molecule photovoltaics. Figure 22 clearly illustrates that fullerenes have the most significant impact compared to other materials, and so the relative mass contribution in the device design will directly influence the device CED. Small molecules and semiconductor polymers have similar embodied energy between them, except for PdPc, so the nature of processing conditions will also impact the device CED. Figure 23 summarizes the CED for both polymer and small molecule photovoltaics as a function of materials, processing, and other components. In general, the CED spans the same magnitude of 3-6 MJ/Wp for both cases. Also, the CED shows a trend of decreasing value with increasing device efficiency. The CED of small molecule devices is on average slightly higher than polymer devices, but this is largely due to the lower device efficiency for

reported measurements. In general, if the efficiency is lower, it increases the contribution from the background system (substrate, contacts and encapsulation, etc.) which is required to produce equivalent peak power, thus increasing the impact.

Another apparent difference between the polymer and small molecule photovoltaics is in the major contributors. The polymer devices show material contributions dominating the processing conditions, whereas the opposite trend is true for small molecule devices where it is more balanced. As an example, the total thickness of small molecule photovoltaics is lower (<60 nm) and these structures utilize pure C_{60}, which has a dramatically lower embodied energy than the modified fullerenes in polymer devices. In addition to the higher impact fullerene material, polymer photovoltaics require a thicker layer (e.g. 80-250 nm), which necessitates an increased material requirement using, modified fullerenes and polymers. Ultimately, the differences in device design present an interesting tradeoff where the overall CED is similar between organic approaches. These results can also influence the discussion between the research community over the respective merits of each approach.

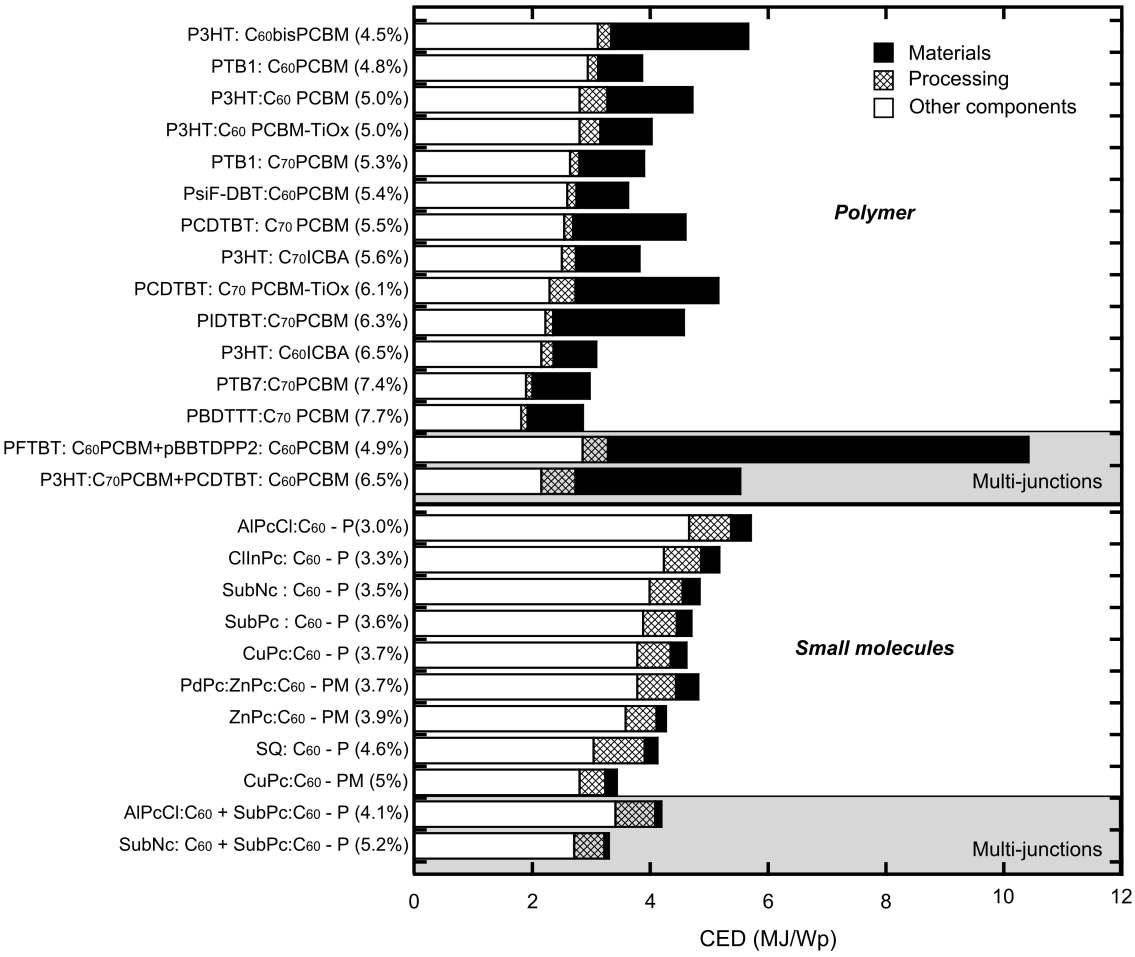

Figure 23: Cumulative energy demand (CED) for all organic photovoltaics considered in this work. For small molecule P refers to planar and PM, planar-mixed device structures.

For small molecules photovoltaics, various approaches have been explored to increase device efficiency. One of the most popular is layer optimization by controlling the successive evaporation of single material layer and mixed heterojunction material, such as in the case of the 3.9% efficient ZnPc/C_{60} photovoltaic [91]. An alternative approach is to use a thin layer of a different material absorbing in a different region of the spectrum and also acts as an EBL. For example, in the case considered here, 15 nm of palladium phthalocyanide (PdPc) is evaporated prior to deposition of the ZnPc/C_{60} photovoltaic. Because PdPc has much higher embodied energy than other small molecules (Figure 22),

this thin layer is enough to affect the total impact of the materials. As shown in Figure 23 the CED for the device increases compared to similar device architectures with lower efficiency. The optimization of layers for small molecules seems to be the most successful approach to reduce the overall impact of small molecules. For example, this is evident with CuPc where a typical planar junction yields an efficiency of 3.7%, but use of a planar mixed heterojunction approach increases the efficiency to 5% for the same total device thickness. From a CED standpoint, this corresponds to more than a 25% reduction in energy/Wp even when evaporation energy is increased by 5% due to the layer sequence.

A more detailed breakdown of the relative contributions from each material component on the overall CED for the highest efficiency organic photovoltaics and most prevalently reported P3HT:C_{60}PCBM device is shown in Figure 24. Details about other devices considered in this work are available in the SI including the material inventory. The largest contribution is the ITO sputtering onto the corresponding substrate material (i.e. PET) and the electrical contacts with encapsulation. An important observation is that there are opportunities to develop alternative transparent conductive electrode substrates with less embodied energy, which would dramatically reduce the overall CED for all organic photovoltaics further. Figure 24 a-b also illustrates the relative impact of various active material components from the most common P3HT:C_{60}PCBM device to the highest efficiency polymer photovoltaic made using the block-copolymer PBDTTT.

In both polymer photovoltaics, the major material contributor is the electron acceptor. It's importance increase with increasing device efficiency because larger amount of larger fullerenes are being used. There is a small increase in the direct contribution from a block-copolymer compared to the P3HT, but it is actually an improvement when

considering all other factors. The block copolymer has a lower bandgap with higher absorption coefficient that allows for a thinner layer (80-100 nm compared to 150-200 nm for P3HT) and higher efficiency which reduces the amount of material required. In addition, optimal polymer chain organization can be obtained by solvent optimization with the copolymer, which eliminates the need for post-processing annealing treatment compared to P3HT, thereby reducing the contribution from annealing even further. In both polymer cases, the solvent shows minimal contribution on the overall CED, and is not a motivating influence towards "greener" polymer photovoltaic manufacturing from an energy standpoint, although it may be a significant component on a mass basis during fabrication. In contrast, it is a direct contributor compared to both fullerenes and polymer which both have a much higher impact, but their impact is not visible during device fabrication.

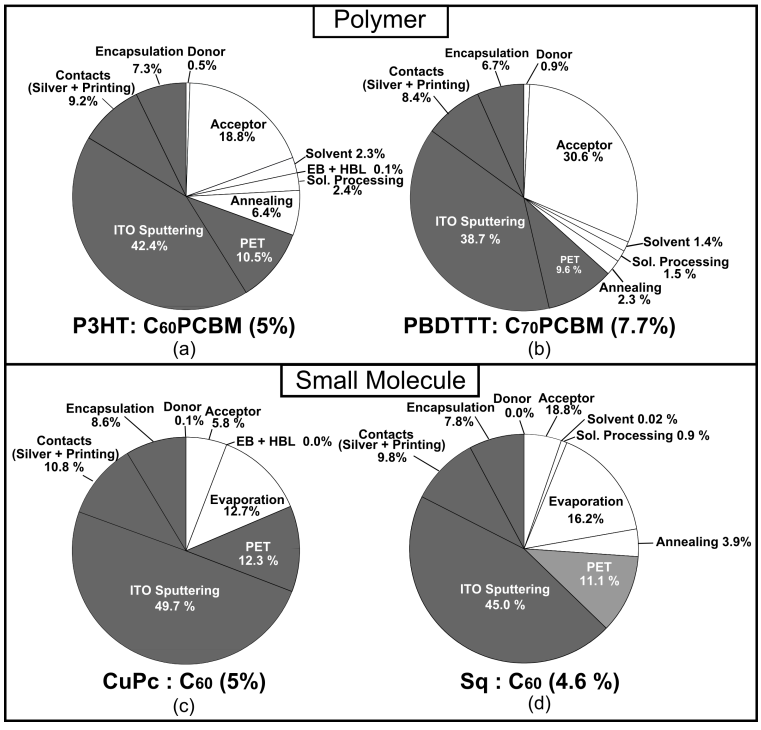

Figure 24: Analysis of each device component for (a) P3HT:C_{60} PCBM , (b)PBDTTT:C_{70} PCBM, (c) CuPc:C_{60} and (d) Sq:C_{60}.

Comparison of Figure 24 a and c highlights the different contributions of materials and processing between the same efficiency polymer and small molecule photovoltaics. The contribution from the ITO sputtering onto the PET and the electrical contacts with encapsulation is even more pronounced with the small molecule devices. In addition, it is apparent that the impact of processing for small molecule photovoltaics is greater than the materials. The relative contribution of the electron acceptor in the small molecule devices, which is unmodified C_{60}, is nearby 30% the amount in polymer photovoltaics. The comparison of Figure 24 c and d, corresponds to a conventional small molecule device which requires thermal evaporation for active material deposition in relation to a solution processed SQ active layer device. In both cases, the main component is the evaporation step since the SQ devices require evaporation of the EBL (MoO_3) prior to the solution-processed SQ deposition, which is then followed by C_{60} and HBL evaporation. Since the major contribution from evaporation comes from the energy used during the chamber evacuation, the overall impact of the evaporation is higher for solution processed SQ than thermally evaporated small molecule photovoltaics. Thus, if all layers in a SQ or PC device are deposited through solution-processing, the CED would greatly be reduced.

3. Multi-junction photovoltaics

The fabrication of multi-junction photovoltaics requires additional processing and material to obtain higher efficiency, but it is the predominant option to increase organic photovoltaic efficiencies above 13%. There are limited published studies on multi-junction photovoltaics, but efficiencies of 8.3% have been reported for double junction small molecule photovoltaics [12]. As illustrated in Figure 23 the multi-junction polymer photovoltaics increases in efficiency, from 6.1% to 6.5%, but the overall impact is an increase in CED, mostly due to the total amount of active material required. The effect is

even more pronounced for devices with lower efficiencies such as PFTBT:pBBTDPP2 which has an embodied energy more than twice the energy from a P3HT:C_{60}PCBM device mainly due to the amount of material used.

The tunnel junction using material such as TiO_x and Pedot:PSS has negligible impact and although the contribution from processing seems the same, there is actually a lower impact from annealing and greater impact from solution processing since six layers have to be deposited rather than three. For small molecule multi-junction devices, the overall impact decreases with increasing efficiency, as there is little increase in processing energy since most of the energy is associated with the initial chamber evacuation. Since all of the materials used in small molecule photovoltaics have lower impact and require only a small amount during fabrication, the overall result is a large reduction in total energy with multi-junction structures compared to single layer small molecule photovoltaics. In Figure 23 two types of small molecule multi-junction photovoltaics are shown to illustrate the impact for higher efficiency devices on the overall impact. In this case, the tandem small molecule photovoltaic made of SubNc+SubPc has a slightly lower CED than P3HT:PCBM for a similar efficiency.

4. Sensitivity analysis

Sensitivity analysis is used to verify the validity of the initial assumptions and provide a range of possible CED values considering the best and worst case scenario. In Figure 25 the shaded area represents the range of results for the best and worst scenarios for each photovoltaic. The range is much larger for polymer photovoltaics, and particularly for photovoltaics using C_{70}PCBM and multi-junction photovoltaics since C_{70}PCBM has a

wider range of embodied energy (see Figure 20) and larger amount of material is required for a polymer multi-junction cell.

For polymer photovoltaics, moving from a single junction to a multi-junction at a given efficiency increases the total cumulative energy. Overall, there is an observed decrease with increasing efficiency. The variation due to the different scenarios is much less for small molecule devices compared to polymer photovoltaics since a lower amount of material with lower embodied energy is being used. The most important result from Figure 25 is that all organic photovoltaics have lower impact than inorganic photovoltaics, regardless of the scenario considered, and that the impact of organic photovoltaics is going down with increasing device efficiencies.

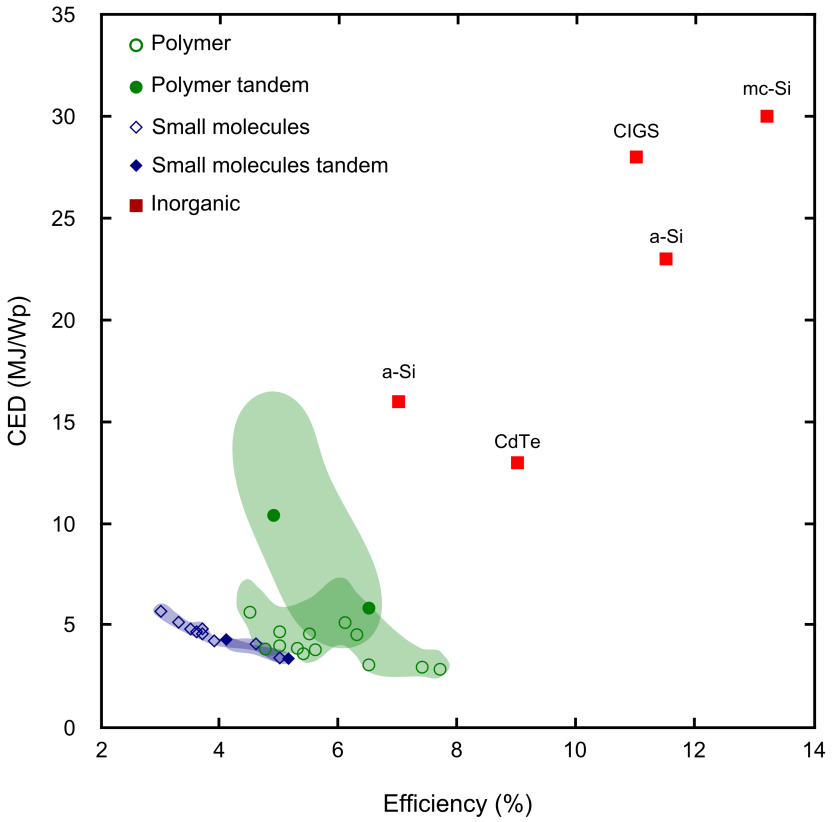

Figure 25: Comparison of all types of organic photovoltaics compared to the reported inorganic photovoltaics (adapted from [60]), including uncertainty analysis for organic photovoltaics using scenario analysis.

One important result from this figure is the rate at which embodied energy is being reduced with increasing efficiency. In previous studies, it was assumed that for future organic photovoltaics, the embodied energy of a photovoltaic with twice the device efficiency would be half the initial device. It is obviously not the case from the results since there is additional processing and material requirements which are responsible for the increased device efficiency. For example with polymer photovoltaics, a 54% increase in device efficiency (from P3HT to PBDTTT) resulted in 32% reduction in embodied energy. In order to reach higher device efficiencies, a multi-junction will be necessary. Therefore the overall, the total embodied energy will likely be higher for the multi-junction compared to the single junction, unless the efficiency is significantly higher to compensate for the extra processing and material requirement. For small molecules, it is shown that the largest energy contribution is associated with the evaporation process, which requires the creation of a vacuum. Adding additional layers for a multi-junction doesn't significantly increases the CED.

DISCUSSION

One result from this work was the creation of life cycle inventory data for 15 new semiconductor materials, which are currently used in organic photovoltaics but also in other organic electronics devices therefore can be used to establish the impact of new technologies such as organic light emitting diodes (OLED). The primary goal of this work was to study the impact of various pathways which have been pursued over the last few years to improve device efficiencies, including the comparison of small molecules and polymer photovoltaics, the use of thermal treatment, interface layers, low bandgap polymer and multi-junctions. In the case of single junction devices, both the small molecule and polymer photovoltaics were found to have similar CED. For polymer photovoltaics, there is

a trend in using larger and higher quantity of fullerenes, which reduces the rate of CED/Wp. While the interface layers where considered, the material has negligible impact, but the deposition and annealing of those were significant in particular for the multi-junction approach. Low bandgap polymers have higher CED than traditional P3HT, but it remains considerably much lower than fullerenes.

The focus of this work was the active layer in organic photovoltaics but from the results in Figure 23 the rest of the devices is the largest contributor, in particular the ITO sputtering alone accounts for more than 35% of the total CED. While increasing device efficiency reduces the contribution from the rest of the device, further reduction in embodied energy will require reduction of those components. This work was performed using CED/Wp and was not converted to energy payback-time (EPBT) as it is commonly done in photovoltaics LCA. EPBT calculates the time a photovoltaics device needs to operate to compensate for the energy required for its fabrication. Since organic photovoltaics are expected to be used mainly under non ideal insolation such as in building integrated photovoltaics or portable electronics, using an optimized insolation value will not be an appropriate method, but actual insolation conditions should be considered in future work.

5.2. Life cycle assessment of greener options

INTRODUCTION

One of the main advantages of polymer phovoltaics is the ability to use solution processing to rapidly produce large area devices. However, the use of hazardous organic solvents such as toluene, chloroform, dichlorobenzene and *o*-xylene conflict with the idea of developing clean, low cost energy sources. A green chemistry and engineering approach is

desirable to identify in the early stage of technology development to favor solutions that eliminate or reduce the use and generation of hazardous substances while contributing to the long-term success of the technology. In particular, water-soluble dyes and polymers have received scant research attention so far, however, the prospect of water-soluble polymers and fullerenes have been investigated [94]. The alternative materials were obtained through the chemical modification of the basic molecules, therefore increasing the number of synthesis steps. Using the results from the life cycle assessment of polymer and fullerenes (section 5.1), the energy associated with the production of those new materials is calculated and used to compare with other types of organic photovoltaics processed using aromatic solvents.

METHODOLOGY

The energy required to produce water soluble fullerene derivative (C_{60}-WS) and polymer (Poly-(4-(2,3-dihydroxypropoxy)-2-methylbutan-2-yl5,5'-dimethyl [2,2'-bithiophene] -4-carboxylate)) (P3CT) is calculated based on recently published synthesis conditions [94] and using the results from Chapter IV for the basic conditions of fullerenes. For the polymer, since the derivative is similar to P3HT, the embodied energy is estimated based on previously calculated values as a function of synthesis steps (Figure 21). For the fullerene derivative, the detailed calculation is performed, and details about the input-output material flow are available in A2. The reported device fabrication conditions and device power efficiency is used to compare with standard P3HT:C_{60}PCBM and PTB7:C_{70}PCBM photovoltaics using the conditions described in Table 3. Both types of solar cells are compared using Cumulative Energy Demand (CED) as well as TRACI 2, which is a method developed by the U.S. EPA to assess environmental impacts.

Table 3: Active layer material input considered for 1kWp organic solar cells

Device (n %)	Donor		Acceptor		Solvent	
	Name	g	Name	g	Name	g
P3CT – C_{60}WS (0.7%)	P3CT	80.36	C_{60} -WS	80.36	23.75% Water/ 23.75% IPA/ 52.5% THF	8040
P3CT – C_{60} WS (5%)	P3CT	11.25	C_{60}-WS	11.25	23.75% Water/ 23.75% IPA/ 52.5% THF	1130
P3HT- C_{60} PCBM (5%)	P3HT	11.25	C_{60} PCBM	9.00	CB	1130
P3HT- C_{60} ICBA (6.5%)	P3HT	11.54	C_{60} ICBA	11.54	*o*-DCB	1150
PTB7-C_{70} PCBM (7.4%)	PTB7	5.07	C_{70} PCBM	7.61	*o*-DCB	510

RESULTS AND DISCUSSION

Using the results from chapter 5.1, the embodied energy of P3CT is estimated to be 3827 MJ/kg. The embodied energy of modified fullerenes to be used with the P3CT is shown in Figure 26 for Pyro-tetralin. There is a five fold increase in the embodied energy of C_{60}-WS compared to the unmodified C_{60}.

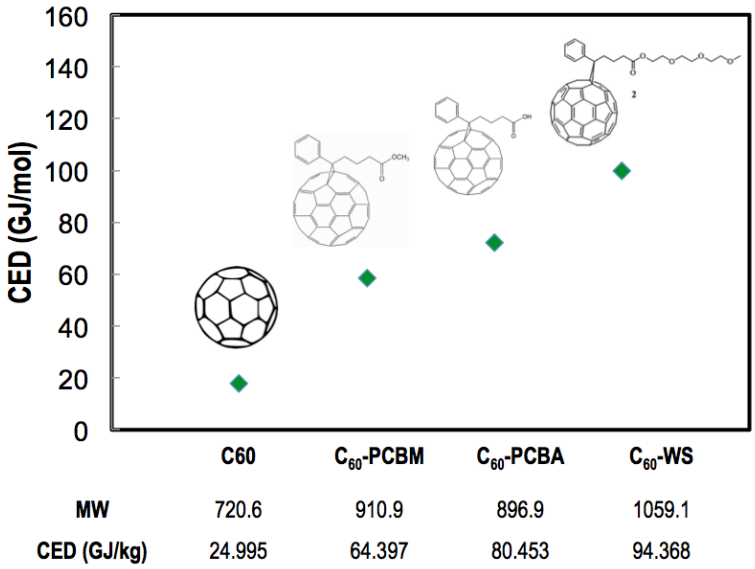

Figure 26: Embodied energy of water soluble fullerene compared to unmodified and other fullerenes derivatives.

Using the conditions described in Table 3, the cumulative energy demand (CED) for the production of P3HT:C_{60} PCBM (η=5%) is compared to the water compatible option in Figure 27a. For the water processing option, the current efficiency of 0.7% results in a total 7 fold increase in CED because larger solar cells are required to produce the same amount of

output power. Even if the efficiency of this type of solar cell was increased to 5%, the total CED required to produce the solar cell would be 4.26 MJ/Wp which is still higher than the 4.00 MJ/Wp from P3HT:C_{60}PCBM (considering only pyto-tetralin method for fullerenes production). Therefore from a CED standpoint, this type of device would require an efficiency of 5.32% to be equivalent to a P3HT:C_{60}PCBM solar cell.

Cumulative energy demand is often used as an indicator for environmental impact since current databases often lack information about chemical emissions. Therefore, this can lead to an underestimation of the environmental impacts. Since detailed inventory analysis regarding air emissions was performed for the active layer (section 5.1), and considering the different active layer materials, the scope of this study can be limited to the impact of producing the solvent, polymer, and fullerenes as well as the direct solvent impact. There is some concern about the direct impact from solvent since solvent represents 98-99% by weight of all the material input during the assembly phase (see Table 3). Even when considering 5% loss due to fugitive emissions, which is much higher than the suggested value of 0.2% [95], the direct impact of solvent is negligible compared to the indirect impact of all the other inputs as illustrated in Figure 27b.

The energy necessary to produce a material (in this case the non-renewable energy) is strongly correlated to most environmental impacts, except for ozone layer depletion, since in this particular case the polymer synthesis involves brominated compounds.

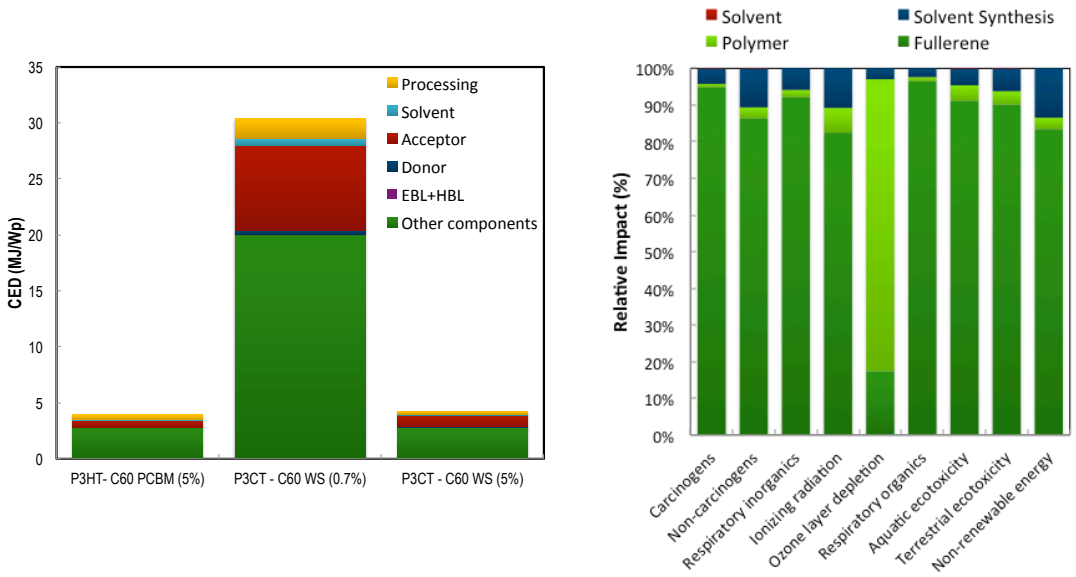

(a) (b)

Figure 27: (a) Embodied energy of water soluble fullerene compared to other fullerenes derivatives and (b) relative impact of various components on different indicators.

For all other indicators, the synthesis of the fullerene has the largest impact, mostly because of the large amount of solvent being used in the process. While the fabrication of a P3HT:C_{60} PCBM solar cell requires only 9 g of C_{60}PCBM, which seems negligible compared to the 1130 g of chlorobenzene, the pyrolysis reaction is highly inefficient. Therefore, the main product is carbon emissions (136.9 kg) for each kg of C_{60} being produced (Figure 12). In addition to the emissions during synthesis, the separation and purification of fullerenes requires 1876 kg of o-xylene per kg of C_{60}PCBM produced. Therefore, 9 g of C_{60} PCBM actually includes 16,884 g of *o*-xylene, whichhas a much larger impact than the direct use of chlorobenzene in the fabrication stage.

An additional analysis is done considering two different types of environmental impacts: respiratory organics and aquatic ecotoxicity for the various types of devices described in Table 3. Even when considering a power conversion efficiency of 5% for the water soluble option, the overall environmental impact for these two indicators are higher

for the proposed greener option than the traditional devices, mainly because the main contributor is the fullerene, not the solvent (see Figure 28).

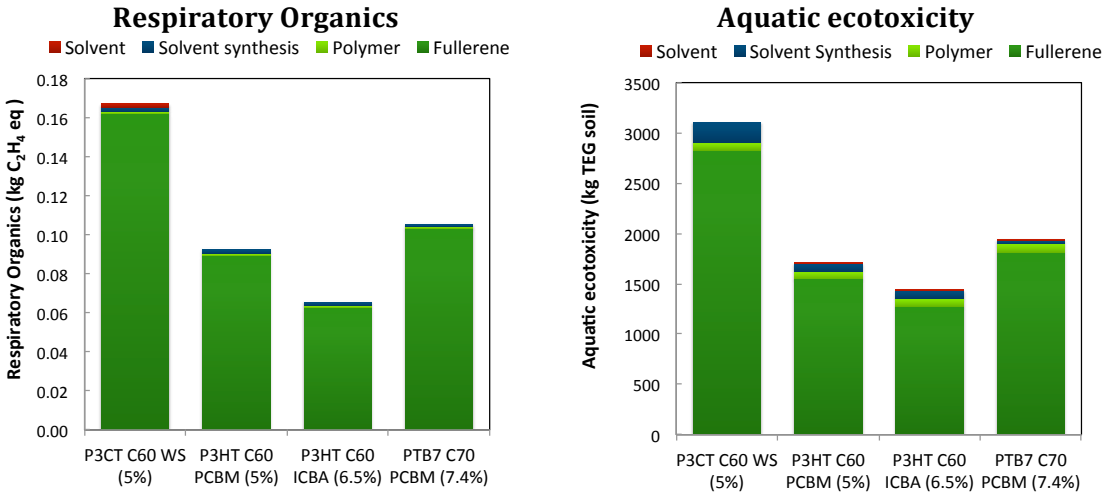

Figure 28: Comparative impacts of P3CT:WS C_{60} compared to current other organic solar cells for (a) respiratory organics and (b) aquatic ecotoxicity.

BROADER IMPLICATIONS

The results from this work illustrate the capability of LCA to identify areas where the greatest reduction can be accomplished as well as identifying the tradeoffs associated with an alternative solution. While considering only the assembly phase, the use of aromatic solvents might seem a major issue and lead to solutions such as aqueous processing of organic photovoltaics. However, the present results show that such a strategy may have an even greater impact when considering all the fabrication stages. The additional functionalization and the lower efficiency of the resulting device, results in greater harm than a traditional P3HT:C_{60}PCBM organic solar cell. According to this result, to reduce the environmental footprint of organic photovoltaics, the focus should be the fullerene production rather than the solvent being used during the assembly stage.

5.3. Economics of organic photovoltaics

INTRODUCTION

The prospect for low cost photovoltaics is the main motivation for organic solar cells. There has been some basic investigation of the cost of organic photovoltaics considering the current cost of the technology and using various assumptions regarding the cost of new semiconductor materials [42, 96].

For small molecules the cost was calculated to be between $1.00 and $2.83 /Wp for a 5% solar cells using CuPc, SnPc and C_{60}[96]. Some of the issues with this estimate originate from the assumptions, which assume a density of 1 g/cm^3, 75% material utilization and a cost of $1/g for CuPc. This calculation underestimate the material usage by at least 110% considering that the actual density of C_{60} is 1.72 [97] while CuPc is 1.63 [98] and the highest reported material utilization for sublimated material is 50% [75]. Also, while CuPc is indeed a widely used pigment, mostly in the automotive industry, the purity of the material used for electronic applications is much higher to limit the amount of electronic traps and therefore the cost increases rapidly with purity. For example, from Sigma [99], the cost for 97% CuPc is $/g 1.47 while the high purity material (99.99%) is $/g 317. Therefore the cost of small molecule photovoltaics is likely to be underestimated due to over-optimistic material usage and material cost.

For polymer solar cells, a similar study has been done considering a 5% P3HT:C_{60}PCBM solar cells which resulted in a cost of 2.803 €/Wp ($/Wp 3.89) where only 0.346 €/Wp was attributed to material cost and device processing(ITO+ PEDOT:PSS + P3HT + C_{60}PCBM + printing + aluminum contact evaporation) [42]. In this case, the cost of both

materials were assumed to be 40 €/Wp ($/Wp 55.52), which is much less than the actual cost of both materials. Considering a density of 1 g/cm^3, 10% material loss and a 5% efficient solar cell, the amount of material for a P3HT:C_{60} PCBM solar cell is assumed to be 0.001 g/Wp for both the polymer and fullerenes. This number is significantly lower than the 0.011 g P3HT/Wp and 0.009 g C_{60}PCBM/Wp calculated in section 5.1 as well as reported in other published studies [60, 61].

Current organic photovoltaics cost analyses underestimate both the amount of material as well as the cost of high purity semiconductor material. An alternative approach that uses Life Cycle Inventory for the active layer of the photovoltaic device is presented in this work.

METHODOLOGY

The cost of photovoltaics is estimated using two methods. First, the direct material input based on the material inventory from section 5.1 and the current cost of materials is used for the active layer. Then, the rest of the device is estimated based on the reported cost of an optimized large area process [100] for the production of a solar module. This first method is referred to as the current cost (CC). The second method uses the raw material inventory (natural gas, coal and crude oil) to estimate the cost of the new materials. Details about the calculations are available in A4. Since the cost is based on raw material only, it is easier with this method to calculate the future cost of the technology and therefore, costs are calculated for 2010 (LCI_{2010}) and 2012 (LCI_{2012}). In all cases, the total energy corresponds to the sum of all material inputs, the rest of the device, and the direct electricity to process the active layer.

RESULTS AND DISCUSSION

The cost of various materials and raw material is presented in Table 4 for the various scenarios. The cost of P3HT is extrapolated based on current cost to a scale of 1kg while the cost of low bandgap polymers was assumed to be 10 times lower than current cost, to account for larger scale production of the material.

Table 4: Overview of unit costs for different scenarios

	Unit	CC	LCI_{2010}	LCI_{2012}
Polymer				
P3HT	$/g	170 [101]	4.3	5.2
PCDTBT	$/g	200 [102]	14.9	17.9
PSIFDBT	$/g	250 [102]	12.5	15.1
PTB1	$/g	350 [102]	12.5	15.1
PTB7	$/g	400 [102]	12.5	15.1
PBDTTT	$/g	500 [102]	12.5	15.1
PIDTBT	$/g	350 Assume PTB1	12.5	15.1
Fullerenes				
C_{60} 99%	$/g	59 (See A2)	53.1	68.4
C_{70} 98%	$/g	338 (See A2)	78.1	100.8
C_{60} PCBM	$/g	245 (See A2)	142.2	180.7
C_{70} PCBM	$/g	833 (See A2)	192.9	246.6
C_{60} ICBA	$/g	1280 [102]	88.3	112.3
C_{70} ICBA	$/g	1765 (See A4)	107.8	137.8
C_{60} bisPCBM	$/g	240 [102]	146.2	185.5
Small molecules				
InPcCl	$/g	119 [99]	41.1	42.0
SuBPc	$/g	94 [99]	2.7	3.5
AlPcCl	$/g	48.4 [99]	1.7	2.5
ZnPC	$/g	4.8 [99]	1.5	1.8
CuPc	$/g	76.5 [99]	1.3	1.8
Electron/hole blocking layers				
PEDOT:PSS	$/g	36.7 [99]		
BPhen	$/g	93.6 [99]	2.1	2.5
BCP	$/g	69.6 [99]	2.1	2.5
Solvents				
o-DCB	$/g	0.0313 [99]		
CB	$/g	0.0253 [99]		
DCM	$/g	0.054 [99]		
Rest of the device [100]				
PET-ITO	$/m^2	108.7		
Silver	$/m^2	22.3		
Barrier	$/m^2	18.9		
Adhesive	$/m^2	8.6		
Raw resources [6]				
Electricity	$/ kWh	0.1158		0.1174
Crude oil	$/barrel		79.4	104.8
Natural gas	$/mcf		11.18	11.92
Coal	$ / ston		125.3	131.1

Using the same single-junction organic photovoltaic as in Chapter 5.1, the cost of various technologies is calculated in Table 5 using the specific cost described in Table 4.

Table 5: Price for the active layer in organic photovoltaics to produce 1kWp photovoltaic device for three different scenarios.

	η (%)	EBL (g)	Donor (g)	HBL (g)	Direct energy kWh	$/Wp CC	$/Wp LCI 2010	$/Wp LCI 2012
Polymer								
P3HT- C_{60} bisPCBM	4.5	3.33	20.83		62.77	**14.1**	**8.3**	**9.3**
PTB1 C_{60} PCBM	4.8	3.15	7.88		48.51	**9.0**	**5.5**	**5.8**
P3HT- C_{60} PCBM	5.0	3.00	11.25		130.56	**8.2**	**5.4**	**5.8**
P3HT- C_{60} PCBM - TiOx	5.0	3.00	11.25	0.12	98.33	**8.2**	**5.4**	**5.8**
PTB1 -C_{70} PCBM	5.3	2.83	7.08		43.57	**13.4**	**5.6**	**6.1**
PsiF-DBT - C_{60} PCBM	5.4	2.78	4.86		42.76	**7.4**	**5.2**	**5.6**
PCDTBT: C_{70} PCBM	5.5	2.73	7.50		41.98	**17.7**	**6.7**	**7.6**
P3HT- C_{70}ICBA (5.6%)	5.6	2.68	13.39		66.34	**17.1**	**5.2**	**5.6**
PCDTBT: C_{70} PCBM TiOx	6.1	2.46	4.92	0.03	122.10	**20.7**	**7.2**	**8.3**
PIDTBT: C_{70} PCBM	6.3	2.38	5.95		36.65	**20.2**	**6.8**	**7.7**
P3HT- C_{60} ICBA	6.5	2.31	11.54		57.16	**19.9**	**4.2**	**4.5**
PTB7 C_{70} PCBM	7.4	2.03	5.07		31.20	**11.1**	**4.3**	**4.7**
PBDTTT-C_{70} PCBM	7.7	1.95	4.87		29.99	**11.2**	**4.1**	**4.5**
Small molecules								
AlPcCl/C_{60}	3.00		3.21	1.19	197.11	**7.3**	**7.0**	**7.1**
ClInPc / C_{60}	3.30		3.13	1.08	175.72	**6.9**	**6.5**	**6.6**
SubNc/ C_{60}	3.50		1.10	1.02	155.36	**6.2**	**6.0**	**6.1**
SubPc/ C_{60}	3.60		3.15	0.99	158.56	**6.2**	**5.8**	**5.9**
CuPc/ C_{60} (h)	3.70		2.75	0.96	156.72	**6.0**	**5.7**	**5.8**
PdPc -ZnPc/ C_{60}	3.70	2.10	1.35	1.44	182.53	**6.9**	**7.4**	**7.5**
ZnPc/ C_{60}	3.90		4.49	0.91	146.28	**5.4**	**5.3**	**5.3**
SQ/C_{60}	4.60	2.43	0.34	0.77	240.41	**4.7**	**4.6**	**4.7**
CuPc/C60 (pm-hj)	5.00		2.02	0.71	121.18	**4.4**	**4.2**	**4.3**

From this table, the current cost method (CC) estimates the cost of polymer photovoltaics to be between $/Wp 7.4 to 20.7 while small molecules are expected to be much cheaper, between $/Wp 4.4 and 7.3. Using the raw material cost, the range for polymer photovoltaics in 2010 is much lower, between $/Wp 4.1 and 8.3, while the difference for small molecules is not as important, and is now in between 4.2 and 7.4 $/Wp. As shown in Table 4, the difference between the current cost of the polymer and the estimate based on the raw material is the largest for the semi-conducting polymer. There

are actually only a few semiconductor producing companies and they are mainly producing laboratory scale amounts of material, therefore keeping the price high. However PBDTTT, PTB1 and PTB7 follow the same chemical synthesis steps, and therefore, should have similar production costs. The actual cost difference can only be attributed to the demand and since only one company produces the material, it has the ability to fix the price. For this reason, using the current cost method provides an unrealistic estimate of the technology cost, in particular when using new materials. As illustrated in Figure 29, the LCI method provides a much lower cost estimate for the cost of polymer photovoltaics compared to using the current cost of the polymer. The cost of P3HT:C_{60}PCBM is estimated to be between 5.4 and 5.8 $/Wp, which corresponds to almost a 40% increase in cost compared to previous estimates. Similarly, a 5% small molecule device cost is estimated to vary between 4.2 and 4.3 $/Wp, more than 45% higher than the highest cost estimate for small molecules.

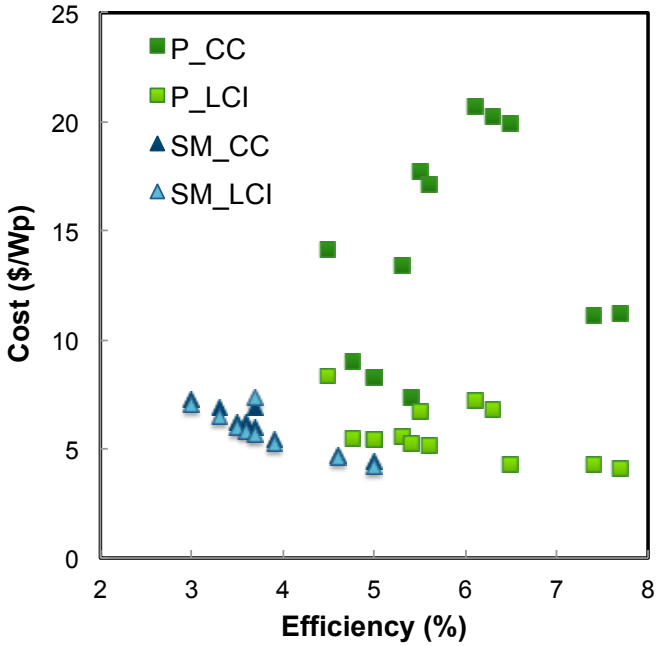

Figure 29: Cost of organic photvoltaics considering the current cost of raw materials (CC) and using the LCI method to calculate the cost based on the cost of raw materials, for both polymer (P) and small molecules (SM).

In all cases, the cost of organic photovoltaics is higher than the desired 1$/Wp. This is further illustrated in Figure 30, where the expected minimum cost of the technology is clearly higher than expected for all the devices considered in this work.

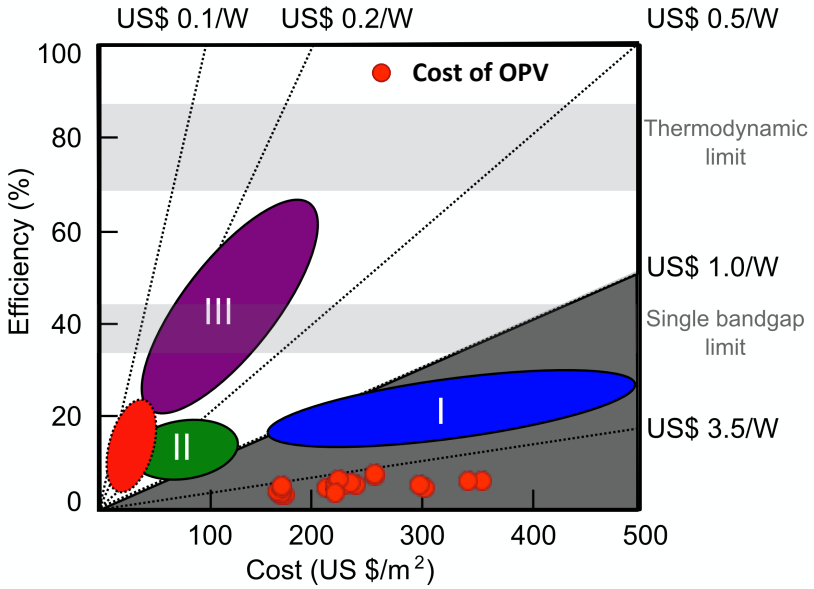

Figure 30: Current cost of OPV relative to other generation photovoltaics (considering the 2010 LCI cost for active material).

In addition to providing a cost estimate based on physical relationships, the LCI cost approach provides a way to forecast the cost of various technologies based on resources use. For example in Table 5, from LCI_{2010} to LCI_{2012}, the cost increase of devices containing a larger amount of polymer are expected to be more important due to the expected increase in the cost of oil over this period. Because small molecule devices use a lower amount of material, the impact is much lower. The life cycle inventory can further provide insight on the use of raw materials either for energy purposes or directly as raw materials. This is illustrated for a PTB7:C_{70} PCBM solar cell in Figure 31. The impact of fullerene production compared to the polymer or the solvent is clear in this figure. The most interesting aspect of

this analysis is the ability to distinguish between resources used as a starting material or for energy since the material component will have a direct impact on the future cost of the technology.

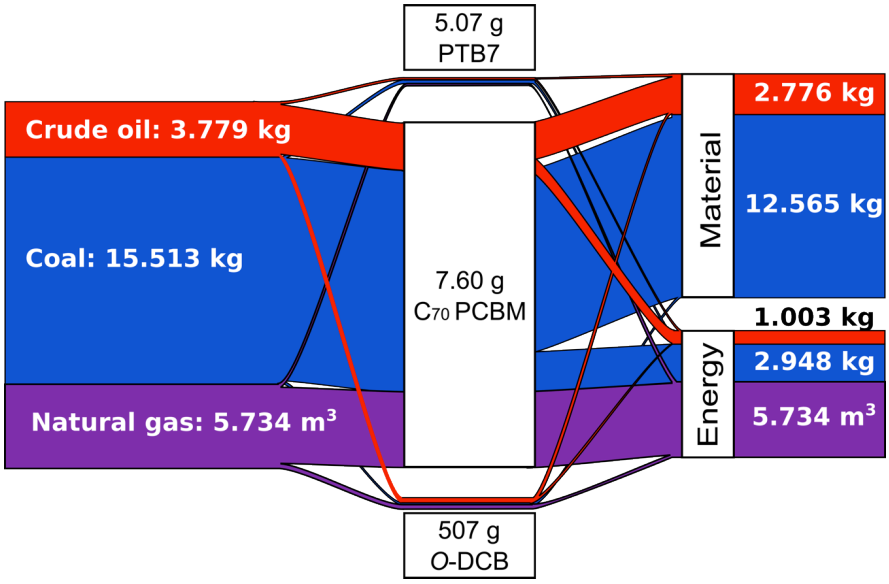

Figure 31: Material flow for the fabrication a 1kWp PTB7:C_{70}PCBM.

BROADER IMPLICATIONS

This works demonstrates an alternative method to estimate the cost of material using the life cycle inventory to correct for the price of new semi-conductor materials. The life cycle approach is also useful to determine future cost of technologies, using the expected cost of raw resources. Overall, all organic photovoltaic technologies have higher cost than the desired $1/Wp and with increasing cost of raw materials, the future cost is likely to increase unless significant improvement in material synthesis or energy reduction is attained.

VI. SOLUTION PROCESSED NIR DYES FOR ORGANIC PHOTOVOLTAICS

In previous chapters, LCA has been used to evaluate the impact of current photovoltaics technologies. For materials, small molecules were found to have a lower impact than polymer while the embodied energy of fullerenes was found to be lower for smaller and unmodified fullerenes. Solution processing was found to require a lower amount of energy than evaporation, but mostly, the use of the same process for all device layers was found to be significant. While the cumulative energy demand was found to decrease with increased efficiency, current multi-junction devices were shown to have much higher CED than single junction and still suffer from low efficiency. In this chapter, using the LCA results, the potential for a solution processable multi-junction device using a combination of small molecules and polymer is demonstrated to illustrate the ability to design organic photovoltaics with lower embodied energy by design. Parts of this works have been published as a proceeding paper as A. Anctil, B. J. Landi, and R. P. Raffaelle, "Multi-junction Polymer Solar Cells," in *34rd IEEE PHOTOVOLTAIC SPECIALISTS CONFERENCE*, Philadelphia, 2009.

INTRODUCTION

There are several challenges restricting the commercial viability of polymer solar cells involving derivatized fullerene-polymer blends. The most notable of these are modest device efficiency and the environmental stability of active materials. In previous work, empirical modeling was used based on current-voltage and spectral measurement to calculate the maximum efficiency of organic solar cells [104]. For C_{70}PCBM-MEH-PPV: C_{70}PCBM and P3HT:C_{60}PCBM systems, efficiency was calculated to be between 6 and 8%, under 1 sun AM1.5 illumination. Theoretically, the incorporation of molecular dyes absorbing between 800-900 nm was shown to increase the power conversion efficiency to

16% under AM1.5 illumination. While absorption in the desired range is a necessary condition, it is not sufficient. The addition of dyes directly to a bulk heterojunction polymer device resulted in charge recombination due to unfavorable energy alignment. Based on those findings, a multi-junction approach for polymer photovoltaics is presented. Two different approaches can be used to fabricate a tandem structure. Devices can be connected in parallel, simply by fabrication of the polymer bulk heterojunction on top of an evaporated dye device [105]. The second approach takes advantage of the easy processability of a sol-gel TiOx solution to create series connection. The TiOx solution can be spin-coated and annealed at a temperature compatible with the polymer device. The same TiOx solution can later be used as a hole blocking layer, which also reduces degradation [106].

In Chapter V the processing of small molecules was found to be the main contributor to the total embodied energy of the device, since large amount of energy is consumed by vacuum equipment. Since both the polymer and the junction material can be solution processed, the ideal solution would be a solution processable NIR small molecule device. For phthalocyanines devices, various methods have been investigated by other groups such as layer-by-layer deposition of 20 bilayers copper phthalocyanine derivative with C_{60} for which the maximum efficiency was η =0.012%[107]. Spin-coating has also be considered for phthalocyanines but so far it has produced device efficiency lower than 1% except for subnaphthalocyanine which has reached 1.29% [108], a value still considerably lower than solution processed polymer photovoltaics or evaporated small molecules devices.

As an alternative, spray-coating is explored in this work since it has the advantage to be a high-throughput method for large area that allow ideal coating on a variety of surfaces for a variety of fluids [109]. Spray-coating methods have been used previously for the

deposition of polymer photovoltaics [109] and photodiodes [110] with performance similar to devices produced with alternative methods but has not been applied to small molecule photovoltaics. While numerous groups recognize the benefit of solution processing over thermal evaporation techniques for large scale production, there has been so far little success in that area mainly due to the limited solubility of small molecules in most organic solvents as well as their tendency to aggregate during spin-coating [108, 111]. Spray-coating techniques have the advantage of allowing diluted solutions since most of the solvent is evaporated before reaching the surface. Multiple parameters such as the number of layers, the solvent, the concentration, the substrate temperature, the ultrasonic power, etc. can be easily modify to affect the film morphology. For those reasons, spray-coating is chosen to deposit NIR small molecules for use in multi-junction photovoltaics.

METHODOLOGY

Glass coated ITO substrates are cleaned by ultrasonication in acetone and isopropyl alcohol and dried at 120 °C for 20 minutes. A layer of poly(3,4-ethylenedioxythiophene):poly(4-styrene sulfonate) (PEDOT:PSS) is spin-coated at 4000 rpm to obtain a 60 nm thick hole conductive layer which is annealed at 120 °C for 1 hour. The polymer/fullerene active layer is obtained by spin-coating a mixture of [6,6]- phenyl-[C_{61}]-butyric acid methyl ester (C_{60}PCBM) with Poly[2-methoxy-5-(2-ethylhexyloxy)-1,4-phenylenevinylene] (MEH-PPV) using a 4:1 PCBM:polymer ratio solution in *o*-xylene. Cyclic voltammetry is used to select candidate small molecules which are evaporated successively using a multi-source PVD75 evaporator. In general a C_{60} layer is evaporated after the coevaporation of a small molecule:C_{60} layer for which the ratio and amount of small molecule is varied.

For tandem solar cells fabrication, a solution of TiOx is prepared following Kim et al. procedure [78]. The resulting solution is diluted using a 1:4 ratio in isopropanol prior to spin-coating on top of the first device. Annealing is performed on a hot plate in air at 120 °C for 10 minutes. Similarly, a thin layer of PEDOT:PSS is spin-coated and dried for 10 minutes at 120°C. The second device is then fabricated on top of the first one. Spray-coated devices are fabricated using the Sono-Tek system, which allows control over the sonic head power, deposition speed and pattern, liquid flow and substrate temperature. A solution is made by mixing 5 mg of ZnPc with 5 mg of AlPcCl and 10 mg of C_{60} in 20 mL of chloroform and sonicated for 30 min. For all devices, evaporation of aluminum as top contacts results in devices with an area of 8 mm^2. The current-voltage characteristics (J-V) are obtained using an Agilent source-measure unit and a Newport Oriel Instrument light source calibrated under air mass 1.5 (AM1.5) followed by spectral response measurements. Surface morphology of the films is studied using an atomic force microscope (AFM) in contact mode.

RESULTS AND DISCUSSION

1. Multi-junction and evaporated NIR dyes

The ability to fabricate tandem devices is demonstrated using two standard MEH-PPV:C_{60} PCBM devices. Figure 32a shows the current versus voltage photoresponse as compared to a single MEH-PPV junction device where an approximate doubling of the open-circuit voltage is observed. The reduced short-circuit current is due to the use of the same material which absorbs in the same region of the solar spectrum. To overcome this issue, the use of a dye with absorption in the desired 700-1100 nm is investigated since it could be used structure similar to the one illustrated in Figure 32b. Using various tandem connections between the individual layers and proper current-matching could result in dramatic improvement in polymer photovoltaics.

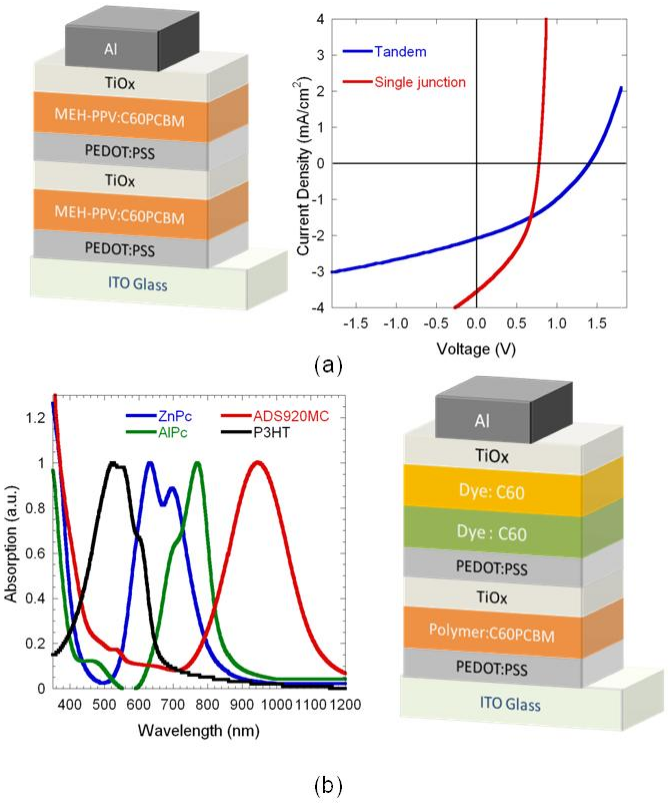

Figure 32: (a) The comparison of the current versus voltage photoresponse of MEH-PPV:C_{60}PCBM tandem device compared to its single junction counterpart and (b) the multi-junction approach combining series and parallel connection of individual devices with potential small molecules absorbing in different regions of the solar spectrum.

In a bulk heterojunction device, a proper excited state energy cascade between the materials with regard to electron affinities and ionization potentials is required to ensure exciton generation and collection. The two small molecules, zinc phthalocyanine (ZnPc) and aluminum 1,8,15,22-tetrakis(phenylthio)-29*H*,31*H*-phthalocyanine chloride (AlPcCl), are chosen based on their absorption spectrum as well as their proper energy alignment with C_{60} as measured using cyclic voltammetry. One of the main obstacles in using small molecule semi-conductors is their low carrier mobilities [112], which limits the maximum thickness of the active layer to the exciton diffusion length. Due to their high absorption coefficients, the selected dyes could be used in thin films to partially mitigate the transport

problem. A second option uses a different structure or co-evaporation of dye and fullerenes to create a diffuse heterojunction by physical vapor deposition. The co-evaporation of the donor and acceptor creates a morphology similar to the one of a bulk heterojunction. The presence of distributed interface increases excition dissociation rate, which results in increasing current density [113]. This approach has been demonstrated for other systems; the most popular using copper phthalocyanine (CuPc) as the donor material [112].

For the purpose of this work, ZnPc is preferred to CuPc due to its absorption at longer wavelengths which does not overlap with the polymer absorption. ZnPc also has a higher absorption coefficient than CuPc which would require thinner layer for full light absorption. For ZnPc, the successive evaporation of two layers with different ratio of ZnPc:C_{60} is a more successful approach than the planar heterojunction, similarly to what has been previously found for CuPc [93]. Using this approach, light absorption is increased since a thicker layer can be fabricated. Devices made with zinc phthalocyanine in combination with lead phthalocyanine have been shown to increase the current density, but not the open circuit voltage while evaporated sucessively. Becausee of its toxicity, lead phthalocyanine is replaced by AlPcCl. Not only AlPcCl has a proper energy alignment with both the zinc phtalocyanine and the fullerenes (Figure 33 a), but it has a smaller bandgap which improves the near-infrared absorption. As shown in Figure 33b, the successive evaporation of the two small molecules results in a film with caracteristic absorption peaks related to the pure materials.

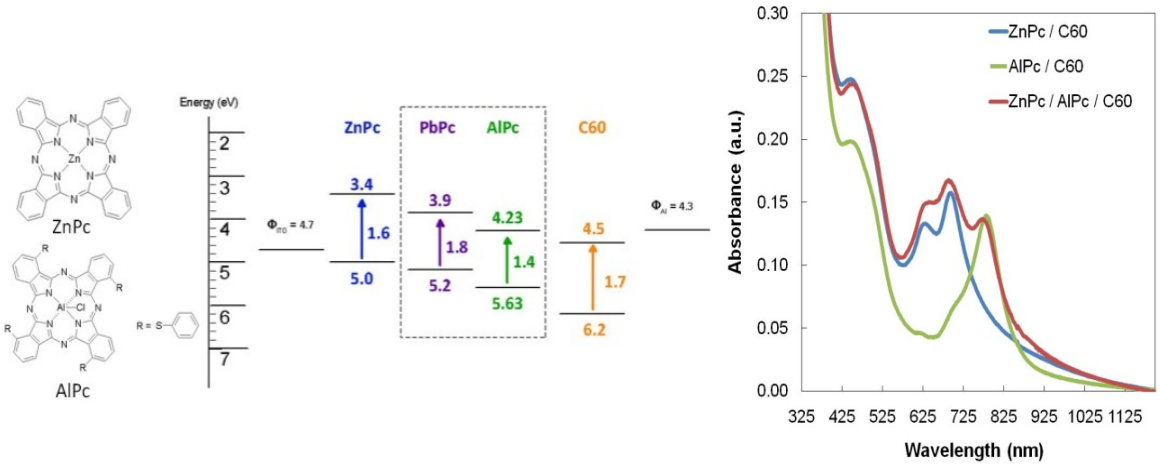

(a) (b)

Figure 33: (a) Energy alignment of different components with values from [103] for C_{60}, ZnPc and PbPc and (b) absorption from devices containing only zinc phthalocyanine, aluminum phthalocyanine and finally a combination of both aluminum and zinc phthalocyanine.

According to the energy diagram, AlPcCl has not only a smaller bandgap than PbPc but also a larger difference between the LUMO level of the acceptor and the HOMO level of the donor. This difference in energy levels should create a larger open circuit voltage [114] compared to the ZnPc/PbPc combination. This is demonstrated in Figure 34a where the addition of AlPcCl to the ZnPc device actually caused an increase in the open circuit voltage, while other parameters remained similar, therefore increasing the overall efficiency. While the combination of both dyes improves the spectral response range, optimization of the layers thickness and composition need to be completed to improve the overall efficiency of the devices. In particular, AFM measurements have shown that the addition of aluminum significantly increases the surface roughness as illustrated in Figure 34b, which has been shown for other systems to negatively impact the overall performances of the devices [112].

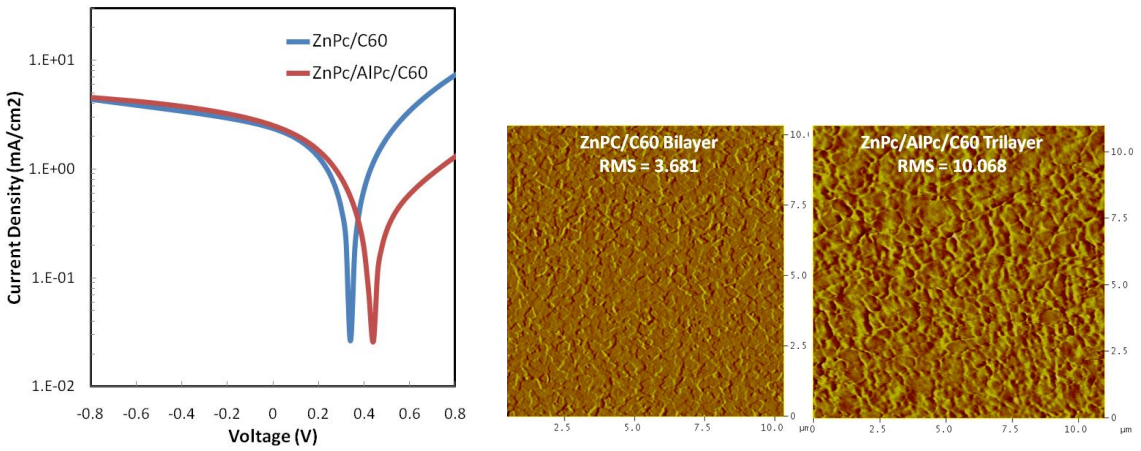

(a) (b)

Figure 34: Current density-voltage (J-V) characteristics of a ZnPc/C_{60} bilayer and a ZnPc/AlPcCl/C_{60} 3 layers cell measured under AM1.5 and (b) contact AFM of the same devices.

2. Solution processing of organic solar cells

The work previously described has shown the potential of using a combination of AlPcCl and ZnPc for tandem solar cells. However thermal evaporation is often not considered a suitable process for large scale production of organic solar cells and for this reason spray-coating is investigated using the same material combination for large area solution processing. The deposition method as well as the solvent influences the material stacking as illustrated by UV-Vis absorption results in Figure 35. A shift in the maximum absorption indicates a different molecular stacking.

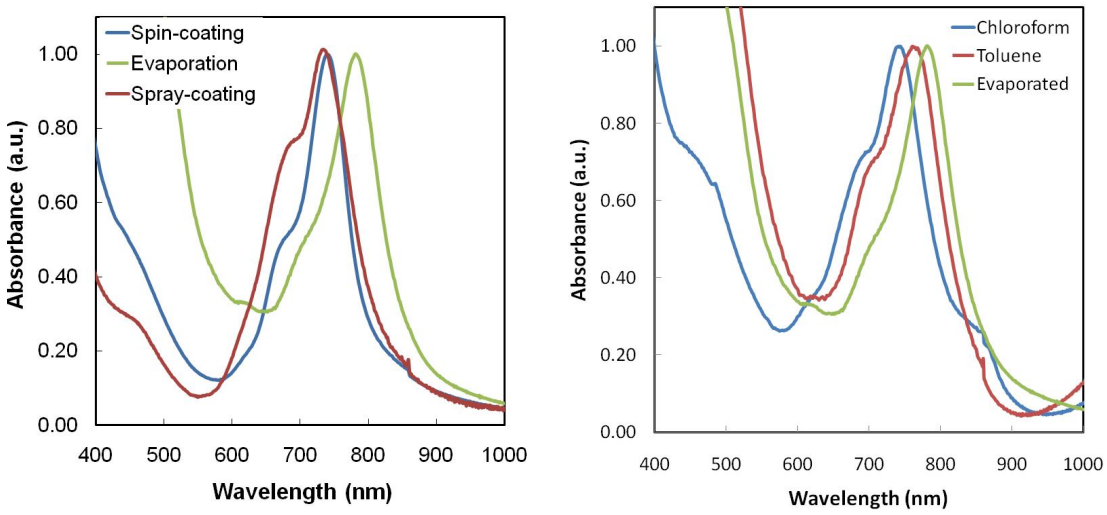

(a) (b)

Figure 35: Effect of processing conditions on absorption for (a) different depositions methods using chloroform as the solvent and (b) different solvents in spray-coated devices compared to evaporated devices.

Complete devices are made using chloroform as a solvent since it reduces the roughness of the layer compared to devices made with toluene. As illustrated in Figure 36, the spray-coated devices have an increased open circuit voltage but a lower current density than evaporated devices. The device is produced using a mixture of ZnPc/AlPcCl/C_{60} where all small molecules are deposited simultaneously rather than in successive layer as illustrated in Figure 36a for simplicity. Since aluminum contacts are evaporated, a thin layer of C_{60} is also evaporated prior to the aluminum deposition. Best efficiencies were obtained for a single layer deposited at a rate of 5 mm/s with a liquid flow of 0.04 mL/ min using 2.5 W sonic head and keeping the substrate temperature at 80°C.

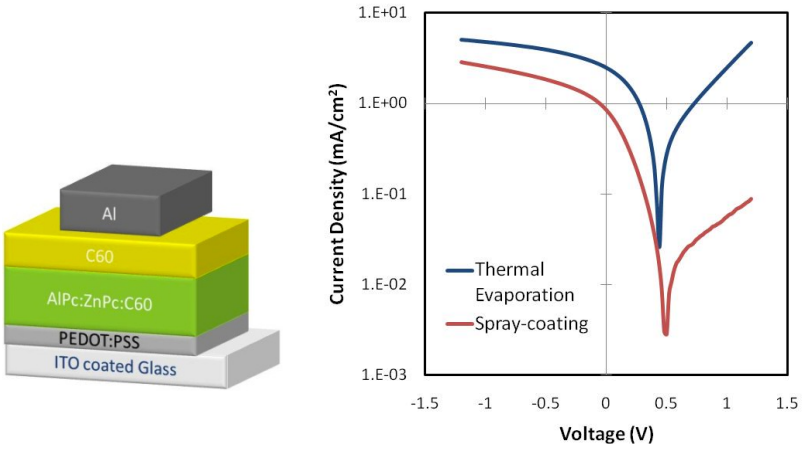

(a) (b)

Figure 36: (a) device structure of spray-coated device and (b) comparison in current-voltage for thermal evaporation and spray-coated devices.

Device efficiency for the spray-coated device is lower than the thermally evaporated device but could be improved by depositing the ZnPc layer followed by a mixture of AlPcCl/C_{60} similar to what was done with the evaporated devices. Additionally, the use of electron blocking layer has not been investigated and it has been shown to be essential to improve performance in small molecules photovoltaics since it reduces the roughness before contacts deposition [93]. Overall, the spray-coating approach can be an interesting approach for solution processing of small molecules.

BROADER IMPLICATIONS

Life cycle assessment is used is to evaluate the proposed alternative NIR multi-junction approach and compare it to current device performance. As discussed in Chapter V, small molecules devices are mainly affected by processing energy. Using the results from Chapter IV and V and the specific energy measured during fabrication of the devices using spray-coating, the energy impact of a solution-processed multi-junction solar cell is

estimated in Figure 37 and compared to previously calculated values for single junctions (Chapter 5.1).

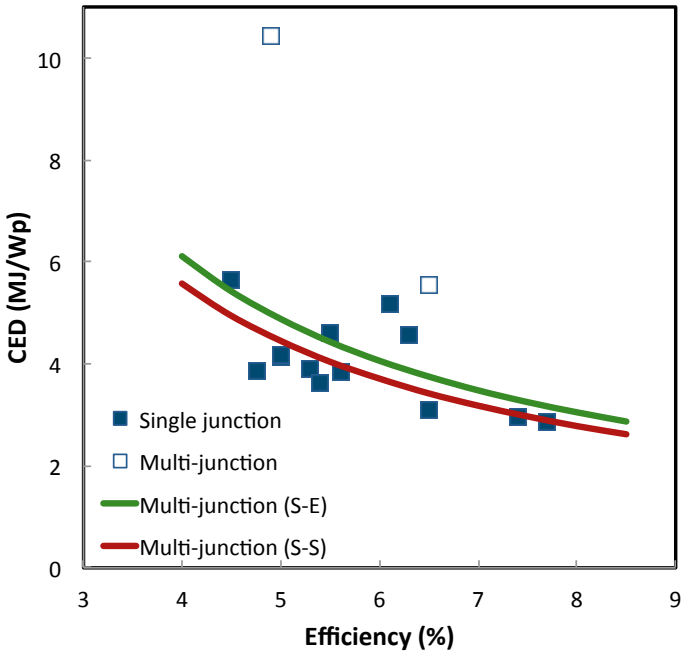

Figure 37: Estimated impact of producing the proposed multi-junction cell using solution processing of the polymer layer and evaporation of the small molecule layers (S-E) and all solution processing as a function of device efficiency.

By choosing both low embodied energy materials (P3HT, C_{60}PCBM for first junction and ZnPc, AlPc and C_{60} for the second device) as well as a low energy solution-processable process, the cumulative energy demand is found to be in the range of the single junction devices. Therefore, the proposed device has by design a much lower impact than previously reported multi-junction devices.

CONCLUSION

Organic photovoltaics are expected to be a low cost energy option with unique properties such as low weight and flexibility that will contribute to their use in new applications such as building-integrated photovoltaics and portable electronics. To date, most work has been directed toward increasing power efficiency while reducing the cost of the technology, whereas little work has been done to evaluate potential negative aspects of the technology. This work addresses the latter by using life cycle analysis (LCA) on current organic photovoltaic technologies. Since the quality of LCA is strongly dependent on the quality of the material inventory, the impact of fullerenes, which are the main acceptor molecule in organic photovoltaics, has been investigated in Chapter IV. It has been shown that purification and modification of the fullerenes greatly increases the embodied energy of the material, which is an order of magnitude higher than most common chemicals. Therefore, the use of fullerenes in products, even in small amount, is likely to influence the overall impact. Therefore, cut-off rules which are often used in LCA to limit the complexity of the study should not be employed. This result is useful for organic photovoltaics, but can also be used to evaluate the impact of other products containing fullerenes.

The embodied energy of fullerene production was used in Chapter V to calculate the life cycle impact of current photovoltaic technologies, including small molecule, polymer, single and multi-junction devices. The work herein increases the LCA literature from 1 type of device to a total of 26 while providing new inventory data for 15 new materials. The energy required to produce small molecule devices was found to be similar to polymer one for single junction photovoltaics, and in all cases, lower than reported inorganic photovoltaics. Alternative "greener" options using water soluble polymer and fullerenes

were compared to current best devices, and found to have an even greater environmental impact when considering all the stages, and not simply the impact of the assembly phase. The life cycle inventory data were then used to estimate the cost of the technology using the raw materials, rather than estimating the future cost of semi-conducting material. This approach has illustrated an advantage of providing a better estimate of future cost of the technology as a function of resources costs.

According to the results from Chapter V, small molecule and non-modified fullerenes have lower embodied energy than polymer photovoltaics, but the use of high vacuum equipment is responsible for most of the impact of the active layer deposition. In order to increase efficiency by absorbing a larger portion of the solar spectrum, a multi-junction approach is necessary. Therefore, the ability to produce a multi-junction organic photovoltaics using ZnPc and AlPcCl for NIR absorption has been demonstrated using an alternative spray-coating approach. The expected CED was calculated to be similar to currently developed single junction photovoltaics, therefore, illustrating how life cycle assessment can be used to better design organic photovoltaics.

APPENDICES

A.1 Supporting Information for "Life Cycle Implications of Fullerene Production

1. Detailed methodology

1.1 Synthesis and separation

Pyrolysis and plasma (arc and radio frequency) synthesis techniques are selected for comparison in this study since they are the most common techniques for commercial production of fullerenes [47]. Arc plasma was the original method for fullerene synthesis, but requires high purity graphite electrodes and high power. While plasma generation allows precise control over fullerene allotrope ratios, it cannot synthesize large amounts of fullerenes, and it requires helium and small diameter graphite rods that need to be changed regularly as the arc distance increases with time, thereby continuously changing synthesis conditions. To overcome this issue, radio-frequency (RF) plasma techniques have been developed that use a large amount of argon and helium to create a plasma in which graphite powder can be continuously fed [115, 116]. Fullerene production rate dramatically increases from 1.2 to 2.7 g/hr by changing from arc to RF plasma (see Table A1) [115]. In comparison, the most common industrial process, pyrolysis, can produce up to 70 g/h of fullerenes by burning a carbon precursor in the presence of a controlled amount of oxygen under reduced pressure [47]. Since the most stable form is not the desired fullerenes, the reaction requires a large amount of hydrocarbon feedstock to produce a small amount of desired material (1-2% wt). The remainder consists of carbon by-products in either solid (graphite and amorphous carbons) or gas form (carbon dioxide, methane and other hydrocarbons) depending on process conditions. The most common hydrocarbon precursor employed is toluene (designated here as pyro-toluene), although recent work has shown where 1,2,3,4-tetrahydronaphthalene (designated as pyro-tetralin) is able to synthesize higher amounts of fullerenes in the as-produced carbon soot [117]. Details used in the present analysis about typical fullerene yield, production rate, and types of fullerenes produced from those methods are given in Table A1.

Table A 1: Reported values for fullerene production under different synthesis process conditions.

Process	Carbon source	Fullerene yield in soot (%)	Production rate (g fullerene/hr)	Ratio C_{60}/C_{70}/ higher fullerenes	Ref.
Arc Plasma	High purity graphite electrodes	13.1	1.2	69 / 24 / 7	[116]
Pyrolysis	Toluene	17.5	44	43 / 28.5 / 28.5	[117]
	1,4-tetrahydronaphtalene (tetralin)	30	70	39 / 30.5 / 30.5	[117]
RF Plasma	Graphite powder	5.9	2.7	70 / 23 / 7	[115]

Once synthesized, fullerenes can be separated through solubility differences with other carbon allotropes by organic solvent extraction [118]. However, separation of C_{60} from C_{70} and higher order fullerenes is complex and requires a large amount of solvent with multiple purification steps, which produces a proportional amount of waste and solvent to be regenerated. In the present analysis, the purification method is based on an iterative process [118] that allows industrial scale production of high purity C_{60} and C_{70}: (Step 1) fullerenes are separated from other carbon material by extraction in *o*-xylene (10 liters of *o*-xylene/kg of carbon soot); (Step 2) fullerene extract solution is filtered and the process is repeated 3 times; (Step 3) filtrate containing the fullerenes and 95% of the solvent is assumed to be recovered and regenerated; (Step 4) the fullerene mix is then separated into C_{60} and C_{70} fractions using fractional enrichment where C_{60} crystallizes in the range of 80-85 °C and can be removed from the other fullerenes using filtration. The filtrate also contains C_{70} and higher order fullerenes that are difficult to separate (which explains the lower purity of commercially sold C_{70} compared to C_{60}).

1.2 Purification

Previous work [42, 43] on the impact of fullerene production only included production and separation steps described above (section 1). However, most medical and energy applications require electronic grade fullerenes, necessitating additional purification steps. Both the C_{60} and the C_{70} fractions can be further purified using flash chromatography with a saturated solution of fullerenes (15 mg/ml in *o*-xylene) [118]. In the case of C_{60}, 15% of the fullerenes are lost due to irreversible adsorption onto the activated carbon, while the last fraction (10%) of the starting solution contains more than more than 0.5% of C_{70} and can be returned to the fullerene mix fraction for further separation, resulting in a 75% yield. Flash chromatography is also used for the C_{70} fraction, but the yield is typically 65% and the

last fraction containing higher fullerenes is discarded. Additional information about synthesis and separation steps are available in Figures A1 to A3. where grey boxes correspond to information from previous inventory data as defined in Table A2, while the black boxes represent the direct process emissions illustrated in Figure 12 for all 4 different processes.

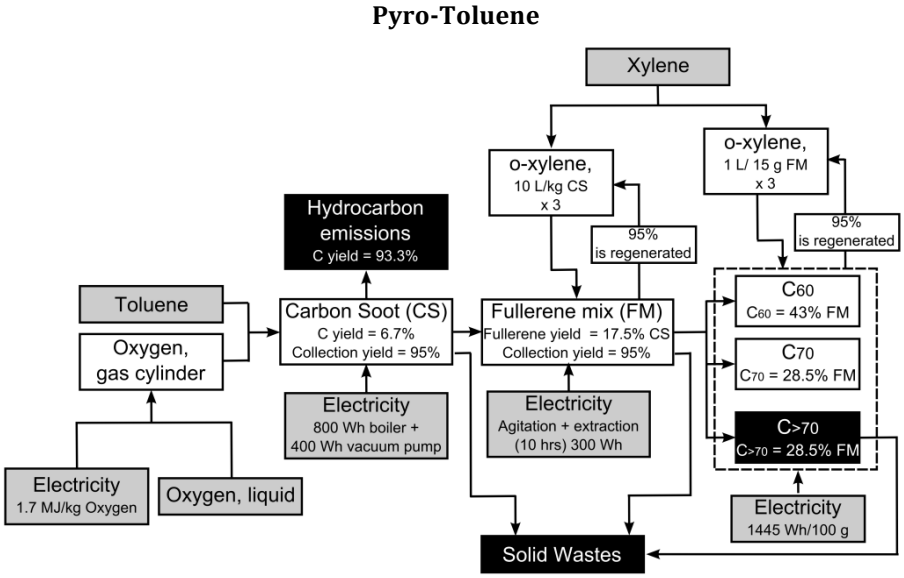

Figure A1: Flow diagram for the production of C_{60} and C_{70} (synthesis and separation steps).

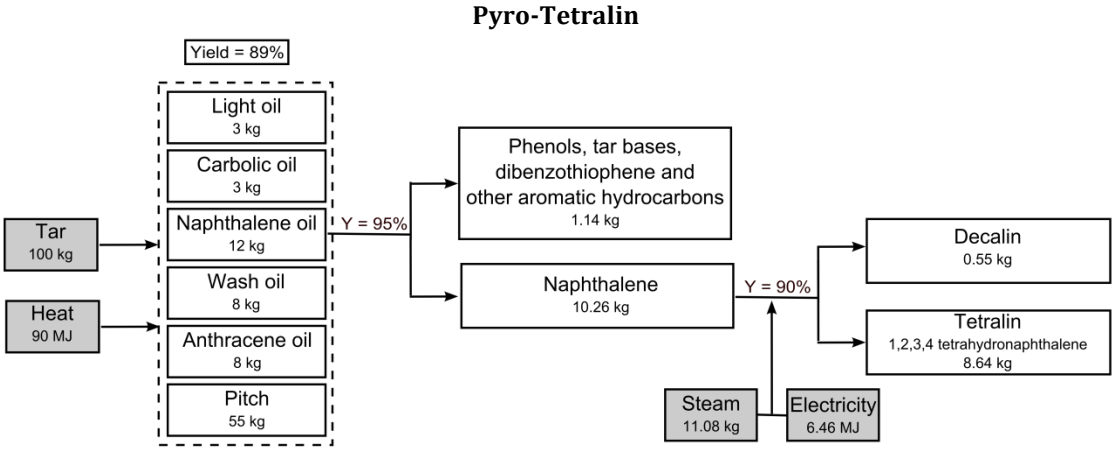

Figure A2: Production of tetralin from coal tar.

The main feedstock for naphthalene production is coal tar which is distillated around 210-220 °C. At an average content of around 10 %, naphthalene represents the most important compound in high temperature coal tar (coke-oven tar) in terms of quantity. It can already be concentrated to over 90% in primary tar distillation. Tetralin is

produced industrially by selective hydrogenation of low-sulphur naphthalene in the presence of nickel catalysts at 180-260 °C and 1.5 MPa [71].

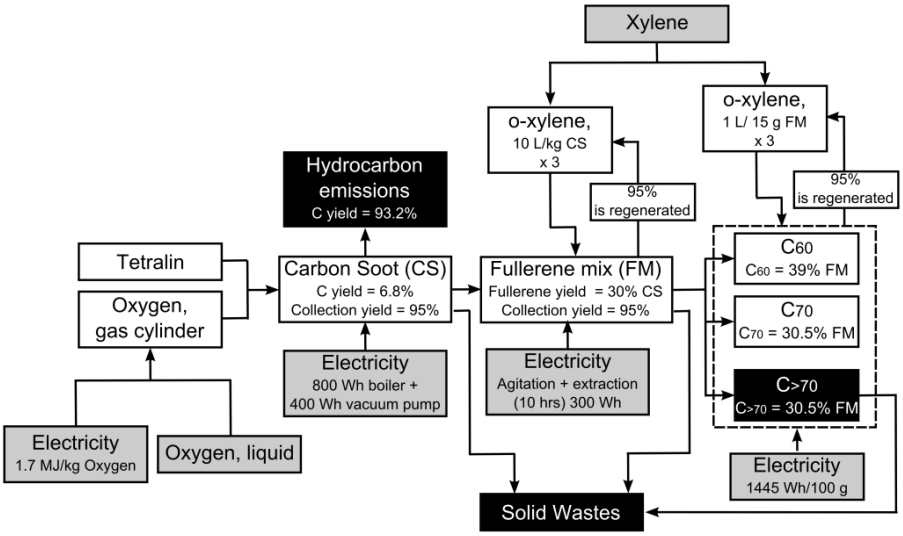

Figure A3: Flow diagram for the production of C_{60} and C_{70} (synthesis and separation steps) from pyro-tetralin.

Arc Plasma

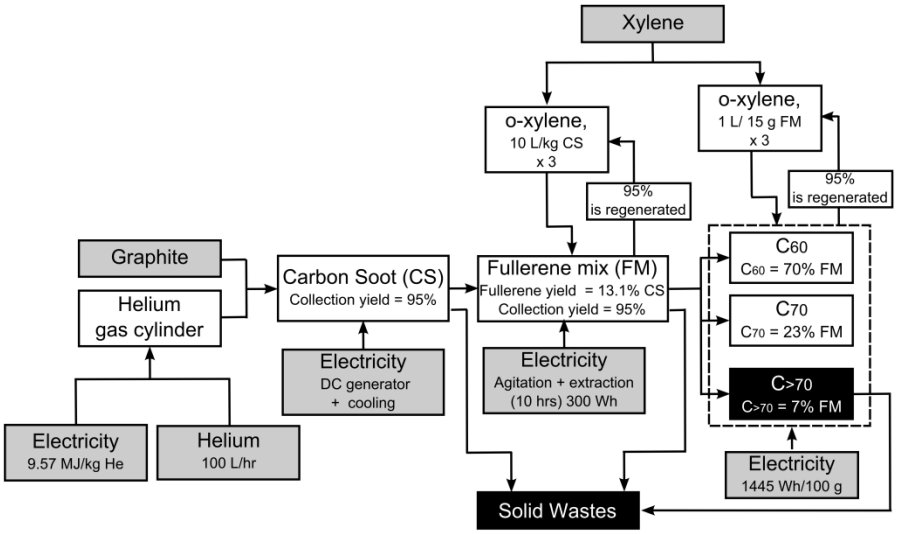

Figure A4: Flow diagram for the production of C_{60} and C_{70} (synthesis and separation steps) from arc plama.

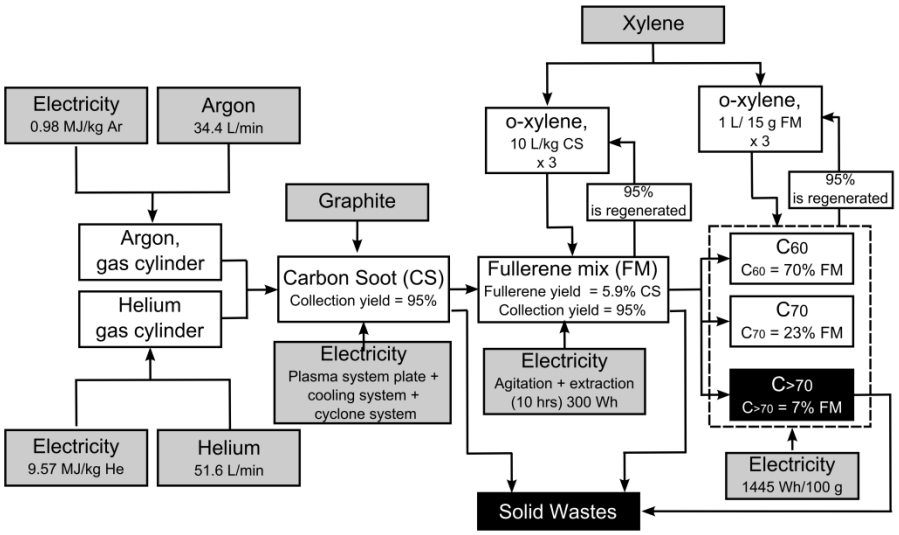

Figure A5: Flow diagram for the production of C_{60} and C_{70} (synthesis and separation steps) from RF plasma.

1.3. Functionalization

Modified fullerenes are increasingly used for organic solar cell applications and methano-fullerenes previously shown in Figure 1 are used to illustrate nanomaterial functionalization. Fullerenes are modified to the PCBM derivative to increase their solubility and enhance their electronic properties [119].

The reaction steps, yields, and chemical assumptions in the present calculations are based upon the reactions and yield described by Hummelen [119] (Figure A6). The bis-adduct is a minor by-product of the functionalization stage and has been pursued as a possible fullerene material for organic solar cells, but has not shown significant performance improvements compared to the major products C_{60} or C_{70}-PCBM compounds [79] and is therefore excluded from this study. Pyridine is obtained by distillation from lower-boiling fractions of tar distillates (light and carbolic oil) at a yield of 85% [71].

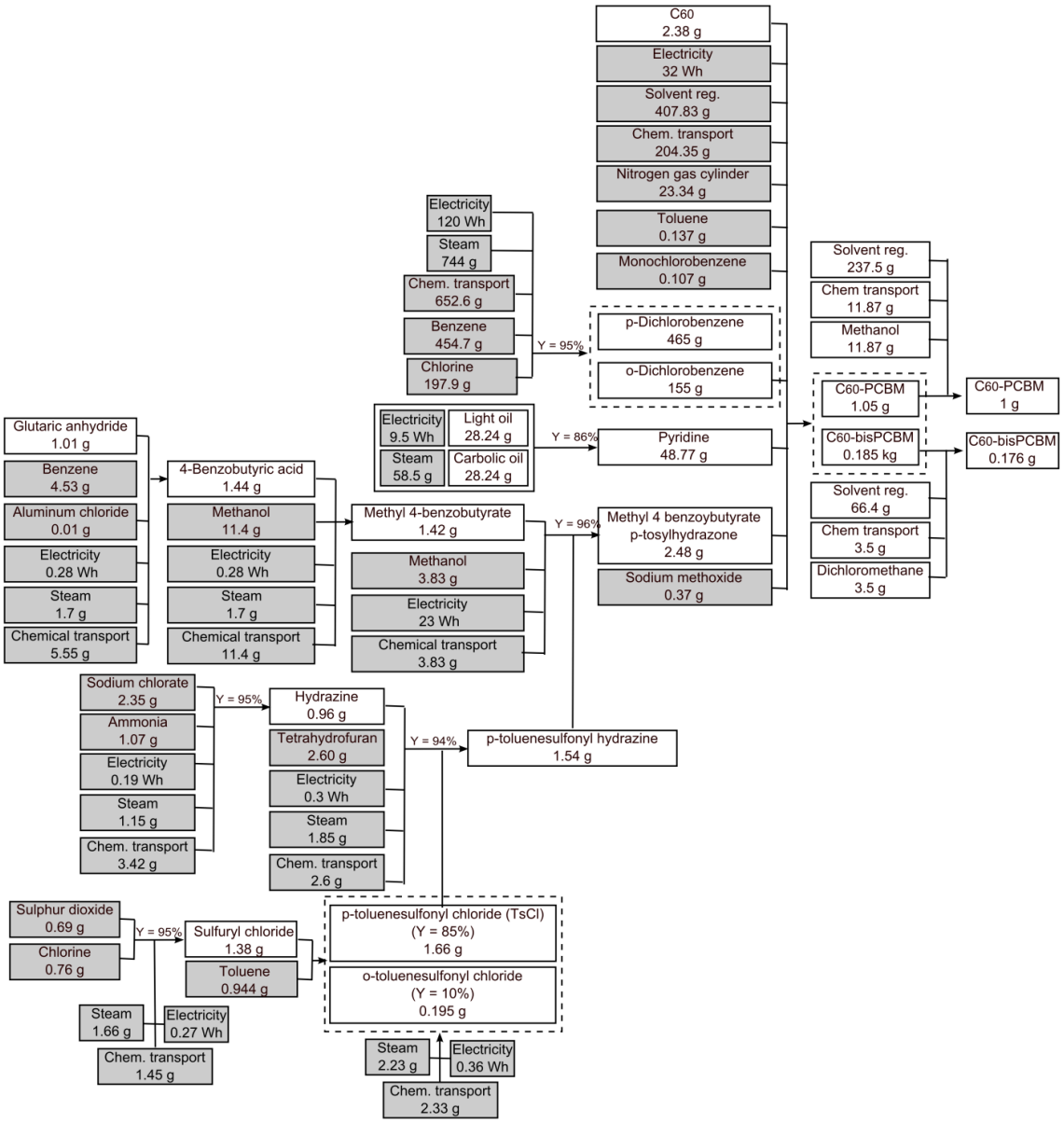

Figure A6: Flow diagram for the production of C_{60}-PCBM.

2. Data source for life-cycle assessment

2.1. Materials

Table A 2: Data sources for materials and energy used in the inventory analysis

	Details	Ref.
Tar	By-product of coke production used in almost all US coke plants in 1998	[120]
Heat, at hard coal industrial furnace	Industrial heating where net efficiency average is 80% under german condition in the early 1990s. Stroker boiler is used as reference technology	[120]
Steam	Steam for chemical processes at plant. Average steam production out of gas and heavy fuel oil by 11 European chemical producers	[121]
Sodium methoxide	Sodium hydrogenation of trimethyl borate Brown-Schlesinger process delivers the co-products sodium tetrahydroborate and sodium methoxide. The inventory is modeled for the world.	[122]
Benzene	Data from the Eco-profiles of the European plastics industry based on 11 European production sites, corrected for US electricity uses.	[123]
Monochlorobenzene	Chlorination of benzene delivers co-products monochlorobenzene, o-dichlorobenzene, p-dichlorobenzene and hydrochloric acid based on mass balance.	[71]
Toluene	Production by catalytic reforming out of naphtha. Data from the Eco-profiles of the European plastics industry based on 11 European production sites	[124]
Methanol	Production of methanol from natural gas through steam reforming process. Data from various plants of different locations.	[124]
Chlorine	Average European chlorine production from the 3 different electrolysis cell techniques (mercury, diaphragm and membrane).	[124]
Oxygen	Cryogenic air separation	[124]
Argon	Catalytic burning of oxygen impurities in argon using hydrogen	[124]
Helium	Production of helium from natural gas	[124]
Sulphur dioxide	Inventory is based on numerous industrial processes from literature...	[124]
Sodium chlorate	Manufacturing process by means of electrolysis of a sodium chloride solution	[124]
Ammonia	Present state of the art technology used in european ammonia production plants, based on reports from 1995 and 2000 Manufacturing	[124]
Tetrahydrofuran	Production of tetrahydrofuran from 1,4-butanediol using stoichiometric calculation	[125]
Dichloromethane	Data from various plants within Europe	[124]
o-xylenes	Mixed xylenes are all produced together and mass allocation is used for various products (o-xylene: 32.3%, p-xylene 64.2% and m-xylene and ethylbenzene: 3.5%) Extractive distillation with yield of 95% is performed to separte the products.	[71]
Chemicals transportation	Standard transport distances for basic chemicals in Europe: 600 km train and 100 km lorry 16 t	[28]
Gas transport	Standard transport distances for gases cylinder in Europe: 200 km train and 100 km lorry 16 t	[28]
Operation lorry 16 t	Includes fuel consumption for an average European lorry in the year 2005	[126]
Operation freight train	Average goods transport condition in Europe for diesel and electric trains	[126]
Electricity	Electricity medium voltage at grid US. Total electricity losses at 13 at medium voltage approximated along with Swiss data	[127]
Solvent regeneration	Best case scenario with 1.5 kg steam/kg product and 0.2 MJ of electricity/kg of product	[29]
Utility inputs for reaction and workout	For new chemicals where there is no specific available information, the reaction is based on the stochiometric reaction, assuming a 95% yield and 1.2 kg steam/kg of product and 0.7 MJ/kg of product	[29]

2.2. Gas cylinder energy

Table A 3. Specific compression work for gas cylinder at 175 bar.

Gas	Adiabatic coefficient (n)	Initial specific volume (m^3/kg) [128]	Specific compression work (MJ/kg)
Argon	1.67	0.561	0.98
Oxygen	1.4	1.43	1.70
Helium	1.66	5.56	9.57

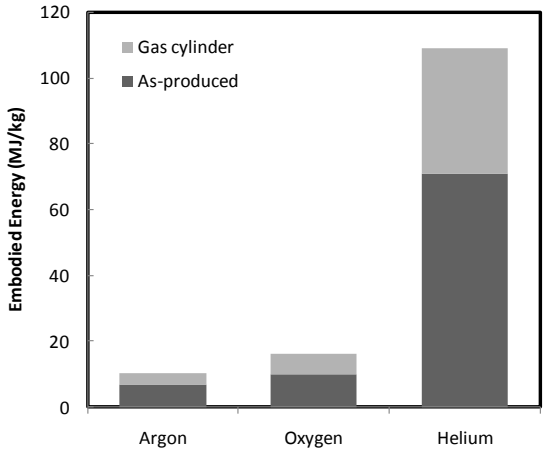

Figure A7: Embodied energy from gas cylinder

3. Review of previous studies and inputs

Table A 4: Summary of previous methods and inputs for fullerene production and the resulting embodied energy calculated.

	Method	Publication year (method year)	Inputs	Embodied energy (GJ/kg C_{60})
Previous Work	Pyro-Benzene	2009 [42] (1992) [129]	Benzene and oxygen	32
	Pyro-Toluene	2008 [43] (2005) [74]	Toluene	8.8
	Plasma-Arc	2009 [42](1997) [130]	Electricity	91
	Plasma-RF	2009 [42](2000) [131]	Electricity	118
This Work	Pyro-Toluene	(2005) [74]	(Figure A1)	17.0
	Pyro-Tetralin	(2008) [132]	(Figure A3)	12.7
	Plasma-Arc	(2007) [116]	(Figure A4)	88.6
	Plasma-RF	(2006) [115]	(Figure A5)	106.9

4. Inventory results

Table A 5: Inventory for the production of 1kg of C_{60}

	Units	Pyro-toluene	Pyro-tetralin	Arc Plasma	RF Plasma
O-xylene	kg	24.0	20.0	21.0	45.1
Toluene	kg	137.1			
Tetralin	kg		81.9		
Electrode pitch	kg			8.3	25.3
Oxygen, gas cylinder	kg	109.7	68.9	0.9	2.8
Helium gas cylinder	kg			15.4	127.1
Argon gas cylinder	kg				844.8
Chemical transport	kg	260.8	252.9	37.6	70.4
Gas cylinder transport	kg	109.7	69.4	16.3	974.7
Solvent regeneration	kg	456.4	380.1	398.4	857.0
Electricity	kWh	223.3	167.8	6399.6	6140.3

Table A6: Inventory for the production of 1kg of different fullerenes derivatives using pyro-tetralin process.

		C_{60} 99.5% PCBM	**C_{60} 99.9% PCBM**	**C_{70} 95% PCBM**	**C_{70} 98% PCBM**	**C_{60} 99.9% bisPCBM**
Toluene	kg	5.1	5.1	5.1	5.1	5.2
Tetralin	kg	221.8	277.2	277.1	426.4	279.0
Pyridine	kg	41.6	41.6	41.6	41.6	41.8
Methanol	kg	11.9	11.9	11.9	11.9	0
o-xylene	kg	66.1	93.8	80.1	134.8	94.4
o-dichlorobenzene	kg	6.6	6.6	6.6	6.6	6.6
Methyl 4 benzoylbutyrate p-tosylhydrazone	kg	2.1	2.1	2.1	2.1	2.1
Dichloromethane	kg	0	0	0	0	19.9
Nitrogen, gas cylinder	kg	19.9	19.9	19.9	19.9	20.0
Oxygen, gas cylinder	kg	186.6	233.2	233.2	358.7	234.7
Gas cylinder transport	kg	207.9	254.9	254.8	381.3	256.5
Chemical transport	kg	815.5	1017.0	990.4	1494.4	1031.5
Solvent regeneration	kg	1829.2	2355.5	2095.9	3133.7	2521.7
Electricity	kWh	567.5	698.8	681.6	1010.2	710.8

5. <u>Fullerenes products cost</u>

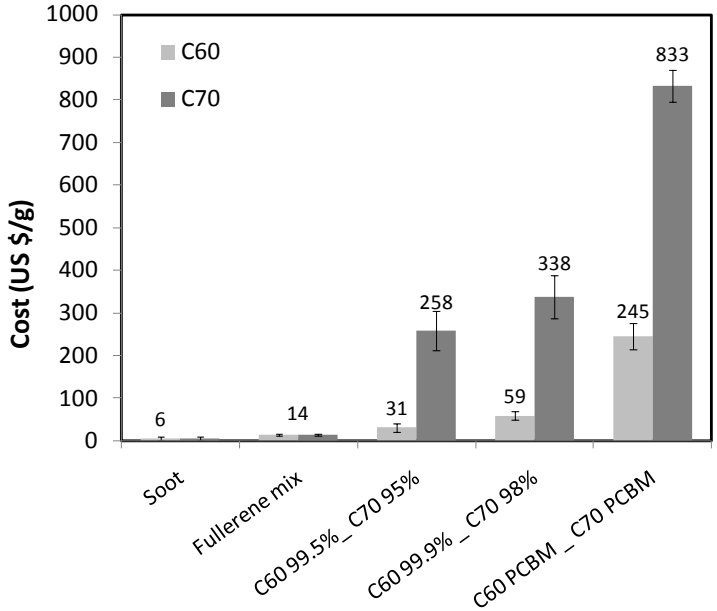

Figure A8: Cost of various fullerenes products from 7 companies as of March 2010 (SES Research, MTR Ltd., Term-USA, American Dye Source Inc., BuckyUSA, NeoTech Product, Solenne). For european companies, Euro/USD conversion factor was taken as 1.388 which corresponds to the average 2009 exchange rate.

A.2 Material input-output for new chemicals

Table A 6: Synthesis of PCDTBT [67]

Outputs	PCDTBT_2	**21.07**	g		
Inputs		**Used**		***Total***	**Regenerated solvent**
	Ethyl formate	7.408	g		
	Octyl magnesium bromide -> hexylmagnesium bromide	65.229	g		
	THF	6.46		*129.15*	122.7
	Methanol	1.67		*33.37*	31.7
	NH4Cl			*5.00*	
	Diethyl ether	4.46		*89.25*	
	Aqueous NaCl solution			*5*	
	nitrogen (75-500 g/kg product) (g)	1.58025			
Process Inputs					
	Stir 8 hrs room temperature (Wh)			0.104	
	Solvent regeneration (g)				154.39
	Chem transport (g)	12.59			
Outputs	PCDTBT_3	**14.25**	g		
Inputs		**Used**		***Total***	**Regenerated solvent**
	PCDTBT_2	10.00	g		
	p-toluenesulfonyl chloride	11.13	g		
	Triethylamine	9.84	g		
	Trimethylamine	2.49	g		
	Dichloromethane	10.11	g	202.20	192.1
	Hexane	2.52		50.39	47.9
	Ethyl acetate	0.38		7.67	7.3
	nitrogen (75-500 g/kg product) (g)	1.07			
Process Inputs					
	Stirred 90 min (Wh)			0.0195	
	Solvent regeneration (g)				247.24
	Chem transport (g)	13.01			
	Chem reaction (g)	1.77			
Outputs	PCDTBT_5	**8.203**	g		
Inputs		**Used**		***Total***	**Regenerated solvent**
	Potassium hydroxide	5.611	g		
	PCDTBT_4	6.5	g		
	PCDTBT_3	12.32	g		
	DMSO	2.688		53.77	51.1
	Distilled water	2.461		49.22	46.8
	Hexanes	1.611		32.23	30.6
	Dichloromethane	3.265		65.29	62.0
	nitrogen (75-500 g/kg product) (g)	0.61523	g		
Process Inputs					
	Chem transport (g)	10.03	g		
	Solvent regeneration (g)				190.48
	Stirr 6 hrs room temperature (50 ml)	0.03			
Outputs	PCDTBT_6	**6.081**	g		
Inputs		**Used**		***Total***	**Regenerated solvent**
	PCDTBT_5	6	g		
	Butyllithium in hexane	1.4	g		
	2-isopropoxy,4,4,5,5,tetramethy1,3,2...	4.359	g		
	THF	1.045		20.9	19.9
	Diethyl ether	1.288		25.8	24.5
	Methanol	0.241		4.8	4.6
	Acetone	0.024		0.5	0.5
	nitrogen (75-500 g/kg product) (g)	0.456	g		
Process Inputs					
	Chem transport (g)	2.60	g		
	Solvent regeneration (g)				49.36
	Stir 10 hrs (Wh)	0.03			
	2 hrs 78 C (Chem reaction) g	8.58			
Outputs	PCDTBT	**0.1781**	g		

Inputs		Used		Total	Regenerated solvent
	PCDTBT_6	0.723	g		
	PCDTBT_7	0.504	g		
	Pd2(dba)3	0.005	g		
	Tri-o-tolyl phosphine	0.007	g		
	Aqueous tetraethylammonium hydroxide	3.000	g		
	Bromobenzene	0.001	g		
	Phenylboronic acid	0.013	g		
	Toluene	0.737		15	14.0
	Methanol	0.085		2	1.6
	Hexanes	0.070		1	1.3
	Toluene	0.093		2	1.8
	Dichloromethane	0.142		3	2.7
	Chloroform	0.158		3	3.0
	nitrogen (75-500 g/kg product) (g)	0.01336	g		
Process Inputs					
	Chem transport (g)	1.28			
	Solvent regeneration (g)				24.407
	Stir 72 hrs (Wh)	0.12			
	95 C 72 hrs (Chem reaction) g	33.07			
Outputs	2,7–dibromo-9-H-carbazole (p4)	**0.29**	g		
Inputs		**Used**		***Total***	**Regenerated solvent**
	4,4-dibromo-2,2-diaminobiphenyls (1c)	0.5	g		
	Nafion H	0.025	g		
	o-xylene	0.88		0.88	0.0
	nitrogen (75-500 g/kg product) (g)	0.0218			
Process Inputs					
	Chem transport (g)	0.88			
	Solvent regeneration (g)	0			
	Refluxed 12 hrs (Chem reaction) g	0.92			
Outputs	**4,4,-dibromo2,2, diaminobiphenyls (1c)**	3	g		
Inputs		**Used**		***Total***	**Regenerated solvent**
	4,4,dibromo-2,2-dinitrobiphenyl	4.02	g		
	hydrochloric acid	2.4	g		
	tin	0.474	g		
	sodium hydroxide	3	g		
	ethanol	0.59		11.83	11.2
	diethyl ether	0.64		12.71	12.1
	nitrogen (75-500 g/kg product) (g)	0.2250			
Process Inputs					
	Chem transport (g)	1.23			
	Solvent regeneration (g)				23.307
	30 min reflux (Chem reaction) g	1.42			
Outputs	**4,4,-dibromo2,2, dinitrobiphenyl**	6	g		
Inputs		**Used**		***Total***	**Regenerated solvent**
	2,5-dibromonitrobenzene	12	g		
	Cupper	3	g		
	DMF	1.13		22.66	21.5
	Benzene	1.58		31.55	30.0
	nitrogen (75-500 g/kg product) (g)	0.45			
Process Inputs					
	Chem transport (g)	5.71			
	Solvent regeneration (g)				51.4995
	Heated 120 C for 2 hrs (Chem reaction) g	2.20			
Outputs	**2,5-dibromonitrobenzene**	140.4	g		
Inputs		**Used**		***Total***	**Regenerated solvent**
	1,4-dibromobenzene	118	g		
	Sulphuric acid	506	g		
	Nitric acid (50%)	82.8	g		
	Sodium hydroxide 50% solution	22.7	g		
	Dichloromethane	15.65		313.08	297.4
	Water	3.51		70.20	66.7

	Nitrogen (75-500 g/kg product) (g)	10.53			
Process Inputs					
	Chem transport (g)	630.69			
	Solvent regeneration (g)				364.11
Outputs	P7 (4.7-di(2bromothien 5 yl) 2,1,3 benzothiadiazole	**1**	**g**		
Inputs		**Used**		***Total***	**Regenerated solvent**
	4,7-di-2thienyl-2,1,3-benzothiadizole	2	g		
	NBS	2.5	g		
	chloroform	0.33		6.66	6.3
	acetic acid	4.72		4.72	0.0
	nitrogen (75-500 g/kg product) (g)	0.075			
Process Inputs					
	Chem transport (g)	5.05			
	Solvent regeneration (g)				6.327
	Stirred at room temperature overnight (10 mL)	0.01	Wh		
Outputs	4,7-Di-2thienyl-2,1,3-benzothiadiazole	**1.8**	**g**		
Inputs		**Used**		***Total***	**Regenerated solvent**
	4,7-dibromo-2,1,3-benzothiadiazole	2	g		
	tributyl(2-thienyl)stannane	6.1	g		
	THF	0.36		7.20	6.8
	Dichloromethane	0.36		7.16	6.8
	Hexane	0.18		3.54	3.4
	nitrogen (75-500 g/kg product) (g)	0.135			
Process Inputs					
	Chem transport (g)	0.9			
	Solvent regeneration (g)				17.005
	Refluxed 3 hrs in THF (Chem reaction equivalent)	2.24	g		
Outputs	Tributyl(2-thienyl)stannane	**50.1**	g		
Inputs		Used		Total	Regenerated solvent
	Butylithium	9.61	g		
	Thiophe	12.6	g		
	Chlrotributyltin	51.3	g		
	THF	3.3		65.4	62.1
	Nitrogen	3.758	g		
Process Inputs					
	Chem transport (g)	3.27			
	Solvent regeneration (g)				62.08
	Mix 50 C 30 min Chem reaction	0.41	g		

Table A 7: Synthesis of P3HT [66]

Outputs	P3HT	**21.07**	g		
Inputs		**Used**		***Total***	**Regenerated solvent**
	2-5-Dibromo-3hexylthiophene	2.56	g		
	Cyclohexylmagnesium chloride	1.18	g		
	THF	0.6650	g	13.3	12.6345
	Methanol	0.3098	g	6.2	5.8853
	Hexane	0.2562	g	5.1	4.8670
	Chloroform	0.5790	g	11.6	11.0005
	nitrogen (75-500 g/kg product) (g)	1.58025			
Process Inputs					
	Mix 30 min			0.001	Wh
	Solvent regeneration (g)				34.387
	Chem transport (g)	1.81			
Outputs	**2,5-Dibromo-3-alkylthiophene**	**309.79**	g		
Inputs				***Total***	**Regenerated solvent**
	3-hexylthiophene	168.30	g		
	NBS	391.56	g		

	Acetic acid	16.25	g	324.97	308.72
	Chloroform	22.92	g	458.49	435.56
	nitrogen (75-500 g/kg product) (g)	23.23			
Process Inputs					
	Distillation product (Chem reaction)	18.8	g		
	Solvent regeneration (g)	744.29	g		
	Chem transport (g)	39.17	g		
Outputs	3-hexylthiophene	**1.183**	g		
Inputs				***Total***	**Regenerated solvent**
	3-bromothiophene	1.00	g		
	Hexyl magnesium bromide	2.80	g		
	Diethyl ether	0.27	g	*5.37*	5.10
	Dichloromethane	0.47	g	*9.42*	8.95
	Hexane	0.23	g	*4.65*	4.42
	nitrogen (75-500 g/kg product) (g)	0.0887			
Process Inputs					
	Mix	0.02	Wh		
	Solvent regeneration (g)	18.46			
	Chem transport (g)	0.97			
Outputs	Hexyl magnesium bromide	**181.8**	g		
Inputs				***Total***	**Regenerated solvent**
	1-bromohexane	165.07	g		
	Magnesium	24.30	g		
	THF	8.33	g	*166.65*	158.31
	nitrogen (75-500 g/kg product) (g)	13.64			
Process Inputs					
	Mix 190 mL 1 hr at 45C (Chem reac)	10.4	g		
	Solvent regeneration (g)	158.31	g		
	Chem transport (g)	8.33	g		
Outputs	1-bromohexane	**165.07**	g		
Inputs				***Total***	**Regenerated solvent**
	Hexane	89.5	g		
	Hydrogen bromide	80.9	g		
	H2SO4	1	g		
	nitrogen (75-500 g/kg product) (g)	12.38			
Process Inputs					
	Chem reaction	165.07	g		
	Chem transport (g)	90.5	g		
Outputs	3-bromothiophene	**101.36**	g		
Inputs				***Total***	**Regenerated solvent**
	Thiophene	84.14	g		
	Br2	159.80	g		
	Chloroform	18.05	361.03	*342.98*	
	nitrogen (75-500 g/kg product) (g)	7.60			
Process Inputs					
	Mix 12 hrs + heat (Chem react)	208.67	g		
	Solvent regeneration (g)	342.98	g		
	Chem transport (g)	18.05	g		
Outputs	Thiophene	**79.9**	g		
Inputs	**CS2**	**38.05**	**g**	***Total***	**Regenerated solvent**
	2-butanol	74.10	g		
	nitrogen (75-500 g/kg product) (g)	5.99			
Process Inputs					
	Chem reaction	79.9	g		
	Chem transport (g)	74.1	g		

Table A 8: Synthesis of phthalocyanines [24, 25]

Outputs	ZnPc	1.257	g		
Inputs				***Total***	**Regenerated solvent**
	Phthalonitrile	1.28	g		
	ZnCl2	0.341	g		
	Water	0.251	g	*5.0*	4.8
	Acetone	0.199	g	*4*	3.8
	Dichloromethane	0.334	g	*6.7*	6.3
	Acetonitrile	0.593	g	*11.9*	11.3
Process Inputs					
	490 W microwave for 5 min	147	kJ		
	Solvent regeneration (g)	26.162			
	Chem transport (g)	1.13			
Outputs	CuPc	1.257	g		
Inputs				***Total***	**Regenerated solvent**
	Phthalonitrile				
	CuCl2				
	Water	0.265	g	*5.3*	5.0
	Acetone	0.210	g	*4.2*	4.0
	Dichloromethane	0.352	g	*7.0*	6.7
	Acetonitrile	0.625	g	*12.5*	11.9
Process Inputs					
	300 W microwave for 10 min	336	kJ		
	Solvent regeneration (g)	27.577			
	Chem transport (g)	1.19			
Outputs	PdPc	1.006	g		
Inputs				***Total***	**Regenerated solvent**
	Phthalonitrile	1.28	g		
	PdCl2	0.443	g		
	Water	0.201	g	*4.0*	3.8
	Acetone	0.159	g	*3.2*	3.0
	Dichloromethane	0.267	g	*5.3*	5.1
	Acetonitrile	0.474	g	*9.5*	9.0
Process Inputs					
	630 W microwave for 10 min	378	kJ		
	Solvent regeneration (g)	20.938	g		
	Chem transport (g)	0.90	g		
Outputs	AlPcCl	0.2415	g		
Inputs				***Total***	**Regenerated solvent**
	Phthalic anhydride	0.355	g		
	AlCl3	0.08	g		
	Water	0.048	g	*1.0*	0.9
	Acetone	0.038	g	*0.8*	0.7
	Dichloromethane	0.064	g	*1.3*	1.2
	Acetonitrile	0.114	g	*2.3*	2.2
Process Inputs					
	300 W microwave 10 min	90	kJ		
	Solvent regeneration (g)	5.026	g		
	Chem transport (g)	0.216	g		
Outputs	SubPc	0.9690	g		
Inputs				***Total***	**Regenerated solvent**
	Phthalonitrile	1.2813	g		
	BCl3	0.2929	g		
	Water	0.194	g	*3.9*	3.7
	Acetone	0.154	g	*3.1*	2.9
	Dichloromethane	0.257	g	*5.1*	4.9

	Acetonitrile	0.457	g	*9.1*	8.7
Process Inputs					
	650 W microwave 10 min	390	kJ		
	Solvent regeneration (g)	20.167	g		
	Chem transport (g)	0.868	g		
Outputs	InPcCl	0.9776	g		
Inputs				***Total***	**Regenerated solvent**
	Phthalonitrile	1.28	g		
	InCl3	0.5529	g		
	Water	0.196	g	*3.9*	3.7
	Acetone	0.155	g	*3.1*	2.9
	Dichloromethane	0.259	g	*5.2*	4.9
	Acetonitrile	0.461	g	*9.2*	8.8
Process Inputs					
	490 W microwave for 5 min	180	kJ		
	Solvent regeneration (g)	20.347	g		
	Chem transport (g)	0.88	g		
	Chem transport (g)				
	Chem transport (g)				
	Chem transport (g)				
	Chem transport (g)				

Table A 9: Synthesis of Squaraine [133]

Outputs	Diisobutylamine	125.36	g		
Inputs				***Total***	**Regenerated solvent**
	Sec-butylamine	73.14	g		
	2-Bromobutane	137.02	g		
			g		
			g		
			g		
			g		
	nitrogen (75-500 g/kg product) (g)	9.402			
Process Inputs					
	Reflux in 2-bromobutane 24 hrs (Chem reaction eq)	174	g		
Outputs	Squaraine intermediate	4.4	g		
Inputs				***Total***	**Regenerated solvent**
	1,3,5-trihydroxybenzene	7.9	g		
	Diisobutylamine	16.2	g		
	1-butanol	0.489	g	*9.78*	9.29
	toluene	1.570	g	*31.41*	39.84
	hexane	0.695	g	*13.89*	13.2
	acetone	0.210	g	*4.30*	3.99
	nitrogen (75-500 g/kg product) (g)	12.38			
Process Inputs					
	Refluxed 6 hrs (chem react eq)	25.92	g		
	Solvent regeneration (g)	56.32	g		
	Chem transport (g)	27.12	g		
Outputs	2,4-bis[4- (N,N-diisobutylamino)-2,6-dihydroxyphenyl]squaraine	65.98	g		
Inputs				***Total***	**Regenerated solvent**
	SQ intermediate	70.4	g		
	Squaric acid	17.1	g		
	1-butanol	1.77	g	*35.42*	33.65
	toluene	5.69	g	*113.76*	108.08
	hexane	12.96	g	*259.22*	246.26
	methanol	15.69	g	*313.74*	298.05
	nitrogen (75-500 g/kg product) (g)	4.95			
Process Inputs					
	Refluxed 5 hrs in 1-butanol and toluene (Chem react eq)	78.80	g		
	Solvent regeneration (g)	686.04	g		
	Chem transport (g)	123.59	g		

Table A 10: Synthesis of C_{60} derivatives

Outputs	C60- WS	83	g		
Inputs				***Total***	**Regenerated solvent**
	C60 PCBA	97	g		
	DMAP	44	g		
	Triethyleneglycol monemethyl ether	72	g		
	DCC	108	g		
	DCM	18.71	g	*374.1*	355.40
	Ethyl acetate	11.17	g	*223.35*	212.19
	Toluene	10.79	g	*215.86*	205.07
	nitrogen (75-500 g/kg product) (g)	6.225			
Process Inputs					
	Heat + mixing	5.25	MJ		
	Solvent regeneration (g)	772.65	g		
	Chem transport (g)	112.67	g		
Outputs	C_{60} ICMA	0.428	g		
	C_{60} ICBA	0.653	g		
Inputs				***Total***	**Regenerated solvent**
	C60 99.9	1.44	g		
	Indene	4.63	g		
	1,2,4-trichlorobenzene	4.38	g	*87.6*	83.22
	Methanol	8.56	g	*171.19*	162.63
	Toluene	5.39	g	*107.87*	102.48
	Hexane	7.08	g	*141.57*	134.49
Process Inputs					
	Heat	1.23	MJ		
	Mixing	0.07	Wh		
	Solvent regeneration (g)	428.81	g		
	Chem transport (g)	30.04	g		
Outputs	C60PCBA	40.45	g		
Inputs				***Total***	**Regenerated solvent**
	C60 PCBM	50	g		
	HCl	87.5	g		
	Acetic Acid	524.5	g		
	Chlorobenzene	11.10	g	*222*	210.9
	Methanol	3.20	g	*64.1*	60.85
	nitrogen (75-500 g/kg product) (g)	3.03			
Process Inputs					
	Chem reaction (Heat)	330.2	g		
	Solvent regeneration (g)	271.75	g		

Table A 11: Synthesis of PTB7 [68]

Outputs	PTB7_2	1.04	g		
Inputs				***Total***	**Regenerated solvent**
	4,6-dihydrothieno[3,4-b]thiophene-2-carboxylic acid	1.46	g		
	Butyllithium	1.11	g		
	N-fluorobenzenesulfonimide	3.22	g		
	THF	0.51	g	*10.29*	9.78
	Ethyl Acetate	0.31	g	*6.24*	5.93
	nitrogen (75-500 g/kg product) (g)	0.078			
Process Inputs					
	Mix RT for 12 hrs				
	Solvent regeneration (g)	15.71	g		
	Chem transport (g)	1.93	g		
Outputs	PTB7_3	1.42	g		
Inputs				***Total***	**Regenerated solvent**
	DCC	1.58	g		

	DMAP	0.26	g		
	2-ethylhexanol	8.20	g		
	PTB7_2	1.04	g		
	Dichloromethane	0.95	g	*18.99*	18
	Hexane	0.37	g	*7.39*	7.0
	nitrogen (75-500 g/kg product) (g)	0.107			
Process Inputs					
	Solvent regeneration (g)	25.06	g		
	Chem transport (g)	9.52	g		
Outputs	PTB7_4	1.25	g		
Inputs				***Total***	**Regenerated solvent**
	MCPBA	0.78	g		
	PTB7_3	1.42	g		
	Ethyl acetate	0.2	g	*3.95*	3.7
	nitrogen (75-500 g/kg product) (g)	0.09375			
Process Inputs					
	Heat		MJ		
	Solvent regeneration (g)	3.75	g		
	Chem transport (g)	0.2	g		
Outputs	PTB7_5	0.95	g		
Inputs				***Total***	**Regenerated solvent**
	Acetic anhydride	0.13	g		
	PTB7_4	1.25	g		
	Hexane	0.124	g	*2.49*	2.4
	Dichloromethane	0.126	g	*2.52*	2.4
	nitrogen (75-500 g/kg product) (g)	0.07125			
Process Inputs					
	Reflux in acetic anhydride for 2.5 hrs (Chem react)	0.67	g		
	Solvent regeneration (g)	7.13	g		
	Chem transport (g)	0.38	g		
Outputs	PTB7_6	0.98	g		
Inputs				***Total***	**Regenerated solvent**
	NBS	1.34	g		
	Sodium sulfite solution	2.29	g		
	PTB7_5	0.95	g		
	DMF	0.22	g		
	Dichloromethane	0.49	g		
	Hexane	0.14	g		
	nitrogen (75-500 g/kg product) (g)	0.07350			
Process Inputs					
	Solvent regeneration (g)	16.11	g		
	Chem transport (g)	3.14	g		
Outputs	PTB7_8	0.8	g		
Inputs				***Total***	**Regenerated solvent**
	Benzo[1,2-b]dithiophene-4,8 dione	1.00	g		
	Zinc dust	0.65	g		
	NaOH	18.45	g		
	2-ethylhexyl-p-toluenesulfonate	4.3	g		
	Ethanol	0.17	g	*3.39*	3.22
	Chloroform	0.36	g	*7.12*	6.76
	Dichloromethane	0.16	g	*3.18*	3.02
	Hexane	0.08	g	*1.57*	1.49
	nitrogen (75-500 g/kg product) (g)	0.06			
Process Inputs					
	Refluxed 1 hr (Chem react eq)	6.06	g		
	Solvent regeneration (g)	13.0	g		
	Chem transport (g)	19.2	g		
Outputs	PTB7_9	0.867	g		
Inputs				***Total***	**Regenerated solvent**
	Butyllithium solution	0.22	g		
	Trimethyltin chloride solution	0.84	g		
	PTB7_8	0.62	g		

	THF	0.15	g	*2.99*	2.84
	Hexanes	0.17	g	*3.41*	3.24
	IPA	0.68	g	*0.68*	0
	nitrogen (75-500 g/kg product) (g)	0.06503			
Process Inputs					
	Stirred RT 12 hrs				
	Chem transport (g)	2.06	g		
	Regeneration	6.08	g		
Outputs	PTB7	0.355	g		
Inputs				***Total***	**Regenerated solvent**
	PTB7_6	0.236	g		
	PTB7_9	0.386	g		
	Pd(PPh3)4	0.025	g		
	DMF	0.03	g	*0.61*	0.58
	Toluene	0.08	g	*1.68*	1.60
	Methanol	0.17	g	*3.37*	3.20
	Chloroform	0.32	g	*6.30*	5.99
	Hexane	0.14	g	*2.79*	2.65
	nitrogen (75-500 g/kg product) (g)	0.02663			
Process Inputs					
	120 C for 12 hrs (chem react eq)	3.141	g		
	Chem transport (g)	0.74	g		
	Regeneration	14.02	g		

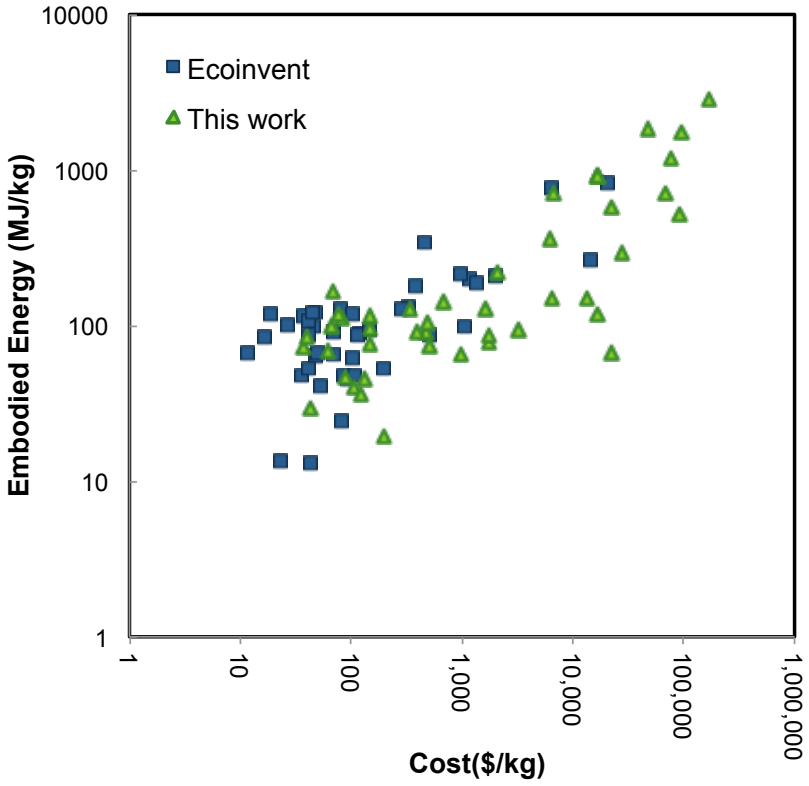

Figure A 9: Relationship between CED and cost of material from the Ecoinvent database and the fine chemicals calculated.

A.3 Supporting Information for Cumulative Energy Demand for Small Molecule and Polymer Photovoltaics

S.1. Process description

S1.1 Evaporation of small molecules

The system characteristics have been measured for various materials (ZnPc, AlPc and C60) and adjusted for other materials using physical properties.
Assume deposition speed to be 1Å/s and initial pump down time to be 0.5 hour.
Assume max area = 0.1 m^2

Table A 12: Base case systems parameters

	Power	Usage
Vacuum pump	400 W	Pump-down (30 min) + Deposition time
System idle power	91.2 W	Pump-down (30 min)
Evaporation power	See Figure	60 s + Thickness/1Å/s

To calculate the evaporation power, we assume a 60 s. soaking at lower power, followed by the material evaporation.

Table A 13: Angstrom evaporator evaporation conditions

Material	Soaking Power (%)	Evaporation Power (%)
Phthalocyanines dyes	15	25
C60 – MoO_3	15	30
BCP- BPhen- PTCDI	5	15

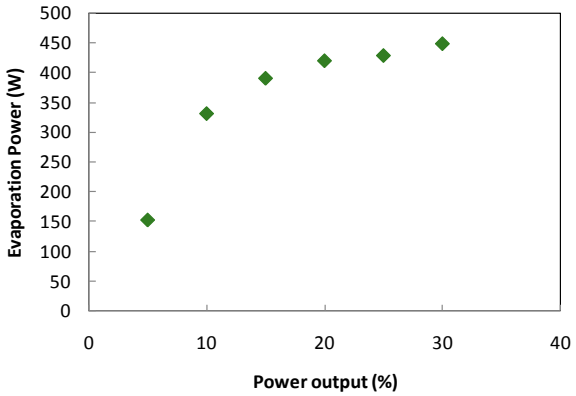

Figure A10: Energy consumption of Angstrom Evaporator

S1.1 Cumulative Energy demand of materials

Table A 14: Cumulative energy demand of small molecules (MJ/kg)

	ZnPc	CuPc	SubPc	AlPcCl	PdPc	Sq
Phthalonitrile	89	85	116		111	
Phthalic anhydride	0	0	0	116	0	
M-Cl	14	15	16	24	50512	
Chemicals	64	62	64	271	64	1084
Solvent regeneration	138	128	138	138	138	160
Energy	407	883	1402	1298	1309	62
TOTAL (MJ/kg)	**713**	**1174**	**1736**	**1848**	**52134**	**1305**

S1.2 Polymer and small molecules synthesis

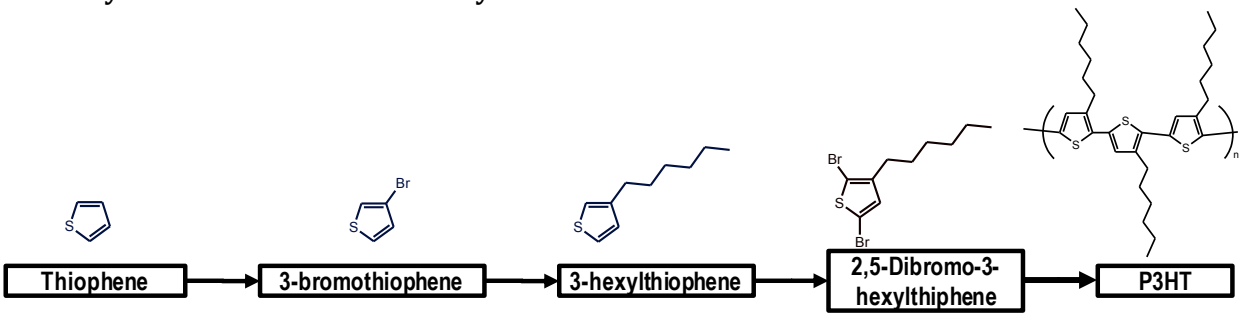

Figure A11: Synthesis of P3HT [66]

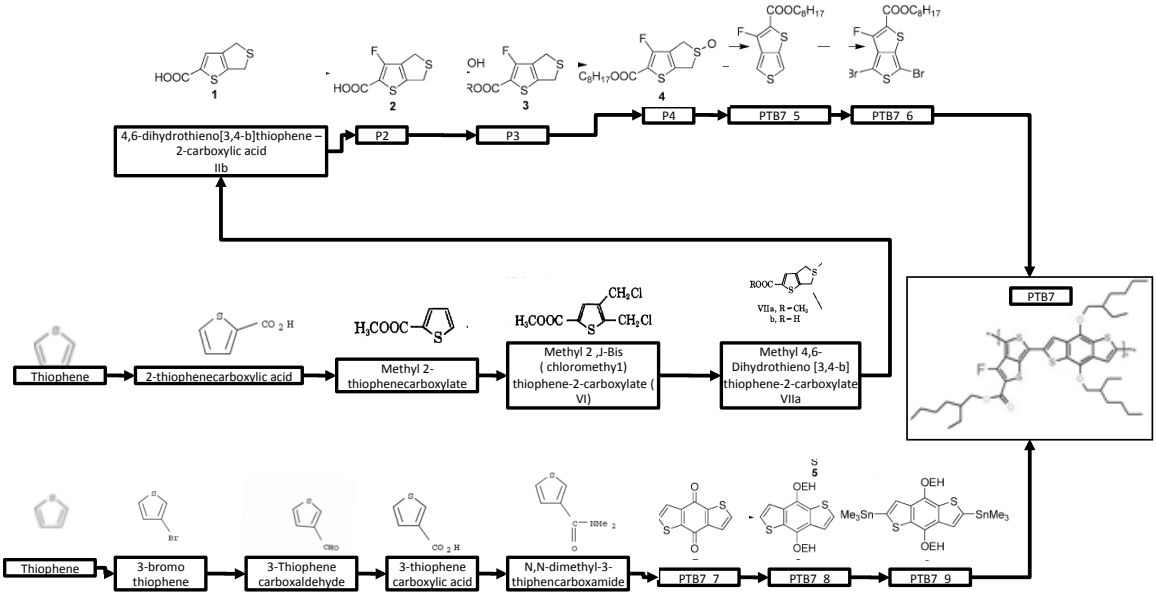

Figure A12: Synthesis of PTB7 (based on [68])

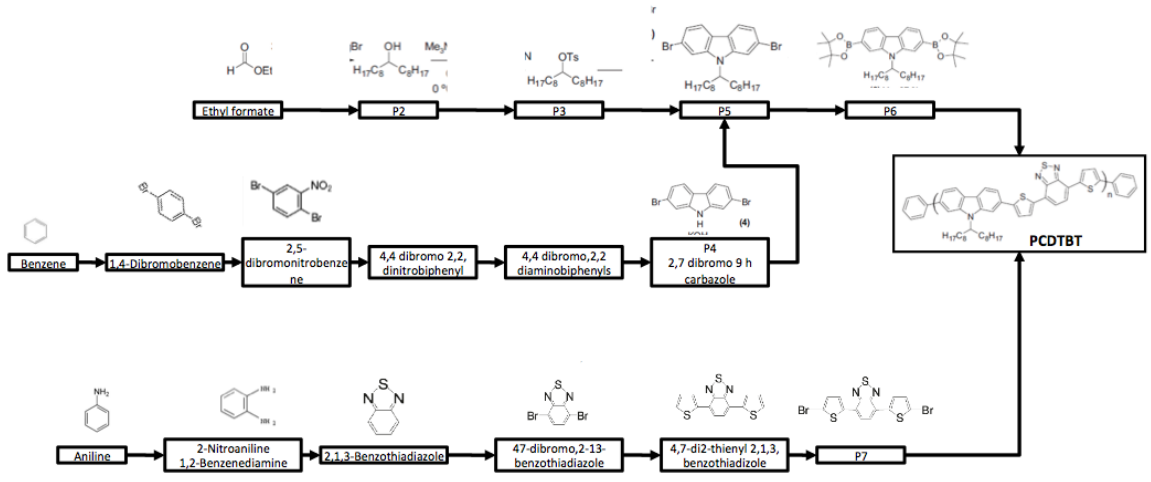

Figure A13: Synthesis of PCDTBT (based on [67])

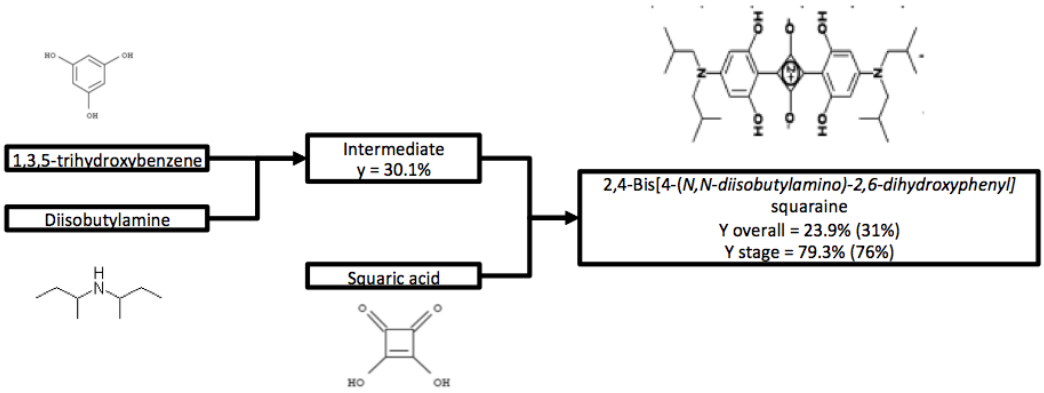

Figure A14: Synthesis of SQ (based on [133])

Table A 15: Material and direct energy inventory to produce 1 kWp photovoltaics.

g/kW	Efficiency %	EBL (g)	Donor (g)	HBL (g)	Direct energy kWh
Polymer					
P3HT- C_{60} bisPCBM	4.50	3.33	20.83		62.77
PTB1 C_{60} PCBM	4.76	3.15	7.88		48.51
P3HT- C_{60} PCBM	5.00	3.00	11.25		130.56
P3HT- C_{60} PCBM - TiOx	5.00	3.00	11.25	0.12	98.33
PTB1 -C_{70} PCBM	5.30	2.83	7.08		43.57
PsiF-DBT - C_{60} PCBM	5.40	2.78	4.86		42.76
PCDTBT: C_{70} PCBM	5.50	2.73	7.50		41.98
P3HT- C_{70}ICBA (5.6%)	5.60	2.68	13.39		66.34
PCDTBT: C_{70} PCBM TiOx	6.10	2.46	4.92	0.03	122.10
PIDTBT: C_{70} PCBM	6.30	2.38	5.95		36.65
P3HT- C_{60} ICBA	6.50	2.31	11.54		57.16
PTB7 C_{70} PCBM	7.40	2.03	5.07		31.20
PBDTTT-C_{70} PCBM	7.70	1.95	4.87		29.99
Small molecules					
AlPcCl/C_{60}	3.00		3.21	1.19	197.11
ClInPc / C_{60}	3.30		3.13	1.08	175.72
SubNc/ C_{60}	3.50		1.10	1.02	155.36
SubPc/ C_{60}	3.60		3.15	0.99	158.56
CuPc/ C_{60} (h)	3.70		2.75	0.96	156.72
PdPc -ZnPc/ C_{60}	3.70	2.10	1.35	1.44	182.53
ZnPc/ C_{60}	3.90		4.49	0.91	146.28
SQ/C_{60}	4.60	2.43	0.34	0.77	240.41
CuPc/C60 (pm-hj)	5.00		2.02	0.71	121.18

Table A 16: Cumulative energy demand of organic solar cells (kJ/Wp)

	Donor	Acceptor	Solvent	EB+ HBL	Sol. Process.	Evap	Annealing	PET	ITO sputtering	Contacts (Silver + printing)	Encap-sulation	Total (KJ/Wp)
P3HT-C_{60} bisPCBM (4.5%)	40.8	2146.5	139.2	0.4	72.2	0.0	153.8	469.4	1897.2	411.1	327.8	5658.4
PTB1 C_{60} PCBM (4.76 %)	40.2	661.2	52.6	0.4	68.3	0.0	106.4	443.8	1793.6	388.7	309.9	3865.0
P3HT- C_{60}PCBM (5%)	20.0	760.0	90.0	0.3	65.0	0.0	405.0	422.5	1707.5	370.0	295.0	4135.3
P3HT- C_{60}PCBM (5%)	22.0	755.4	92.0	5.2	97.5	0.0	405.0	422.5	1707.5	370.0	295.0	4172.2
PTB1 C_{70}PCBM (5.3%)	36.1	1020.5	47.3	0.3	61.3	0.0	95.5	398.6	1610.8	349.1	278.3	3897.8
PsiF-DBT C_{60} PCBM (5.4%)	28.4	816.0	39.8	0.3	60.2	0.0	93.8	391.2	1581.0	342.6	273.1	3626.4
PCDTBT: C_{70} PCBM (5.5%)	43.9	1802.8	61.4	0.3	59.1	0.0	92.0	384.1	1552.3	336.4	268.2	4600.4
P3HT- C_{70}ICBA (5.6%)	26.2	966.7	89.5	0.3	58.0	0.0	180.8	377.2	1524.6	330.4	263.4	3817.0
PCDTBT: C_{70} PCBM TiOx (6.1%)	28.8	2364.4	32.9	1.6	79.9	0.0	359.6	346.3	1399.6	303.3	241.8	5158.1
PIDTBT:C_{70} PCBM	34.8	2146.2	39.8	0.3	51.6	0.0	80.4	335.3	1355.2	293.7	234.1	4571.3
P3HT- C_{60}ICBA (6.5%)	22.6	629.4	77.1	0.3	50.0	0.0	155.8	325.0	1313.5	284.6	226.9	3085.1
PTB7 C_{70} PCBM (7.4%)	25.8	913.6	33.9	0.2	43.9	0.0	68.4	285.5	1153.7	250.0	199.3	2974.4
PBDTTT-CF C_{70} PCBM (7.7%)	24.8	878.0	39.8	0.2	42.2	0.0	65.7	274.4	1108.8	240.3	191.6	2865.8
AlPcCl/C_{60} (3%)	5.9	330.5	0.0	0.8	0.0	709.6	0.0	704.2	2845.8	616.7	491.7	5705.2
ClInPc/C_{60} (3.3%)	5.5	300.5	0.0	0.8	0.0	632.6	0.0	640.2	2587.1	560.6	447.0	5174.2
SubNc /C_{60} (3.5%)	1.9	283.3	0.0	0.7	0.0	559.3	0.0	603.6	2439.3	528.6	421.4	4838.1
SubPc /C_{60} (3.6%)	5.5	241.0	0.0	0.7	0.0	570.8	0.0	586.8	2371.5	513.9	409.7	4700.0
CuPc/C_{60} (h) (3.7%)	3.2	268.0	0.0	0.7	0.0	564.2	0.0	570.9	2307.4	500.0	398.6	4613.1
ZnPc/C_{60} (PdPc) (3.7%)	1.0	268.0	0.0	110.0	0.0	657.1	0.0	570.9	2307.4	500.0	398.6	4813.1
ZnPc/C_{60} (3.9%)	3.2	158.9	0.0	0.5	0.0	526.6	0.0	541.7	2189.1	474.4	378.2	4272.5
SQ/C_{60} (4.6%)	0.2	215.6	0.7	0.8	35.3	668.8	161.4	459.2	1856.0	402.2	320.7	4120.8
CuPc/C_{60} (pm-hj) (5%)	2.4	199.0	0.0	0.5	0.0	436.3	0.0	422.5	1707.5	370.0	295.0	3433.1
SubNC + SubPc tandem	3.9	128.0	0.0	0.6	0.0	507.0	0.0	410.2	1657.8	359.2	286.4	3353.1
ClAlPc + SubPc tandem	6.5	178.6	0.0	0.8	0.0	669.8	0.0	515.2	2082.3	451.2	359.8	4264.3

A4. Supporting information for "Economics of organic photovoltaics"

Since P3HT has been produced for many years, there are multiple suppliers and material is available in bulk amounts, therefore we can extrapolate the cost of P3HT.

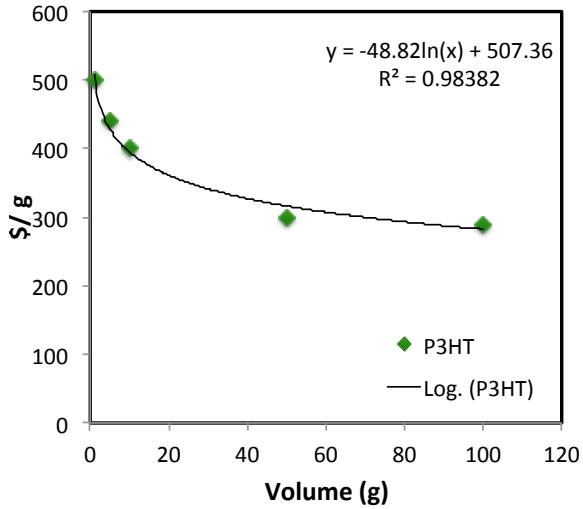

Figure A 15: Decrease in cost/g for P3H

Table A 17: Material inventory (m = material and e = energy).

		Oil Crude (kg)	Coal brown (kg)	Coal hard (kg)	NG (m3)	Br (kg)	Li (kg)	Zn (kg)	NaCl (kg)	M in MPc (kg)
C_{60}	m	94.2	5.5	89.8					0.6	
	e	26.7	20.5	459.1	178.6					
C_{60} PCBM	m	198.6	17.1	1078.0					8.9	
	e	121.4	54.5	212.0	511.0					
C_{70} PCBM	m	309.0	63.7	1580.0					9.5	
	e	122.0	35.3	307.0	675.9					
C_{60} PCBA	m									
	e	401.626	92.68	1600.02	640.98					
C_{60} ICBA		190.23	49.07	842.92	322.17					
C_{70} ICBA		216.22	60.90	1138.97	400.11					
C_{60} bis PCBM		328.19	70.87	1295.50	532.55					
C_{70}		175.7	39.55	841.9	260					
CuPc	m	1.52	0.0	0.0						
	e	1.50	2.7	21.8	0.1				0.4	0.129
InPcCl	m	2.579	0	0						
	e	3.371	6.73	27.5	12				0.642	0.309
SubPc		3.96	4.19	34.3	10.86					
ZnPc		2.55	1.42	10.62	6.19					0.163
AlPcCl		4.83	4.53	32.4	1.154					0.081
PdPc		131.99	574.1	364.2	466.21					0.278
Sq		8.97	3.13	4.95	15.57					
BCP	m	4.9	0.0	0.4					1.2	
	e	0.8	1.3	2.3	8.3					
P3HT	m	7.48	0.21	0.673		5.19			1.4	
	e	3.32	4.32	7.647	18.6					
PCDTBT	m	21	0	6.0		5.17	0.18		9.03	
	e	13	23.9	23.7	66.7					
PTB7	m	19.9	0.9	7.6		7.1	0.2	1.6	21.0	
	e	7.8	19.0	22.5	56.8					

REFERENCES

[1] IPCC, *Fourth Assessment Report*. 2007: http://ipccwg1.ucar.edu/wg1/Report/AR4WG1_Print_Ch02.pdf

[2] S. Pacala and R. Socolow, "Stabilization Wedges: Solving the Climate Problem for the Next 50 Years with Current Technologies," *Science,* vol. 305, pp. 968-972, 2004.

[3] H.-H. Rogner*, et al.*, "Climate Change 2007: Mitigation. Contribution of Working Group III to the Fourth Assessment Report of the Intergovernmental Panel on Climate Change," New York2007.

[4] BP Global. *BP Statistical Review of World Energy June 2010*: http://www.bp.com

[5] World Bank.: http://data.worldbank.org/

[6] U. S. Energy Information Administration, "Annual Energy Outlook 2010," http://www.eia.gov/oiaf/aeo/pdf/0383(2010).pdf

[7] A. Cho, "Energy's Tricky Tradeoffs," *Science,* vol. 329, pp. 786-787, 2010.

[8] U. S. Energy Information Administration, *Annual Energy Outlook 2010 Early Release Overview*: http://www.eia.doe.gov/oiaf/aeo/index.html

[9] C. A. Wolden*, et al.*, "Photovoltaic manufacturing: Present status, future prospects, and research needs," *Journal of Vacuum Science and Technology A,* vol. 29, p. 030801, 2011.

[10] A. C. Mayer, S. R. Scully, B. E. Hardin, M. W. Rowell, and M. D. McGehee, "Polymer-based solar cells," *Materials Today,* vol. 10, pp. 28-33, 2007.

[11] R. A. J. Janssen, J. C. Hummelen, and N. S. Sariciftci, "Polymer-fullerene bulk heterojunction solar cells," *MRS Bulletin,* vol. 30, pp. 33-36, 2005.

[12] M. A. Green, K. Emery, Y. Hishikawa, and W. Warta, "Solar cell efficiency tables (version 37)," *Progress in Photovoltaics: Research and Applications,* vol. 19, pp. 84-92, 2011.

[13] *Konarka*: http://www.konarka.com

[14] *Solarmer*: http://www.solarmer.com

[15] *Heliatek:* http://www.heliatek.com

[16] M. K. Siddiki, J. Li, D. Galipeau, and Q. Qiao, "A review of polymer multijunction solar cells," *Energy & Environmental Science,* vol. 3, pp. 867-883, 2010.

[17] United Nations, "Report of the World Commission on Environment and Development: Our Common Future.":http://www.un-documents.net/wced-ocf.htm

[18] International Organization for Standardization, "Environmental management-Life cycle assessment-Requirements and guidelines," vol. 14044, ed. Switzerland, 2006, p. 46.

[19] A. Hadipour, B. de Boer, and P. W. M. Blom, "Organic tandem and multi-junction solar cells," *Advanced Functional Materials,* vol. 18, pp. 169-181, 2008.

[20] T. Ameri, G. Dennler, C. Lungenschmied, and C. J. Brabec, "Organic tandem solar cells: A review," *Energy & Environmental Science,* vol. 2, pp. 347-363, 2009.

[21] B. A. Gregg, "The photoconversion mechanism of excitonic solar cells," *MRS Bulletin,* vol. 30, pp. 20-22, January 2005.

[22] R. P. Raffaelle, A. Anctil, R. DiLeo, A. Merrill, and B. J. Landi, "Dye-Sensitized Bulk Heterojunction Polymer Solar Cell," in *33rd IEEE PHOTOVOLTAIC SPECIALISTS CONFERENCE*, San Diego, 2008.

[23] I. Bruder*, et al.*, "What determines the performance of metal phthalocyanines (MPc, M = Zn, Cu, Ni, Fe) in organic heterojunction solar cells? A combined experimental and theoretical investigation," *Organic Electronics,* vol. 11, pp. 377-387, 2010.

[24] D. Villemin, M. Hammadi, M. Hachemi, and N. Bar, "Applications of Microwave in Organic Synthesis: An Improved One-step Synthesis of Metallophthalocyanines and a New Modified Microwave Oven for Dry Reactions " *Molecules,* vol. 6,, pp. 831-844, 2001.

[25] M. S. Roy, P. Balraju, Y. S. Deol, S. K. Sharma, and G. D. Sharma, "Charge-transport and photocurrent generation in bulk hetero junction based on Chloro-aluminum phthalocyanine (ClAlPc) and Rose Bengal (RB)," *Journal of Materials Science,* vol. 43, pp. 5551-5563, 2008.

[26] G. Wei, R. R. Lunt, K. Sun, S. Wang, M. E. Thompson, and S. R. Forrest, "Efficient, Ordered Bulk Heterojunction Nanocrystalline Solar Cells by Annealing of Ultrathin Squaraine Thin Films," *Nano Lett.,* vol. 10, pp. 3555-3559, 2010.

[27] US Environmental Protection Agency, "Life Cycle Assessment: Principles and Practice," 2006.

[28] R. Frischknecht, N. Jungbluth, H.-J. Althaus, G. Doka, R. Dones, and T. Heck, "Overview and Methodology Final report ecoinvent Data v2.0," Duebendorf, 2007.

[29] G. Geisler, T. B. Hofstetter, and K. Hungerbuhler, "Production of Fine and Speciality Chemicals: Procedure for the Estimation of LCIs," *International Journal of Life Cycle Analysis,* vol. 9, pp. 101-113, 2004.

[30] J. Rostalski and D. Meissner, "Monochromatic versus solar efficiencies of organic solar cells," *Solar Energy Materials and Solar Cells,* vol. 61, pp. 87-95, 2000.

[31] M. S. Mauter and M. Eliimelech, "Environmental Applications of Carbon-Based Nanomaterials," *Environmental Science and Technology,* vol. 42, pp. 5843-5859, 2008.

[32] H. Kroto, "Symmetry, space, stars and C60," *Reviews of Modern Physics,* vol. 69, pp. 703-722, 1997.

[33] N. Martin, N. Solladie, and J. Nierengarten, "Advances in Molecular and Supramolecular Fullerene Chemistry," *The electrochemical Society Interface,* vol. Summer, pp. 29-33, 2006.

[34] T. Da Ros, "Twenty Years of Promises: Fullerene in Medical Chemistry," in *Medicinal Chemistry and Pharmacological Potentital of Fullerenes and Carbon Nanotubes*, S. Science, Ed., ed, 2008.

[35] F. Diederich, "Covalent fullerene chemistry," *Pure and Applied Chemistry,* vol. 69, pp. 395-400, 1997.

[36] D. E. Meyer, M. A. Curran, and M. A. Gonzalez, "An examination of existing data for the industrial manufacture and use of nanocomponents and their role in the life cycle impact of nanoproducts," *Environmental Science & Technology,* vol. 43, pp. 1256-1263, 2009.

[37] H. Sengul, T. L. Theis, and S. Ghosh, "Toward Sustainable Nanoproducts: An Overview of Nanomanufacturing Methods," *Journal of Industrial Ecology,* vol. 12, pp. 329-359, 2008.

[38] C. Bauer, J. Buchgeister, R. Hischier, W. R. Poganietz, L. Schebek, and J. Warsen, "Towards a framework for life cycle thinking in the assessment of nanotechnology," *Journal of Cleaner Production,* vol. 16, pp. 910-926, 2008.

[39] M. Jacoby, "The Power of Plastic," *Chemical & Engineering News,* vol. 88, pp. 12-16, 2010.

[40] C. Som, M. Berges, Q. Chaudhry, M. Dusinka, and T. F. Fernandes, "The importance of life cycle concepts for the development of safe nanoproducts," *Toxicology,* vol. 269, pp. 160-169, 2010.

[41] W. Kloepffer, M. A. Curran, P. Frankl, R. Heijungs, A. Koehler, and S. I. Olsen, "Nanotechnology and Life Cycle Assessment: Synthesis of Results," Washington DC2007.

[42] A. L. Roes, E. A. Alsema, K. Blok, and M. K. Patel, "Ex-ante Environmental and Economic Evaluation of Polymer Photovoltaics," *Progress in Photovoltaics: Research and Applications,* vol. 17, pp. 372-393, 2009.

[43] D. Kushnir and B. A. Sanden, "Energy Requirements of Carbon Nanoparticle Production," *Journal of Industrial Ecology,* vol. 12, pp. 360-375, 2008.

[44] C. Jimenez-Gonzalez, S. Kim, and M. R. Overcash, "Methodology for Developing Gate-to-Gate Life Cycle Inventory Information," *International Journal of Life Cycle Assessment,* vol. 5, pp. 153-159, 2000.

[45] J. Gonzalez-Aguilar, M. Moreno, and L. Fulcheri, "Carbon nanostructures production by gas-phase plasma processes at atmospheric pressure," *Journal of Physics D: Applied Physics,* vol. 40, pp. 2361-2374, 2007.

[46] D. L. Plata, A. J. Hart, C. M. Reddy, and P. M. Gschwend, "Early evaluation of Potential Environmental Impacts of Carbon Nanotube Synthesis by Chemical Vapor Deposition," *Environmental Science and Technology,* vol. 43, pp. 8367-8373, 2009.

[47] H. Takehara, M. Fujiwara, M. Arikawa, M. D. Diener, and J. M. Alford, "Experimental study of industrial scale fullerene production by combustion synthesis," *Carbon,* vol. 43, pp. 311-319, 2005.

[48] Y. Liang*, et al.*, "Development of New Semiconducting Polymers for High Performance Solar Cells," *Journal of American Chemical Society,* vol. 131, pp. 56-57, 2009.

[49] T. Tokunaga, K. Kaneko, K. Sato, and Z. Horita, "Microstructure and mechanical properties of aluminum–fullerene composite fabricated by high pressure torsion," *Scripta Materialia,* vol. 58, pp. 735-738, 2008.

[50] H.-J. Althaus, S. Blaser, M. Classen, and N. Jungbluth, "Life Cycle Inventories of Metals. Final report ecoinvent 2000," 2000.

[51] A. Anctil, C. W. Babbitt, R. P. Raffaelle, and B. J. Landi, "Life-cycle Assessment of Organic Solar Cells Technologies," in *35th IEEE Photovoltaic Specialists Conference*, Honolulu, 2010.

[52] K. Sander and G. S. Murthy, "Life cycle analysis of algae biodiesel," *The International Journal of Life Cycle Assessment,* vol. 15, pp. 704-714, 2010.

[53] W. J. Groot and T. Borén, "Life cycle assessment of the manufacture of lactide and PLA biopolymers from sugarcane in Thailand," *The International Journal of Life Cycle Assessment,* vol. 15, pp. 970-984, 2010.

[54] P. T. Boudreault, A. Najari, and M. Leclerc, "Processable Low-Bandgap Polymers for Photovoltaic Applications," *Chemistry of Materials,* vol. 23, pp. 456-469, 2011.

[55] H.-Y. Chen, *et al.*, "Polymer solar cells with enhanced open-circuit voltage and efficiency," *Nature Photonics,* vol. 3, pp. 649-653, 2009.

[56] D. Venkataraman, S. Yurt, B. H. Venkataraman, and N. Gavvalapalli, "Role of Molecular Architecture in Organic Photovoltaic Cells," *Journal of Physical Chemistry Letters,* vol. 1, 2010.

[57] V. Shrotriya, "Polymer Power," *Nature Photonics,* vol. 3, pp. 447-449, 2009.

[58] L. J. Chen, Q. L. Song, Z. H. Xiong, J. H. Huang, and F. He, "Environment-friendly energy from all-carbon solar cells based on fullerene-C60," *Solar Energy Materials and Solar Cells,* vol. 95, pp. 1138-1140, 2010.

[59] A. Anctil, C. W. Babbitt, R. P. Raffaelle, and B. J. Landi, "Material and Energy Intensity of Fullerene Production," *Environmental Science and Technology,* vol. 45, pp. 2353-2359, 2011.

[60] R. Garcıa-Valverde, J. A. Chermi, and A. Urbina, "Life cycle analysis of organic photovoltaic technologies," *Progress in Photovoltaics: Research and Applications,* vol. 18, pp. 535-558, 2010.

[61] N. Espinosa, R. Garcia-Valverde, A. Urbina, and F. C. Krebs, "A life cycle analysis of polymer solar cell modules prepared using roll-to-roll methods under ambient conditions," *Solar Energy Materials & Solar Cells,* 2010.

[62] C. Capello, G. Wernet, J. Sutter, S. Hellweg, and K. Hungerburger, "A comprehensive environmental assessment of petrochemical solvent production," *International Journal of Life Cycle Assessment,* vol. 14, pp. 467-479, 2009.

[63] M. A. J. Huijbregts, *et al.*, "Is cumulative fossil energy demand a useful indicator for the environmental performance of products? ," *Environmental Science & Technology* vol. 40, pp. 641-648, 2006.

[64] Y. He, H. Y. Chen, J. Hou, and Y. Li, "Indene-C60 Bisadduct: A New Acceptor for High-Performance Polymer Solar Cells," *Journal of the American Chemical Society,* vol. 132, pp. 1377-1382, 2010.

[65] G. Zhao, Y. He, and Y. Li, "6.5% Efficiency of Polymer Solar Cells Based on poly(3-hexylthiophene) and Indene-C60 Bisadduct by Device Optimization," *Advanced Materials,* vol. 22, pp. 4355-4358, 2010.

[66] M. C. Stefan, A. E. Javier, I. Osaka, and R. D. McCullough, "Grignard Metathesis Method (GRIM): Toward a Universal Method for the Synthesis of Conjugated Polymers," *Macromolecules,* vol. 42, pp. 30-32, 2009.

[67] N. Blouin, A. Michaud, and M. Leclerc, "A Low-Bandgap Poly(2-6-Carbazole) Derivative for Use in High-Performance Solar Cells," *Advanced Materials,* vol. 19, pp. 2295-2300, 2007.

[68] Y. Liang, D. Feng, Y. Wu, S. Tsai, C. Ray, and L. Yu, "Highly Efficient Solar Cell Polymers Developed via Fine-Tuning of Structural and Electronic Properties," *Journal of American Chemical Society,* vol. 131, pp. 7792-7799, 2009.

[69] S. H. Park, *et al.*, "Bulk heterojunction solar cells with internal quantum efficiency approaching 100%," *Nature Photonics,* vol. 3, pp. 297-303, 2009.

[70] L. Cai, H. Zhao, W. Zhang, and L. Dai, "One-step Synthesis Method of Symmetrical 1,10-phenanothroline Derivative," China Patent, 2010.

[71] F. Ullmann, "Ullmann's encyclopedia of industrial chemistry," 6th ed, 2003.

[72] "PlasticsEurope's Eco-profiles."

[73] R. Hischier, M. Classen, M. Lehmann, and W. Scharnhorst, "Life Cycle Inventories of Electric and Electronic Equipment - Production, Use & Disposal," Duebendorf and St. Gallen2007.

[74] H. Takehara, M. Fujiwara, M. Arikawa, M. D. Diener, and M. Alford, "Experimental study of industrial scale fullerene production by combustion synthesis," *Carbon,* vol. 43, pp. 311-319, 2005.

[75] R. R. Lunt, B. E. Lassiter, J. B. Benziger, and S. R. Forrest, "Organic vapor phase deposition for the growth of large area organic electronic devices," *Applied Physics Letters,* vol. 95, p. 233305, 2009.

[76] W. Cai, X. Gong, and Y. Cao, "Polymer solar cells: Recent Development and Possible Routes for Improvement in the Performance," *Solar Energy Materials & Solar Cells,* vol. 94, 2010.

[77] W. Ma, C. Yang, X. Gong, K. Lee, and A. J. Heeger, "Thermally stable efficient polymer solar cells with nanoscale control of the interpenetrating network morphology," *Advanced Functional Materials,* vol. 15, pp. 1617-1622, 2005.

[78] J. Y. Kim*, et al.*, "New Architecture for High-Efficiency Polymer Photovoltaic Cells Using Solution-Based Titanium Oxide as an Optical Spacer," *Advanced Materials,* vol. 18, pp. 572-576, 2006.

[79] M. Lenes, G.-J. A. H. Wetzelaer, F. B. Kooistra, S. C. Veenstra, J. C. Hummelen, and P. W. M. Blom, "Fullerene Bisadducts for Enhanced Open-Circuit Voltages and Efficiencies in Polymer Solar Cells," *Advanced Materials,* vol. 20, pp. 2116-2119, 2008.

[80] Y. He, G. Zhao, B. Peng, and Y. Li, "High-Yield Synthesis and Electrochemical and Photovoltaic Properties of Indene-C 70 Bisadduct," *Advanced Functional Mater,* vol. 20, pp. 3383-3389, 2010.

[81] E. Wang*, et al.*, "High-performance polymer heterojunction solar cells of a polysilafluorene derivative," *Applied Physics Letters,* vol. 92, p. 033307, 2008.

[82] Y. Liang*, et al.*, "Development of New Semiconducting Polymers for High Performance Solar Cells," *Journal of American Chemical Society,* vol. 131, pp. 56-57, 2009.

[83] J. Peet*, et al.*, "Efficiency enhancement in low-bandgap polymer solar cells by processing with alkane dithiols," *Nature Materials,* vol. 6, pp. 497-500, 2007.

[84] S. H. Park, *et al.* "Bulk heterojunction solar cells with internal quantum efficiency approaching 100%," *Nature Photonics,* vol. 3, pp. 297-303, 2009.

[85] K.-S. Chena*, et al.*, "Highly efficient indacenodithiophene-based polymeric solar cells in conventional and inverted device configurations," *Organic Electronics,* vol. 12, pp. 794-801, 2011.

[86] Y. Liang*, et al.*, "For the Bright Future - Bulk Heterojunction Polymer Solar Cells with Power Conversion Efficiency of 7.4%," *Advanced Materials,* vol. 22, pp. 1-4, 2010.

[87] J. Y. Kim*, et al.*, "Efficient Tandem Solar Cells Fabricated by All-Solution Processing," *Science,* vol. 317, p. 222, 2007.

[88] J. Gilot, M. M. Wienk, and R. A. J. Janssen, "Optimizing Polymer Tandem Solar Cells," *Advanced Energy Materials,* vol. 22, pp. E67-E71, 2010.

[89] D. Cheyns, B. P. Rand, and P. Heremans, "Organic tandem solar cells with complementary absorbing layers and a high open-circuit voltage," *Applied Physics Letters,* vol. 97, p. 033301, 2010.

[90] W. Wang, D. Placencia, and N. R. Armstrong, "Planar and textured heterojunction organic photovoltaics based on chloroindium phthalocyanine (ClInPc) versus titanyl phthalocyanie (TiOPc) donor layers," *Organic Electronics,* vol. 12, pp. 383-393, 2011.

[91] W. Zeng, K. S. Yong, Z. M. Kam, F. Zhu, and Y. Li, "Effect of blend layer morphology on performance of ZnPc:C60-based photovoltaic cells," *Applied Physics Letters,* vol. 97, p. 133304, 2010.

[92] I. Kim, H. M. Haverinen, J. Li, and G. E. Jabbour, "Enhanced power conversion efficiency of p-i-n type organic solar cells by employing a p-layer of palladium phthalocyanine " *Applied Physics Letters,* vol. 97, pp. 203301-3, 2010.

[93] J. Xue, B. P. Rand, S. Uchida, and S. R. Forrest, "A Hybrid Planar-Mixed Molecular Heterojunction Photovoltaic Cell," *Advanced Materials,* vol. 17, pp. 66-70, 2005.

[94] R. Sondergaard, M. Helgesen, M. Jorgensen, and F. C. Krebs, "Fabrication of Polymer Solar Cells Using Aqueous Processing for All Layers Including the Metal Back Electrode," *Advanced Energy Materials,* vol. 1, pp. 68-71, 2011.

[95] G. Geisler, T. B. Hofstetter, and K. Hungerbuehler, "Production of fine and specialty chemicals: procedure for the estimation of LCIs," *Int. J. Life Cycle Assess.,* vol. 9, pp. 101-113, 2004.

[96] J. Kalowekamo and E. Baker, "Estimating the manufacturing cost of purely organic solar cells," *Solar Energy,* vol. 83, pp. 1224-1231, 2009.

[97] W. P. Beyermann, M. F. Hundley, J. D. Thompson, F. N. Diederich, and G. Gruner, "Low-temperature specific heat of C60," *Physical Review Letters,* vol. 68, pp. 2046-2049, 1992.

[98] C. J. Brown, "Crystal structure of β-copper phthalocyanine," *Journal of the Chemical Society A,* pp. 2488-2493, 1968.

[99] Sigma-Aldrich. *Chemical prices*: http://www.sigmaaldrich.com/

[100] T. D. Nielsen, C. Cruickshank, S. Foged, J. Thorsen, and F. C. Krebs, "Business, market and intellectual property analysis of polymer solar cells," *Solar Energy & Solar Cells,* vol. 94, pp. 1553-1571, 2010.

[101] Rieke Metals, "P3HT prices,": http://www.riekemetals.com/

[102] 1-material. *Low bandgap polymer prices*. 2011

[103] J. Dai, X. Jiang, H. Wang, D. Yan. "Organic photovoltaic cells with near infrared absorption spectrum", in *Applied Physics Letters*, vol. 91, pp. 253503, 2007

[104] A. Anctil*, et al.*, "Inkjet Fabrication of Tandem Dye-Sensitized Bulk Heterojunction Polymer Solar Cells," in *MRS*, Boston, 2008.

[105] C. Zhang, S. W. Tong, C. Jiang, E. T. Kang, D. S. H. Chan, and C. Zhu, "Simple tandem organic photovoltaic cells for improved energy conversion efficiency," *Applied Physics Letters,* vol. 92, pp. 083310/1-083310/3, 2008.

[106] A. Hayakawa, O. Yoshikawa, T. Fujieda, K. Uehara, and S. Yoshikawa, "High performance polythiophene/fullerene bulk-heterojunction solar cell with a TiOx hole blocking layer," *Applied Physics Letters,* vol. 90, pp. 163517/1-163517/3, 2007.

[107] H. Benten, N. Kudo, H. Ohkita, and S. Ito, "Layer-by-layer deposition films of copper phthalocyanine derivative; their photoelectrochemical properties and application to solution-processed thin-film organic solar cells," *Thin Solid Films,* vol. 517, pp. 2016-2022, 2009.

[108] B. Ma, C. H. Woo, Y. Miyamoto, and J. M. J. Frechet, "Solution Processing of a Small Molecule, Subnaphthalocyanine, for Efficient Organic Photovoltaic Cells," *Chemistry of Materials,* vol. 21, pp. 1413-1417, 2009.

[109] C. Girotto, B. P. Rand, J. Genoe, and P. Heremans, "Exploring spray coating as a deposition technique for the fabrication of solution-processed solar cells," *Solar Energy Materials & Solar Cells,* vol. 93, pp. 454-458, 2009.

[110] S. F. Tedde, J. Kern, T. Sterzl, J. Furst, and P. Lugli, "Fully Spray Coated Organic Photodiodes," *Nano Letters,* vol. 9, pp. 980-983, 2009.

[111] *M. T. Lloyd*, *J. E. Anthony*, and *G. G. Malliaras*, "Photovoltaics from soluble small molecules," *Materials Today,* vol. 10, pp. 34-41, 2007.

[112] F. Yang, R. R. Lunt, and S. R. Forrest, "Simultaneous heterojunction organic solar cells with broad spectral sensitivity," *Applied Physics Letters,* vol. 92, pp. 053310/1-053310/3, 2008.

[113] G. U. C. Yu, J. Gao, J. C. Hummelen, F. Wudl, and A. J. Heeger, "Polymer photovoltaic cells: enhanced efficiencies via a network of internal donor-acceptor heterojunctions," *Science,* vol. 270, pp. 1789-1791, Dec 15 1995.

[114] S. Guenes, H. Neugebauer, and N. S. Sariciftci, "Conjugated Polymer-Based Organic Solar Cells," *Chemical Reviews (Washington, DC, United States),* vol. 107, pp. 1324-1338, 2007.

[115] J. Szépvölgyi*, et al.*, "Effects of Precursors and Plasma Parameters on Fullerene Synthesis in RF Thermal Plasma Reactor," *Plasma Chemistry and Plasma Processing,* vol. 26, 2006.

[116] Z. Markovic, et al., "Comparative Process Analysis of Fullerene Production by the Arc and the Radio-Frequency Discharge Methods," *Journal of Nanoscience and Nanotechnology,* vol. 7, pp. 1357-1369, 2007.

[117] J. M. Alford, C. Bernal, M. Cates, and M. D. Diener, "Fullerene production in sooting flames from 1,2,3,4-tetrahydronaphthalene," *Carbon,* vol. 46, pp. 1623-1625, 2008.

[118] Y. S. Grushko, V. P. Sedov, and A. Shilin, "Technology for Manufacture of Pure Fullerenes C60, C70 and a Concentrate of Higher Fullerenes," *Russian Journal of Applied Chemistry,* vol. 80, pp. 448-455, 2007.

[119] J. C. Hummelen, B. W. Knight, F. LePeq, F. Wudl, J. Yao, and C. L. Wilkins, "Preparation and Characterization of Fulleroid and Methanofullerene Derivatives," *Journal of Organic Chemistry,* vol. 60, p. 532, 1995.

[120] A. Röder, C. Bauer, and R. Dones, "Sachbilanzen von Energiesystemen. Final report No. 6 ecoinvent data v2.0," Dübendorf and Villigen, 2007.

[121] R. Zah and R. Hischier, "Life Cycle Inventories of Detergents. Final report ecoinvent data v2.0.," Dübendorf, 2007.

[122] J. Sutter, "Life Cycle Inventories of Highly Pure Chemicals Final report ecoinvent Data v2.0," Dubendorf and St. Gallen, 2007.

[123] R. Hischier, "Life Cycle Inventories of Packaging and Graphical Paper. Final report ecoinvent data v2.0.," Dübendorf, 2007.

[124] H.-J. Althaus, M. Chudacoff, R. Hischier, N. Jungbluth, M. Osses, and A. Primas, "Life Cycle Inventories of Chemicals. Final report ecoinvent data v2.0.," Dübendorf, 2007.

[125] J. Sutter, "Life Cycle Inventories of Petrochemical Solvents Final report ecoinvent Data v2.0," Duebendorf and St. Gallen, 2007.

[126] M. Spielmann, R. Dones, and C. Bauer, "Life Cycle Inventories of Transport Services. Final report ecoinvent Data v2.0," Dübendorf and Villigen, 2007.

[127] R. Frischknecht, M. Tuchschmid, M. Faist Emmenegger, C. Bauer, and R. Dones, "Strommix und Stromnetz. Sachbilanzen von Energiesystemen. Final report No. 6 ecoinvent data v2.0," Dübendorf and Villigen, 2007.

[128] J. A. Dean, *Lange's Handbook of Chemistry*, 15th edition ed., 1999.

[129] J. B. Howard, A. L. Lafleur, Y. Makarovsky, S. Mitra, C. J. Pope, and T. K. Yadav, "Fullerenes synthesis in combustion," vol. 30, pp. 1183-1201, 1992.

[130] T. Alexakis, P. G. Tsantrizos, Y. S. Tsantrizos, and M. J-L., "Synthesis of fullerenes via the thermal plasma dissociation of hydrocarbons," *Applied Physics Letters,* vol. 70, pp. 2102-2104, 1997.

[131] A. A. Bogdanov, D. Deininger, and G. A. Dyuzhev, "Development prospects of the commercial production of fullerenes.," *Technical Physics,* vol. 45, pp. 521-527, 2000.

[132] J. M. Alford and e. al., "Fullerene production in sooting flames from 1,2,3,4-tetrahydronaphthalene," *Carbon,* vol. 46, pp. 1623-1625, 2008.

[133] M. Tian, M. Furuki, I. Iwasa, Y. Sato, L. S. Pu, and S. Tatsuura, "Search for Squaraine Derivatives That Can Be Sublimed without Thermal Decomposition," *Journal of Physical Chemistry B,* vol. 106, 2002.